EFFECT OF PRESSURE ON MECHANICAL BEHAVIOR OF FILLED ELASTOMERS

Thesis by

Keikichi Yagii

In Partial Fulfillment of the Requirements

for the Degree of

Doctor of Philosophy

California Institute of Technology

Pasadena, California

1972

(Submitted October 12, 1971)

ACKNOWLEDGEMENT

Concluding my four year's work at the California Institute of Technology in this form of a thesis, my thanks, most of all, are due to Dr. N. W. Tschoegl, without whose guidance and help I would never have been able to reach this day. I am equally grateful to Dr. K. Ninomiya, who in the first place enabled me to begin and continue my academic study here.

I would like to thank all the professors, friends, and employees of many sections of the Caltech community who helped me pursue the study. Especially, I would like to thank D. G. Fesko for many useful discussions, R. E. Cohen for his help with English, and S. C. Sharda for sharing experiences in the experiments.

I am deeply grateful to the Japan Synthetic Rubber Company for allowing me to stay abroad for so many years.

This work was supported during the first three years by the United States Air Force.

ABSTRACT

The Young's modulus, stress-strain curves, and failure properties of glass bead-filled EPDM vulcanizates were studied under superposed hydrostatic pressure. The glass bead-filled EPDM was employed as a representation of composite systems, and the hydrostatic pressure controls the filler-elastomer separation under deformation. This separation shows up as a volume change of the system, and its infuence is reflected in the mechanical behavior as a reinforcing effect of variable degree.

The strain energy stored in the composite system in simple tension was calculated by introducing a model which is described as a cylindrical block of elastomer with two half spheres of filler on each end with their centers on the axis of the cylinder. In the derivation of the strain energy, assumptions were made to obtain the strain distribution in the model, and strain energy-strain relation for the elastomer was also assumed. The derivation was carried out for the case of no filler-elastomer separation and was modified to include the case of filler-elastomer separation.

The resulting strain energy, as a function of stretch ratio and volume of the system, was used to obtain stress-strain curves and volume change-strain curves of composite systems

under superposed hydrostatic pressure.

Changes in the force and the lateral dimension of a ring specimen were measured as it was stretched axially under a superposed hydrostatic pressure in order to calculate the mechanical properties mentioned above. A tensile tester was used which is capable of sealing the whole system to carry out a measurement under pressure. A thickness measuring device, based on the Hall effect, was built for the measurement of changes in the lateral dimension of a specimen.

The theoretical and experimental results of Young's modulus and stress-strain curves were compared and showed fairly good agreement.

The failure data were discussed in terms of failure surfaces, and it was concluded that a failure surface of the glass-bead-filled EPDM consists of two cones.

TABLE OF CONTENTS

LIST OF FIGURES

LIST OF TABLES

LIST OF SYMBOLS

a	Radius of a spherical filler particle
b	Half length of the model of a composite system
c	Radius of the model
d	Radius of a hook
f	Function determining the shape of strain energy function
l	Axial coordinate of a cylindrical coordinate system after deformation
l'	Axial coordinate of a cylindrical coordinate system before deformation
l_o	Initial distance between the surface of the facing spheres in axial direction
r	Radial element of a cylindrical coordinate system
r_o	Minimum radius of a stretched cylinder
t, t'	Thickness of a specimen
t_o, t_o'	Initial thickness of a specimen
u	Radial or x-element of a displacement vector
v	Ratio of dilatational volume change tangential or y-element of a displacement vector
w	Width of a specimen Axial or z-element of a displacement vector
w_{av}	Average width of a ring specimen
x, y, z	Error factors in the coefficients of a calibration curve of the Hall effect thickness sensor

x	Normalized distance of a point on the surface of a sphere from the bottom of the model
y	Normalized distance of a point on the surface of a vacuole from the bottom of the model
A, B, C	Coefficients of a Hall device calibration curve
$\bar{B}$	Magnetic flux vector
B_1, B_2	Intensity of a magnetic field
C_1, C_2, C_3, C_4	Constants specifying failure surfaces
C_{ij}	Coefficient of the Taylor expansion of a strain energy function
D_o	Outside diameter of a ring specimen
D_i	Inside diameter of a ring specimen
D_a	Average diameter of a ring specimen
E	Young's modulus
$\bar{G}$, $\bar{G}_o$	Shear modulus
I_1, I_2, I_3	Principal invariants of a deformation tensor
$\bar{J}$	Electric current vector
L	Distance between the centers of the hooks of a tensile tester
L_o	Initial distance of the hooks of a tensile tester
P	Hydrostatic pressure
R	Radius of a tube
R_H	Hall coefficient

S_1, S_2	Area
V_H	Output voltage of Hall effect thickness sensor
V	Volume of a system or a tube after deformation
V_o	Volume of a system or a tube before deformation
V_a	Volume of a portion of a vacuole
V_{ao}	Volume of a portion of a sphere corresponding to V_a
W	General notation for strain energy (the meaning of various subscripts is explained in the text)
X, Y	Elements of a rectangular coordinate system
α	Ratio of the minimum and maximum radii of a stretched tube
α_o	A limit of α
α_{ij}	Displacement tensor
β	Ratio of the radii of the ends of a tube before and after stretching
γ_{ij}	Cauchy-Green deformation tensor
ζ	Experimental parameter to correct the theoretical values of strain energy
η	Ratio of the length of a vacuole to the diameter of a filler particle
η_o	Maximum value of η
	Angle between radius of a filler and the axis of the model
λ	Stretch ratio (the meaning of subscripts is explained in the text)
μ	Ratio of enclosed volumes

ν	Exponent of a function that defines the profile of a stretched tube
ν_e	Cross linking density of an elastomer
σ	Nominal (engineering) stress
$\bar{\sigma}$	True stress
σ_b	Stress at break
σ_d	Stress at dewetting
σ_{on}	Octahedral normal stress
σ_{os}	Octahedral shear stress
$\sigma_{on,b}$	Octahedral normal stress at break
$\sigma_{os,b}$	Octahedral shear stress at break
$\sigma_1, \sigma_2, \sigma_3$	Principal stresses of a stress tensor
φ	Volume fraction of filler
ψ	Parameter defining the shape of the model, a b

1. Introduction

Elastomers filled with solid particles show greatly different properties in many respects from those of the matrix of elastic material in which the particles are embedded. The differences appear in Young's modulus, stress-strain response, failure properties, abrasion resistance, etc. When the changes in the properties caused by filler particles are in a desirable direction from the practical point of view, the filler is called a reinforcing, or active filler, or otherwise a non-reinforcing or inactive filler. Restricting our interest to mechanical properties, three features are usually more conspicuous among the effects of filler than the rest of them. These are Young's modulus, the shape of the stress-strain curve, and the failure properties. In order to investigate the effect of filler in an elastic material there may be a number of methods of approach to the problem, either theoretically or experimentally. But our interest is in predicting the properties of a composite system consisting of a matrix of an elastic material and solid particles, provided that the properties of both constituents are known. Molecular theories are not often applied to this special field of interest. Applications of continuum mechanics have been more often used to develop theories for a composite system. From a theoretical point of view, the only difference between a reinforcing

filler and a non-reinforcing filler may be whether or not the rubber matrix separates from the filler particles as a composite system undergoes a deformation. And if this speculation is true, a theory for a composite system with non-reinforcing fillers with controlled degree of filler-elastomer separation will cover the case of reinforcing filler as a special case. A method to control the degree of filler-matrix separation is to carry out measurements under superposed hydrostatic pressure. This leads to the experiments which will be described later.

Of the three features mentioned above, the increase of Young's modulus due to the solid particles is the most frequently studied subject as far as the number of the available theories is concerned.

Einstein's equation for the viscosity[1] of a suspension of rigid spheres in a Newtonian liquid predicts that the viscosity increases linearly with the concentration of the spheres at low concentrations where the interaction between the solid particles are regarded as non-existent.

Smallwood[4], solving the problem by way of the theory of elasticity with some simplifications in his mathematical treatment, derived an equation identical to Einstein's equation for viscosity. Naturally, his equation is useful only for very low concentrations of filler, but this is probably the first attempt to obtain the Young's modulus of a filled system by the theory

of elasticity.

Based on the coincidence of the results from totally different approaches, in some cases the relations that give the increase of viscosity of a liquid due to the suspended particles have been used to predict the Young's modulus of filled elastomers as a function of filler fraction by simply replacing the viscosity terms in the equations by the corresponding moduli. Although this may not be justifiable in a rigorous sense, this method seems to be useful in giving the right information concerning the effect of filler.

Eilers[2], starting from Einstein's viscosity equation of suspension which predicts a linear increase of the viscosity of a suspension with the concentration of solid particles, modified it to give a better fit to experimental results up to higher concentration, mostly empirically. The same equation has been applied to give the increase of the moduli of filled polymers with considerable success.

Guth[3], also starting with Einstein's equation, derived the viscosity of suspension as a power expansion with respect to the concentration of solid particles and gave the coefficients up to the second power of concentration. He also introduced a shape factor for irregular shaped particles which modifies the coefficients in his first equation. This equation was also converted for the purpose of predicting the moduli

of filled polymers simply by replacing viscosity by modulus.

Einstein's and Smallwood's equations are valid only up to filler concentrations of a few percent. The two empirically modified equations mentioned above naturally have wider ranges of applicability, sometimes up to a few tens of percent.

Kerner[23, 24] introduced a three layer model for a composite system which consists of a sphere of filler material inside a concentric shell of material with the properties of the material of continuous phase which is in turn embedded in the material with the overall properties of the composite system. He applied the model to various properites such as electrical conductivity, elasticity, etc. of composite systems. His model was further developed by Van der Poel, and by Furukawa and Sato in their theories.

Van der Poel[5], also by the aid of the theory of elasticity, derived a relation between the moduli of unfilled and filled elastomers. His theory is constructed on a three layer model similar to Kerner's. The model consists of an inner sphere of the material of the disperse phase of radius, a, an intermediate layer of the material of the continuous phase of unit radius, and an outer shell with the properties of the composite, the diameter of which is much larger than those of the other two. The volume fraction of the disperse phase coincides with a^3. The modulus of the material in the outer shell is given a value such that, when the model

is subjected to a uniform tension the overall deformation is not affected if the two inside layers are replaced by a sphere of unit radius of the material in the outer shell. He calculated the modulus of the material in the outer shell and took it as the overall modulus of the system. The relation is not a closed form. Agreement with experimental data is fairly good up to considerable filler concentrations.

Frankel and Acrivos[6] treated the problem from a slightly different direction. Their theory deals with the viscosity of suspension of high concentration. Considering the interaction between the solid particles suspended in the liquid, they derived an equation that gives the asymptote to the viscosity-concentration curve in the high concentration region. Their equation gives good correspondence at high concentration, but not in the region of lower concentrations.

A number of empirical equations have been proposed to express the stress-strain curves of both unfilled and filled elastomers. However, there are very few useful theories to predict the stress-strain curves for filled elastomers from the known properties of filler and elastomer. The most fruitful approach to this problem appears to be choosing an appropriate model that enables us to handle it with reasonable ease.

Sato and Furukawa[7] based their theory on a concentric sphere model similar to Van der Poel's. They chose a simple function for the deformation tensor for the outside layer of the model and calculated the strain energy predicted by the statistical theory of rubber elasticity. With this method, they obtained mechanical properties (such as, e.g , Young's modulus, stress-strain curves, etc.) of composite systems. They ascribed deviations of the theory from the experimental data to vacuole formation and used an adjustable parameter to correct for the deviation. The corrected results agreed with the data for filler fractions up to about 10 -- 15 %.

Although it is quite obvious that vacuole formation around filler particles in a composite system has a great influence on the reinforcing ability of the filler, there has been no theory that directly relates the amount of vacuole formation to the change in the stress strain curves or vice versa. However, a number of experiments have been performed on the measurement and the observation of vacuole formation by deformation of filled elastomers.

Fedors and Landel[8] measured volume changes of elastomers filled with glass beads. Assuming a conical shape for the vacuoles, the height of which increased linearly with the increase of the strain, they derived an expression for the stress-strain curve.

Fishman and Rinde[9], by means of curve fitting, derived an expression that gives the volume change of a deformed, filled system as a function of strain energy, time, and temperature. Experimentally, they measured the volume changes and stress-strain curves under constant strain rate, constant load, and constant loading rate deformation.

Farris[10] measured the volume change of elastomers filled with 'non-reinforcing filler' and analysed the results by a statistical method. He assumed that the probability for a certain particle to dewet at a certain strain is given by a Gaussian distribution, and determined the parameters contained in the distribution function from experimental results. His measurements were performed under superposed hydrostatic pressure as well as at atmospheric pressure.

Some of the work that may be related to the one described herein have been briefly mentioned above. The purpose here is to obtain the mechanical behavior (primarily the stress-strain behavior but also failure behavior) of fillled elastomers as a function of filler fraction and superposed bydrostatic pressure. The superposed pressure is employed to control the degree of vacuole formation or filller-matrix separation under deformation and , consequently, gives some information about the reinforcing mechanism of fillers. In spite of the number of theories mentioned above, none of them is without some kind of experimental para-

meter to give a reasonable fit of the theory to the experimental results. This can hardly be faulted, considering the difficulties involved in solving the problem of the stress-strain behavior of a filled system. For example, non-linearity of the compatibility equations due to large deformation, the non-linear relation between strain and stress, the extremely complicated boundary conditions because of the randomly dispersed particles of filler must be considered. Consequently, some assumptions and simplifications can not be avoided in order to handle the problem and obtain reasonable results.

In chapter 2 we present a theory for obtaining the strain energy in a composite system as a function of stretch ratio and the amount of vacuole formation due to the dewetting on the surfaces of filler particles. The theory contains several assumptions and simplifications. First we assume that matrix material is incompressible , the filler consists of rigid spheres of uniform size and that the strain energy stored during the deformation can be expanded in a Taylor series of the invariants of the strain tensor. Second we assume that time effects and hysteresis effects are absent. A model for the composite system is introduced and the approximate equations for the strain invariants are derived as functions of spatial position in the model when the system is subjected to a simple tension. Combining the Taylor expansion of the strain energy and the approximate equations for the strain invariants, the total strain energy is calculated. The strain energy is obtained both for the case of no vacuole formation and for the case

of vacuole formation

In Section 3 the experimental equipment and procedures, sample preparation, and the method of data analysis are described. Experiments were performed to obtain stress-strain curves and volume change-strain curves of glass-bead filled elastomers with superposed hydrostatic pressure and loading ratio of filler as parameters.

In Section 4 the results of the experiments are compared with the theory. In Subsection 4.1 the material constants of the rubber matrix are obtained from the experimental data. In Subsection 4.2 the initial moduli are calculated both from experimental data and from the theory. In Subsection 4.3 the volume change-stress-strain curves are compared, experimentally and theoretically, and discussed. In Subsection 4.4 the failure behavior of the glass-bead filled rubber vulcanizates is discussed briefly.

In Section 5 the summary and the conclusion are presented.

2. Theory

In this section the strain energy of a deformed composite system will be derived as a function of stretch ratio and amount of volume change. Except for the case specially mentioned the continuum phase is assumed to be incompressible and the filler particles are assumed to be rigid spheres.

2.1. Introduction

When an isotropic and homogeneous material is deformed, a certain amount of strain energy is stored in the system. While the stored energy is a function of the deformation tensor, the energy should be a function of the three invariants of the tensor. These invariants remain unchanged through the rotation of the coodinate system that causes the change of the directions of the three principal axes of the strain tensor. No matter what type of definitions one may choose for the strain tensor and the invariants, these relations will be true.

We will use the Cauchy-Green deformation tensor and the principal invariants in the development of the theory.

Provided that the strain tensor is known at every point in an elastic body, the total strain energy is written,

$$W = \int_V W'(I_1, I_2, I_3)dV \qquad (2 - 1)$$

where W is the total strain energy and W' is the strain energy per unit volume as a function of strain invariants, I_1, I_2, and I_3 in a small volume element dV.

In Section 2.2 we will introduce a model for a composite system of elastomer filled with solid particles. In Section 2.3 a deformation tensor and the strain invariants are introduced, and the strain energy is described as a Taylor expansion of the invariants. In Sections 2.4 and 2.5 the strain invariants are obtained, and consequently the strain energy is calculated. And finally, some applications of the theory will be discussed in Section 4.

2.2. A Model of Composite Systems

It is necessary to introduce a certain simplified model to describe strain, and consequently stress, distribution in a system of elastic material filled with solid particles. A model that is often used is a solid sphere surrounded by elastic material. In our case, however, we are more interested in the effects of interaction between two particles, and consequently the model was chosen to meet this demand. The model is shown schematically in Fig. 1a. As may be clear from the figure, the model is a cylindrical block of elastomer of length, 2b, and of diameter, 2c, with two solid half-spheres of radius, a, embedded on both ends. The relation among a, b, and c is left undetermined

at the moment. The centers of the spheres rest on the axis of the cylinder. This model may be considered as a representative unit cell of a composite system that enables us to obtain the total strain energy simply by multiplying the energy in the model by the number of the particles in the system. This may be the simplest model that can reasonably be treated mathematically but is yet not too different from the real system. As the model is stretched axially, the surface will take a profile that is concave in the middle section. That is, the material belonging to the middle section moves more inward than that near both ends. The question may arise whether or not it is possible for the material to move this way in a real system of the material where other particles may restrict the movement of the elastomer. In reality, however, the filler particles are randomly packed so that not all the particles, or rather, none of the particles are really on the same horizontal plane. Thus when the system is stretched vertically, the surface of the model will have the concave profile as described above, and the void that may be produced will be filled with another particle and the surrounding elastomer that move in. Although this is only a conceptional idea, it will serve to explain the adequacy of the choice of the model.

2.3. Deformation Tensor and the Invariants

When dr_o is a vector connecting two closely located points in an undeformed system and dr_i is the vector for the corresponding points after deformation, the two vectors may be related by a displacement tensor α_{ij} as follows[11, 12]:

$$dr_i = \alpha_{ij}\, dr_{oj} \tag{2.2}$$

where the repeated subscripts imply summation from 1 through 3. From Eq. 2-2 the distances between the two points before and after deformation are related by

$$\begin{aligned}(ds)^2 = dr_i\, dr_i &= \alpha_{\ell k}\, \alpha_{\ell i}\, dr_{ok}\, dr_{oi} \\ &= \gamma_{ki}\, dr_{ok}\, dr_{oi}\end{aligned} \tag{2.3}$$

where ds is the distance, and γ_{ij} is a symmetric deformation tensor. If the principal values of γ_{kl} are γ_1, γ_2, and γ_3, it is easily proved that there exists the following relation between them[13]:

$$\lambda_1^2 = \gamma_1 \qquad \lambda_2^2 = \gamma_2 \qquad \lambda_3^2 = \gamma_3 \tag{2.4}$$

Here stretch ratios are defined as the ratio of the deformed

and undeformed dimensions. Therefore, if we define the invariants, I_1, I_2, and I_3 as follows, they are identical to Rivlin's definitions.

$$I_1 = \gamma_1 + \gamma_2 + \gamma_3 = \gamma_{11} + \gamma_{22} + \gamma_{33}$$

$$I_2 = \gamma_1\gamma_2 + \gamma_2\gamma_3 + \gamma_3\gamma_1 \tag{2.5}$$

$$= \gamma_{11}\gamma_{22} + \gamma_{22}\gamma_{33} + \gamma_{33}\gamma_{11} - \gamma_{23}^2 - \gamma_{12}^2 - \gamma_{31}^2$$

$$I_3 = \gamma_1\gamma_2\gamma_3 = \gamma_{11}\gamma_{22}\gamma_{33} + 2\gamma_{12}\gamma_{23}\gamma_{31} - \gamma_{22}\gamma_{13}^2 - \gamma_{33}\gamma_{12}^2 - \gamma_{11}\gamma_{23}^2$$

A strain energy function of I_1, I_2, and I_3 may be expanded in a power series of the three variables, i.e.,

$$W(I_1, I_2, I_3) = \sum_{i,j,k=1}^{\infty} C_{ijk}(I_1-3)^i(I_2-3)^j(I_3-1)^k \tag{2.6}$$

where $W(I_1, I_2, I_3)$ is the stored energy per unit volume in the system and C_{ijk} are constants. In the case of an incompressible material

$$I_3 = 1$$

and Eq. 2-6 reduces to the following form using similar symbols because the terms containing I_3 vanish.

$$W(I_1,I_2) = \sum_{i,j=1}^{\infty} C_{ij}(I_1-3)^i(I_2-3)^j \qquad (2.7)$$

If an analytical form for the strain energy function is known, the stress in the system can be calculated. This will be shown later.

If u, v, and w are the elements of a displacement vector in the x, y, and z directions, respectively, in cartesian coordinates the displacement tensor, α_{ij} can be written

$$\alpha_{ij} = \begin{bmatrix} 1 + \frac{\partial u}{\partial x} & \frac{\partial u}{\partial y} & \frac{\partial u}{\partial z} \\ \frac{\partial v}{\partial x} & 1 + \frac{\partial v}{\partial y} & \frac{\partial v}{\partial z} \\ \frac{\partial w}{\partial x} & \frac{\partial w}{\partial y} & 1 + \frac{\partial w}{\partial z} \end{bmatrix} \qquad (2.8)$$

If the system is axially symmetric as in our case, the displacement tensor, α_{ij} is written in cylindrical coodinates (r, θ, ℓ') as,

$$\alpha_{ij} = \begin{bmatrix} 1 + \frac{\partial u}{\partial r} & 0 & \frac{\partial u}{\partial \ell'} \\ 0 & 1 + \frac{u}{r} & 0 \\ \frac{\partial w}{\partial r} & 0 & 1 + \frac{\partial w}{\partial \ell'} \end{bmatrix} \qquad (2.9)$$

In this case u and w are the radial and axial elements of the displacement vector, respectively. Details of the derivation of Eq. 2-9 are given in Appendix 1.

From Eq. 2-9 the Cauchy-Green tensor is obtained as,

$$\gamma_{ij} = \alpha_{ik}\alpha_{jk} = \begin{bmatrix} (1+\frac{\partial u}{\partial r})^2 + (\frac{\partial u}{\partial \ell})^2 & 0 & \frac{\partial u}{\partial \ell}(1+\frac{\partial w}{\partial \ell}) + \frac{\partial w}{\partial r}(1+\frac{\partial u}{\partial r}) \\ \cdot & (1+\frac{u}{r})^2 & 0 \\ \cdot & \cdot & (\frac{\partial w}{\partial r})^2 + (1+\frac{\partial w}{\partial \ell})^2 \end{bmatrix} \tag{2-10}$$

The principal invariants are obtained from Eqs. 2-5 and 2-10.

$$I_1 = \left(1+\frac{\partial u}{\partial r}\right)^2 + \left(\frac{\partial u}{\partial \ell}\right)^2 + \left(1+\frac{u}{r}\right)^2 + \left(\frac{\partial w}{\partial r}\right)^2 + \left(1+\frac{\partial w}{\partial \ell}\right)^2$$

$$I_2 = \left[(1+\frac{\partial u}{\partial r})^2 + (\frac{\partial u}{\partial \ell})^2\right]\left(1+\frac{\partial u}{\partial r}\right)^2 + \left(1+\frac{u}{r}\right)^2\left[(\frac{\partial w}{\partial \ell})^2 + (1+\frac{\partial w}{\partial \ell})^2\right]$$

$$+ \left|(1+\frac{\partial u}{\partial r})^2 + (\frac{\partial u}{\partial \ell})^2\right|\left|(\frac{\partial w}{\partial r})^2 + (1+\frac{\partial w}{\partial \ell})^2\right|$$

$$- \left|\frac{\partial u}{\partial \ell}(1+\frac{\partial w}{\partial \ell}) + \frac{\partial w}{\partial r}(1+\frac{\partial u}{\partial r})\right|^2$$

$$= \left|(1+\frac{\partial u}{\partial r})^2 + (\frac{\partial u}{\partial r})^2\right|\left(1+\frac{\partial u}{\partial r}\right)^2 + \left(1+\frac{u}{r}\right)^2\left|(\frac{\partial w}{\partial r})^2 + (1+\frac{\partial w}{\partial \ell})^2\right|$$

$$+ \left|(1+\frac{\partial u}{\partial r})(1+\frac{\partial w}{\partial \ell}) - (\frac{\partial u}{\partial \ell})(\frac{\partial w}{\partial r})\right|^2$$

$$I_3 = \left[\overline{(1 + \frac{\partial u}{\partial r})^2 + (\frac{\partial u}{\partial \ell'})^2}\right]\left(1 + \frac{u}{r}\right)^2 \left[\overline{(\frac{\partial w}{\partial r})^2 + (1 + \frac{\partial w}{\partial \ell'})^2}\right]$$

$$- \left(1 + \frac{u}{r}\right)^2 \left[\overline{\frac{\partial u}{\partial \ell'}(1 + \frac{\partial w}{\partial \ell'}) + \frac{\partial w}{\partial r}(1 + \frac{\partial u}{\partial r})}\right]^2 \quad . \qquad (2 - 11)$$

From Eqs. 2-1, 2-7, and 2-11 we may write for the total stored energy

$$W = \int_0^{2\pi} \int_0^c \int_{-\ell_o}^{\ell_o} \sum_{i,j=1}^{\infty} C_{ij}(I_1 - 3)^i (I_2 - 3)^j \, d\ell' dr(rd\theta) \qquad (2 - 12)$$

provided that the material is incompressible. The displacements u and w must be found. This will be done in the following section.

2.4. Deformation of a Thin Shelled Cylinder

When the model(cf. Fig. 3) is stretched along the axis by the amount $2\Delta b$, the macroscopic stretch ratio, λ is given by

$$\lambda = 1 + \Delta b/b \qquad (2 - 13)$$

We assume that the displacements u, v, and w are given by

$$u = u(r, \ell')$$
$$v = 0 \qquad (2 - 14)$$
$$w = w(r, \ell') = (\lambda' - 1)\ell'$$

where λ' is the internal stretch ratio at radius, r, and thus a function of r, and ℓ' is the distance from the plane of symmetry normal to the axial direction. Physically, this assumption

means that the displacement in the axial direction is proportional to the distance from the middle plane. Direct calculation of the strain invariants leads to difficult nonlinear differential equations. Instead of the deformation of a cylindrical rod we therefore consider the axial stretching of a thin-shelled cylinder (or tube) of radius R, wall thickness dR and length $2\ell_o$ as shown in Fig. 2. Over the thickness, dR, λ' may be assumed to be constant. Here λ' is the overall stretch ratio of a tube which is defined as the ratio of the length of the deformed tube to the original length. The tube is deformed under the condition that the displacements of every point in the material belonging to the tube are described by Eq. 2-14. If the tube was independent of the rest of the material in the system it would take the shape for which the total strain energy stored in it has a minimum. As a matter of fact, the volume enclosed by the tube will be subject to the condition of the material inside. We will discuss this problem later. Now we obtain the strain invariants for the deformed tube by substituting Eq. 2-14 into Eq. 2-11 under the condition that λ' is a constant as follows,

$$I_1 = (1 + \frac{\partial u}{\partial r})^2 + (\frac{\partial u}{\partial \ell})^2 + (1 + \frac{u}{r})^2 + \lambda'^{-2}$$

$$I_2 = \left[(1 + \frac{\partial u}{\partial r})^2 + (\frac{\partial u}{\partial \ell'})^2\right](1 + \frac{u}{r})^2 + \lambda'^{-2}\,(1 + \frac{u}{r})^2$$

$$+ \lambda'^{-2}(1 + \frac{\partial u}{\partial r})^2$$

$$I_3 = (1 + \frac{\partial u}{\partial r})^2\,(1 + \frac{u}{r})^2\,\lambda'^2 \qquad (2 - 15)$$

If the material is incompressible, I_3 must have a value of 1, and we obtain a differential equation in u

$$I_3 \equiv (1 + \frac{\partial u}{\partial r})^2\,(1 + \frac{u}{r})^2\,\lambda'^2 \equiv 1 \qquad (2 - 16)$$

or

$$(1 + \frac{\partial u}{\partial r})(1 + \frac{u}{r}) = \frac{1}{\lambda'} \qquad (2 - 17)$$

Eq. 2-17 can be written

$$\frac{\partial}{\partial r}(r + u)^2 = \frac{2r}{\lambda'} \qquad (2 - 18)$$

Integration gives

$$(r + u)^2 = \frac{r^2}{\lambda'} + f(\ell') \qquad (2 - 19)$$

or

$$r + u = \sqrt{\frac{r^2}{\lambda'} + f(\ell')} \qquad (2 - 20)$$

We have thus made use of the incompressibility condition to derive an expression for u.

Substituting Eq. 2-20 in the first two of Eq. 2-15 the invariants are obtained as an expression containing an unknown function $f(\ell')$ and its derivative $f'(\ell')$. We have

$$I_1 = \frac{r^2}{\lambda'^2\left[\frac{r^2}{\lambda} + f(\ell')\right]} + \frac{\left[f'(\ell')\right]^2}{4\left[\frac{r^2}{\lambda'} + f(\ell')\right]} + \frac{\frac{r^2}{\lambda'} + f(\ell')}{r^2} + \lambda'^2$$

$$I_2 = \frac{1}{\lambda'^2} + \frac{\left[f'(\ell')\right]^2}{4\,r^2} + \lambda^2\,\frac{\frac{r^2}{\lambda'} + f(\ell')}{r^2} + \frac{r^2}{\frac{r^2}{\lambda'} + f(\ell')} \qquad (2-21)$$

The function, $f(\ell')$, may be determined, at least in principle, by substituting Eq. 2-21 into the Taylor expansion of the strain energy, integrating it, and taking the variation to decide the condition at which the total strain energy reaches a mimimum. This procedure, however, yields a highly non-linear differential equation in $f(\ell')$. and it is not likely to be solved precisely. We will assume a certain profile for the tube in the stretched state. The shape of a stretched tube must be a surface of revolution because the system is axially symmetric. Also, it must have mirror symmetry with respect to the plane that is perpendicular to the axis and passes the middle point of the axis. We approximate the function that defines the profile of the surface of revolution at r = R by

$$R + u = r_o + A\ell'^{\nu} \qquad (2 - 22)$$

where r_o, A, and ν are constants. If both ends of the tube are attached to solid surfaces so that the diameter on both ends can not change, $R + u = R$ at $\ell' = \ell_o$. On the other hand, the diameters on the ends change in some cases. This will be discussed later. If this is the case, $R + u = \beta R$ at $\ell' = \ell_o$, where β is a parameter. Using $A=(\beta R - r_o)/\ell_o^{\nu}$, Eq. 2-22 can be rewritten

$$R + u = r_o + (\beta R - r_o)\left(\frac{\ell'}{\ell_o}\right)^{\nu} \qquad (2 - 23)$$

First we consider the case of no change in the volume enclosed by the tube. Geometrically r_o is the minimum radius of the deformed tube and is attained at $\ell' = 0$. This value must be a function of the stretch ratio λ' and the ratio R/ℓ_o. If either R/ℓ_o is very small or λ' is very large, r_o will be $R(1/\lambda')^{\frac{1}{2}}$, provided that the enclosed volume remains constant. This is because both cases correspond to simple tension with negligible end effects. In other words these cases are equivalent to simple extension of a very thin cylindrical block. On the other hand, if R/ℓ_o is very large, i.e. if the radius of the tube is much larger than its length, the fact that the material in the vicinity of both ends restricted in its radial movement gains particular prominence. As a consequence the material near $\ell'=0$ must move further than would beindicated by $R(1/\lambda')^{\frac{1}{2}}$ to satisfy the condition of constant volume of the tube. We shall assume that the value of r_o in this extreme case is given by $R(1/\lambda')$. Then r_o is

$$r_o = R\left(\frac{1}{\lambda'}\right)^{\frac{\lambda'-1 + R/\ell_o}{2(\lambda'-1)+R/\ell_o}} \qquad (2 - 24)$$

This is a rather complicated formula, but the simplest one that satisfies all the conditions mentioned above. While Eq.2-24 is an expression for the case inwhich the volume enclosed by the tube remains constant, the volume must change in the case of vacuole formation as we will discuss later. The original enclosed volume, V_o, is written by

$$V_o = 2\,\pi R^2 \ell_o \qquad (2 - 25)$$

After deformation the volume becomes V and it is calculated from Eq. 2-23

$$\begin{aligned} V &= 2\,\pi \int_o^{\ell_o \lambda'} (R + u)^2\, d\ell \\ &= 2\,\pi \int_o^{\ell_o \lambda'} \left[r_o + (R - r_o)\left(\frac{\ell}{\ell_o \lambda'}\right)^{\nu}\right]^2 d\ell' \\ &= 2\,\pi R^2 \ell_o \lambda' \left[\left(\frac{r_o}{R}\right)^2 + 2\left[\beta - \left(\frac{r_o}{R}\right)\right]\frac{r_o}{R}/(\nu + 1)\right. \\ &\qquad \left. + \left(\beta - \frac{r_o}{R}\right)^2/(2\nu + 1)\right] \end{aligned} \qquad (2 - 26)$$

We term the ratio, V/V_o as the ratio of enclosed volume and

denote it by μ. Then we can write,

$$\frac{\mu}{\lambda} = \left[\left(\frac{r_o}{\beta R}\right)^2 + 2\left(1 - \frac{r_o}{\beta R}\right)\left(\frac{r_o}{\beta R}\right)/(\nu + 1) + \left(1 - \frac{r_o}{\beta R}\right)^2/(2\nu + 1)\right] \quad (2 - 27)$$

Considering the case of volume change suggests that it is more reasonable if we replace $1/\lambda'$ in Eq. 2-24 by $\mu/\beta^2\lambda'$. The result is

$$r_o = R\left(\frac{\mu}{\beta^2\lambda'}\right) \frac{\left(\frac{\beta^2\lambda'}{\mu} - 1\right) + R/\ell_o}{2\left(\frac{\beta^2\lambda'}{\mu} - 1\right) + R/\ell_o} = \beta R\alpha \quad (2 - 28)$$

Substituting Eq. 2-28 in Eq. 2-27 and solving for ν, we obtain

$$\nu = \frac{-(3\alpha_o - 2\alpha - 1) + \sqrt{(3\alpha_o - 2\alpha - 1)^2 - 8(\alpha_o - \alpha^2)(\alpha_o - 1)}}{4(\alpha_o - \alpha^2)} \quad (2 - 29)$$

where $\alpha_o = \mu/\beta^2\lambda'$. The exponent, ν is always larger than 1 and converges to 1 as $\mu/\beta^2\lambda'$ approaches 1. This is desirable geometrically. because, if $\nu \leqq 1$, the profile of the deformed tube would have a cusp at $\ell' = 0$ which is physically unreasonable. Having Eq. 2-23 as the initial condition we can obtain the function, $f(\ell')$ in Eq. 2-20 as

$$f(\ell') = R^2\left[\alpha + (1-\alpha)\left(\frac{\ell'}{\ell_o}\right)^\nu\right]^2 - \frac{R^2}{\lambda'} \quad (2 - 30)$$

In the process of deriving Eq. 2-30, $r_o/\beta R$ was replaced by

α. Substituting Eq. 2-30 in Eqs. 2-21 we obtain the strain invariants in the deformed tube at r = R, as

$$I_1 = \frac{1}{\lambda'^2\left[\alpha + (1-\alpha)\left(\frac{\ell'}{\ell_o}\right)^{\nu}\right]^2} + \frac{\nu^2(1-\alpha)^2\, R^2\left(\frac{\ell'}{\ell_o}\right)^{2(\nu-1)}}{\ell_o^2} + \left[\alpha + (1-\alpha)\left(\frac{\ell'}{\ell_o}\right)^{\nu}\right]^2 + \lambda'^2$$

$$I_2 = \frac{1}{\lambda'^2} + \frac{\nu^2(1-\alpha)^2\, R^2\left(\frac{\ell'}{\ell_o}\right)^{2(\nu-1)}}{\ell_o^2}\left[\alpha + (1-\alpha)\left(\frac{\ell'}{\ell_o}\right)^{\nu}\right]^2 + \lambda'^2\left[\alpha + (1-\alpha)\left(\frac{\ell'}{\ell_o}\right)^{\nu}\right]^2 + \frac{1}{\left[\alpha + (1-\alpha)\left(\frac{\ell'}{\ell_o}\right)^{\nu}\right]^2} \qquad (2-31)$$

We will take Eq. 2-31 as the approximation for the strain invariants at r = R for the model in Fig. 1.

2.5. Strain Energy in the Model of Filled Elastomers

2.5.1. No Vacuole Formation

Since we now have the expression for the strain invariants of the deformation tensor of a deformed composite system as a function of the coordinates (r, θ, ℓ') we can calculate the strain energy in the model by substituting Eqs. 2-31

into Eq. 2-12. Eq. 2-12 can be rewritten as

$$W = 2\pi \int_0^c R\ell_o W_\ell dR \qquad (2 - 32)$$

where r was replaced by the radii of the tubes, R and W_ℓ is given by

$$W_\ell = \frac{2}{\ell_o}\int_0^{\ell_o} \sum_{i,j=0}^{\infty} C_{ij}(I_1 - 3)^i(I_2 - 3)^j d\ell'$$

$$= \frac{2}{\ell_o} \sum_{i,j=0}^{\infty} C_{ij}\int_0^{\ell_o}(I_1 - 3)^i(I_2 - 3)^j d\ell' \qquad (2 - 33)$$

or

$$W_\ell = \frac{2}{\ell_0}\Big[C_{10} \int_0^{\ell_o}(I_1 - 3)d\ell' + C_{01}\int_0^{\ell_o}(I_2 - 3)d\ell'$$

$$+ \sum_{i,j=1}^{\infty} C_{ij} \int_0^{\ell_o}(I_1 - 3)^i(I_2 - 3)^j d\ell'\Big] \qquad (2 - 34)$$

Numerical calculations show that I_1-3 and I_2-3, as given by Eqs. 2-31 vary about 20 % around the average values as ℓ'/ℓ_o changes from 0 to 1 when $\lambda' = 3$ and $R/\ell_o = 1$. The variations decrease as λ' increases. This variation is less when $R/\ell_o < 1$ and increases by 10 -- 15 % as $R/\ell_o \to 3$, which is estimated to be its highest value, attained at the maximum random packing of spheres, 0.63. In ordinary elastomers, the contribution of high terms in the expansion of the strain energy function, C_{ij} $(i+j>1)$, becomes significant only at quite large values of the stretch ratio. For convenience of calculations we may therefore approximate the third term in Eq. 2-34 as follows.

$$\frac{1}{\ell_o}\int_0^{\ell_o}(I_1 - 3)^i(I_2 - 3)^j d\ell' \simeq \left[\frac{1}{\ell_o}\int_0^{\ell_o}(I_1 - 3)d\ell'\right]^i$$

$$x\left[\frac{1}{\ell_o}\int_0^{\ell_o}(I_2 - 3)d\ell'\right]^j \qquad (2 - 35)$$

In fact if i=2, and the variations in I_1-3 or I_2-3 are as large as 50 % the error introduced by this approximation is less than 5 %. If we define W_1 and W_2 as

$$W_1 = \frac{1}{\ell_o}\int_0^{\ell_o}(I_1 - 3)d\ell'$$

$$W_2 = \frac{1}{\ell_o}\int_0^{\ell_o}(I_2 - 3)d\ell' \qquad (2 - 36)$$

Eq. 2-33 gives

$$W_\ell = 2\sum_{i,j=0}^{\infty} C_{ij} W_1^{\,i} W_2^{\,j} \qquad (2 - 37)$$

Values of W_1 and W_2 are obtained by carrying out the integration with the substitution of Eq. 2-31 into Eq. 2-36 to give

$$W_1 = \frac{1}{\beta^2\lambda'^2}\,\Phi + \frac{\nu^2\beta^2R^2(1 - \alpha)^2}{\ell_o^{\,2}}\frac{1}{(2\nu - 1)}$$

$$+ \beta^2\left[\alpha^2 + 2\alpha(1 - \alpha)\frac{1}{\nu + 1} + (1 - \alpha)^2\frac{1}{(2\nu + 1)}\right] + \lambda'^2 - 3$$

$$W_2 = \frac{1}{\lambda'^2} + \frac{\nu^2\beta^2R^2(1 - \alpha)^2}{\ell_o^{\,2}}\left[\frac{\alpha^2}{(2\nu - 1)} + \frac{2\alpha(1 - \alpha)}{(3\nu - 1)} + \frac{(1 - \alpha)^2}{(4\nu - 1)}\right]$$

$$+ \beta^2\lambda'^2\left[\alpha^2 + \frac{2\alpha(1 - \alpha)}{(\nu + 1)} + \frac{(1 - \alpha)^2}{(2\nu + 1)}\right] + \frac{1}{\beta^2}\,\Phi \qquad (2 - 38)$$

where Φ is defined in terms of Gauss' hypergeometric function $F(a, b, c, d)$ by[14]

$$\Phi = \frac{1}{\ell_o}\int_0^{\ell_o} \frac{d\ell'}{[\alpha + (1 - \alpha)(\frac{\ell'}{\ell_o})^{\nu}]^2}$$

$$= \frac{1}{\alpha^2 \nu} \frac{(\nu - 1)}{(2\nu - 1)} F\left(2, \frac{(2\nu - 1)}{(\nu - 1)}, \frac{(3\nu - 2)}{(\nu - 1)}, \frac{(\alpha - 1)}{\alpha}\right) \quad (2 - 39)$$

Substituting Eq. 2-37 into Eq. 2-32 we obtain

$$W = 4\pi \sum_{i,j=0}^{\infty} C_{ij} \int_0^c R\ell_o W_1^{\,i} W_2^{\,j} dR \quad (2 - 32)'$$

In integrating Eq. 2-32 we have to divide the interval into two regions, $0 \leqq R \leqq a$ and $a \leqq R \leqq c$, because both ℓ_0 and λ' are different functions of R in those regions. In the region $0 \leqq R \leqq a$ these quantities are obtained from the following geometrical relations:

$$\ell_o = b - a\cos\theta = b(1 - \psi\cos\theta) \quad (2 - 40)$$

$$R = a\sin\theta = b\psi\sin\theta \quad (2 - 41)$$

and

$$\lambda' = \frac{(\lambda b - a\cos\theta)}{(b - a\cos\theta)} = \frac{\lambda - \psi\cos\theta}{1 - \psi\cos\theta} \quad (2 - 42)$$

Here $\psi = a/b$, and θ is the angle between the axis and a radius that intersects the surface of the sphere to give the radius, R of a tube. Also in this region the material is in contact with the filler surfaces so that the displacements on the boundary

are zero. Consequently, the constant, β in Eqs. 2-35 has a value of 1. The ratio of enclosed volume, μ, is also equal to 1 because we are considering the case of no vacuole formation and the material is assumed to be incompressible. Thus there would be no volume change. Considering these conditions, the values of W_1 and W_2 in the region, $0 \leqq R \leqq a$, $W_{1,IN}$ and $W_{2,IN}$ are written

$$W_{1,IN} = \frac{1}{\lambda'^2}\,\Phi + \frac{\nu^2 R^2 (1-\alpha)^2}{\ell_o^2}\,\frac{1}{(2\nu-1)}$$

$$+ \alpha^2 + 2\alpha(1-\alpha)\frac{1}{(\nu+1)} + (1-\alpha)^2\frac{1}{(2\nu+1)} + \lambda' - 3$$

$$W_{2,IN} = \frac{1}{\lambda'^2} + \frac{\nu^2 R^2 (1-\alpha)^2}{\ell_o^2}\left[\frac{\alpha^2}{(2\nu-1)} + \frac{2\alpha(1-\alpha)}{(3\nu-1)} + \frac{(1-\alpha)^2}{(4\nu-1)}\right]$$

$$+ \lambda'\left[\alpha^2 + \frac{2\alpha(1-\alpha)}{(\nu+1)} + \frac{(1-\alpha)^2}{(2\nu+1)}\right] + \Phi - 3 \qquad (2-43)$$

Here the subscript implies that these values are for the inside region. The value of α is given by

$$\alpha = \left(\frac{1}{\lambda'}\right)^{\frac{(\lambda'-1) + R/\ell_o}{2(\lambda'-1) + R/\ell_o}} \qquad (2-44)$$

and ν is given by Eq. 2-31.

In the region, $a < R \leqq c$, ℓ_o and λ' are given by

$$\ell_o = b \qquad (2 - 45)$$

$$\lambda' = \lambda \qquad (2 - 46)$$

In this case, however, we must obtain the value of β because the ends of the tube are no longer attached to the surfaces of the filler particles. If we assume that the stretch ratio in the axial direction is equal to the overall stretch ratio, λ, at $\ell' = \ell_o$, the radial stretch ratio and tangential stretch ratio may by written in terms of the radial displacement, u, as

$$\begin{aligned} \lambda_1 &= \lambda \\ \lambda_2 &= 1 + \frac{\partial u}{\partial R} \\ \lambda_2 &= 1 + \frac{u}{R} \end{aligned} \qquad (2 - 47)$$

Because the material is incompressible the product $\lambda_1\lambda_2\lambda_3$ must equal 1, i. e.

$$\lambda_1\lambda_2\lambda_3 = (1 + \frac{\partial u}{\partial R})(1 + \frac{u}{R})\lambda = 1 \qquad (2 - 48)$$

Eq. 2-48 is mathematically identical to Eq. 2-17 which gives the following solution

$$R + u = \sqrt{\frac{R^2}{\lambda} + C} \qquad (2 - 49)$$

where C is the constant of integration. Since u must be zero at R = a, we can obtain the constant C as

$$C = (1 - \frac{1}{\lambda})a^2 \qquad (2 - 50)$$

We can also write

$$R + u = R\sqrt{\frac{1}{\lambda} + (1 - \frac{1}{\lambda})\frac{a^2}{R^2}} \qquad (2 - 51)$$

As defined in Eq. 2-23 and its preceding paragraph, β is obtained from Eq. 2-51.

$$\beta = \sqrt{\frac{1}{\lambda} + (1 - \frac{1}{\lambda}) \frac{a^2}{R^2}} \qquad (2-52)$$

Now we can obtain the strain energy stored in the tubes in the region, $a<R<c$. Eq. 2-52 gives β and $\mu = 1$ in this region. W_1 and W_2 can thus be obtained from Eqs. 2-38, denoting them by $W_{1,OUT}$ and $W_{2,OUT}$, respectively, in analogous to $W_{1,IN}$ and $W_{2,IN}$(cf. Eqs. 2-43). $W_{1,OUT}$ and $W_{2,OUT}$ differfrom $W_{1,IN}$ and $W_{2,IN}$ only in α and ν because of the difference in the values assigned to β. Finally the total strain energy in the system is given by the following equation, at stretch ratio, λ

$$W = 2\pi\int_0^a W_{IN} R\ell_o dR + 2\pi\int_a^c W_{OUT} bRdR \qquad (2-53)$$

Thus W_{IN} and W_{OUT} are the values of W_ℓ in Eq. 2-32 in the regions, $0 \leqq R \leqq a$ and $a \leqq R \leqq c$, respectively. Eq. 2-53 can be written, corresponding to Eq 2-32′, as

$$W = 4\pi \sum_{i,j=0}^{\infty} C_{ij} \left[\int_0^a R\ell_o W_{1,IN}{}^i W_{2,IN}{}^j dR + \int_a^c R\ell_o W_{1,OUT}{}^i W_{2,OUT}{}^j dR\right] \qquad (2-53)'$$

The integration can be carried out numerically with the help of Eqs. 2-40, 2-41, 2-42, 2-45 and 2-46. This theory will be extended to the case of vacuole formation in the next subsection. The theory will be compared with experimental results later on.

2.5.2. Vacuole Formation

When an elastic substance separates from the surfaces of filler particles as a composite system is deformed, vacuoles are formed around the particles causing a volume change in the system. This phenomenon is termed 'dewetting' in subsequent discussions. If dewetting occurs under a certain deformation, Eq. 2-53 derived in the previous section is no longer valid and the effect of vacuoles on the total strain energy must be taken into consideration.

Sampson[22], using a system of transparent rubbery material filled with spherical inclusions, photographed the vacuoles formed around the spheres as the system was stretched. Those photographs show that, in most cases, a vacuole originates at the closest point to the neighboring sphere on the surface of the sphere, and that it spreads outward along the surface as the amount of deformation increases. In other words, a vacuole of a finite volume does not come into existence spontaneously, but it increases in size continuously. The shape of the vacuoles resembles an ellipsoid or paraboloid with the major axis coinciding with the direction of stretching, and they are tangentially in contact with the surfaces of spheres. Apparently dewetting is never completed no matter how large the stretch ratio may become, or no matter how large the size of a vacuole may become.

Here, complete dewetting means the state in which a vacuole contacts the filler particle only around its equater. In other words, a finite amount of the surface area of the sphere is always in contact with the continuous phase.

An attempt was made to calculate the strain energy of a dewetting composite system as a function of the overall stretch ratio, λ, and the volume change in the model. This approach required further assumptions and produced unsatisfactory agreement with the data. As this procedure was already rather complicated, its refinement appeared unwarranted. The calculations did show, however, that, at a given stretch ratio, the strain energy of a composite system first decreases sharply as the volume increases, then slows down and reaches a minimum before it increases again. This is easily understood if we consider the internal stretch ratio, λ'. As the volume increases, the stretch ratio decreases because the vacuole formation releases the strain. The strain energy reaches its lowest value when $\lambda'=1$. As the volume increases further, the stretch ratio becomes less than unity and the strain energy increases again. This behavior can be expressed mathematically and can be used to develop simpler approach for calculating the strain energy stored in a de wetting system.

Let $W_o(\lambda)$ be the strain energy before dewetting as obtained in the previous section, and let $W_{min}(\lambda)$ be the minimum strain energy at the same stretch ratio. Then, we can write the strain energy function of the dewetting system, $W(\lambda, v)$ as a function of stretch ratio and volumeratio (which is defined as the ratio of the volume of the

deformed system to that of the original system) as shown below:

$$W(\lambda, v) = W_{min}(\lambda) + [W_o(\lambda) - W_{min}(\lambda)]f(\lambda, v) \qquad (2 - 54)$$

Let $v_o(\lambda)$ be the volume ratio corresponding to the minimum strain energy $W_{min}(\lambda)$. From the definition of $W_o(\lambda)$, $f(\lambda, v)$ must equal unity when $v=1$ and decrease to 0 as v reaches $v_o(\lambda)$. We now assume that the function, $f(\lambda, v)$ has the form

$$f(\lambda, v) = f(\lambda, v/v_o(\lambda)) \qquad (2 - 55)$$

This assumption implies that the pattern of strain energy decrease by dewetting is decided by the ratio of a changed volume to its maximum possible value. For the moment, we leave $v_o(\lambda)$ and $f(\lambda, v/v_o(\lambda))$ undetermined.

$W_o(\lambda)$ was already obtained in the previous subsection. $W_{min}(\lambda)$ is calculated as follows. We consider that, when the volume ratio is $v_o(\lambda)$, the vacuoles are ellipsoids of revolution with the axis of revolution coinciding with the axis of stretching and the two minor radii coinciding with the spherical filler particles. We assume that no radial displacement takes place during the process in which a point of the elastic substance which was in contact with the surface of a particle moves to the new point on the surface of a vacuole. Then the strain energy can be calculated by a method similar to that used in the previous section with slight modifications. That is, the final result is given by Eq. 2-53 as in the case of no vacuole formation.

However, changes must be made in Eq. 2-42 which gives the internal stretch ratios and the ratio of the enclosed volumes, μ, which is contained in the definition of α in Eq. 2-28. The original length of a thin-shelled tube of radius R in the model is given by Eq. 2-40. The length becomes $(\lambda b - a\eta\cos\theta)$ after stretching to a total stretch ratio, λ, for the case of an ellipsoidal vacuole around a sphere instead of $(\lambda b - a\cos\theta)$ given for the case of no vacuole formation. This is because the distance of a point on the vacuole from the bottom of the model is given by $a\eta\cos\theta$ instead of $a\cos\theta$ for the case of a sphere, where η is a constant that changes the radius, a, into the major axis of the ellipsoid, $a\eta$. Consequently, the internal stretch ratio, λ', is given by

$$\lambda' = \frac{\lambda b - a\eta\cos\theta}{b - a\cos\theta} = \frac{\lambda - \eta\psi\cos\theta}{1 - \psi\cos\theta} \qquad (2 - 56)$$

The ratio of the enclosed volumes, μ, is no longer 1 in this case because the volume enclosed by a cylinder does not remain constant after vacuole formation. Fig. 3 shows a schematic of vacuole formation. Although it is a more general case than the one considered here, the change in the enclosed volume is given by the same principle. If the radius of the original cylinder is R, the change in the enclosed volume after deformation is given as the difference between the volume of the shaded portion of the vacuole and the corresponding volume of the sphere.

The volume of the shaded portion of the ellipsoid, V_a, is calculated by

$$V_a = 2\int_{a\eta\cos\theta}^{a\eta} \pi(a\sin\theta)^2 d(a\eta\cos\theta) = \frac{2\pi}{3}a^3\eta(2 + \cos\theta)(1 - \cos\theta)^2 \qquad (2 - 57)$$

The corresponding volume of the sphere, V_{ao}, is

$$V_{ao} = 2\int_{a\cos\theta}^{a} \pi(a\sin\theta)^2 d(a\cos\theta) = \frac{2\pi}{3}a^3(2 + \cos\theta)(1 - \cos\theta)^2 \qquad (2 - 57)'$$

The original volume of the tube, V_o, is

$$V_o = 2\pi\ell_o R^2 = 2\pi b^3(1 - \psi\cos\theta)\sin^2\theta \qquad (2 - 58)$$

The ratio of enclosed volume, therefore, is obtained as

$$\mu = 1 + \frac{V_a - V_{ao}}{V_o} = 1 + \frac{(\eta-1)}{3}\psi^3\frac{(2 + \cos\theta)(1 - \cos\theta)}{(1 - \psi\cos\theta)(1 + \cos\theta)} \qquad (2 - 59)$$

In the calculation of $W_{min}(\lambda)$ by Eq. 2-53, Eq. 2-57 instead of Eq. 2.42 and Eq. 2-59 instead of $\mu = 1$ are used. Integration is carried out numerically as before.

If the form of $f(\lambda, v/v_o(\lambda))$ is known, the total strain energy is given by Eq. 2-54 as a function of stretch ratio and volume ratio. The determination of $f(\lambda, v/v_o(\lambda))$ will be discussed in Section 4.

The method employed to obtain $W_{min}(\lambda)$ can be generalized to obtain the strain energy at any stage of dewetting under

the assumption that shape of the vacuoles is known. Details are given in Appendix 2 for reference.

The relation expressed by Eq. 2-54 will be used to calculate stress-strain and volume change-strain curves of glass bead-filled elastomers under hydrostatic pressure.

3. Experiments and Data Analysis

The purpose of the experiments is to obtain the stress-strain and volume change-strain behavior of an elastic material filled with glass beads which characterize non-reinforcing filler particles as functions of both volumetric loading ratio of filler and superposed hydrostatic pressure.

In this section the experimental equipment and procedures, samples and methods of data analysis will be described.

3.1. Equipment

Two special pieces of equipment were used in the experiments. These are the Pressurized Tensile Tester for measuring the stress-strain curves under superposed hydrostatic pressure and the Hall Effect Thickness Sensor for measuring the volume change accompanying the deformation of a system.

3.1.1. Pressurized Tensile Tester

Details of the pressurized tensile tester were given

in the report by Lim and Tschoegl[15, 16]. Only a brief description will be given in this section.

A detailed diagram of the equipment is shown in Fig. 4. The equipment was designed in the Central Engineering shop of the California Institute of Technology. The equipment is basically a tensile tester designed for simple tension experiments of ring shaped specimens. A hook is attached to the lower crosshead which travels vertically with constant speeds driven by a driving unit. The other hook is connected to a load cell of 5lb. maximum capacity, which is in turn connected to the upper crosshead which is fixed to the frame of the apparatus. The crosshead can travel 18 inches. The whole equipment is built on a base plate with a threaded socket in which a bell shaped steel cover is screwed, when in use. When a measurement is performed the whole system is tightly sealed by means of the cover, the inside is filled with silicone oil and it is pressurized. Two heating units of 1, 000 and 2, 000 watts are installed near the bottom and cooling coils made of copper tubings are located near the top. The cooling coils can be operated by either water or liquid nitrogen. A mixing blade is located at the center of the heating units. The crosshead travel helipot converts crosshead displacements into electric signals to be recorded. Thermocouples are located near the bottom and the upper hook for measuring experimental temperatures and

controlling them. The equipment is connected to the accessories as shown in Fig. 5 and Fig. 6.

Fig. 5 shows the piping schematic diagram. The hydraulic system consists of the pressurized tensile tester, a liquid reservoir, transfer pumps, a control panel, and a nitrogen pressure back-up system. The reservoir can store 40 gallons of silicone oil. The liquid is pumped into the pressurized tensile tester by the transfer pumps. Then, the whole system is pressurized by the pressurizing system. The maximum pressure used is 2,000 psi. (138 bars)

Fig. 6 shows electric connections. The load cell turns a stress into an electric signal, the crosshead travel helipot gives a crosshead displacement as a voltage and these are recorded on the X and Y_1 axes of an X-Y_1-Y_2 recorder.

3.1.2. Hall Effect Thickness Sensor

A number of measurements were carried out to obtain the pressure dependence of stress-strain behavior of glass-bead filled elastomers since the pressurized tensile tester had been built by Lim and Tschoegl[16]. It became clear, however, that not only the stress-strain relation but also the volume change due to stretching of a specimen must be measured in order to interpret the whole nature of the mechanical behavior of a filled material. The Hall-effect thickness sensor was designed to measure the thickness change of a specimen as it is stretched in the pressurized tensile tester.

A charged particle moving in a magnetic field experiences a deflective force termed the Lorentz force. When a solid material carrying a current is placed in a magnetic field, the electrons moving in the material are deflected by the Lorentz force and produce an electromotive force in the direction in which they are deflected. This phenomenon is called the Hall effect[17, 18, 19] after E. H. Hall who discovered it in 1879.

The Hall output voltage is proportional to the vector product of the current vector and the magnetic field intensity, and is given by

$$V_H = wR_H(\overline{J}x\overline{B}) \qquad (3 - 1)$$

where V_H is the Hall output voltage, w is the width of the material, R_H is the Hall coefficient, $\overline{J}$ is the current density and $\overline{B}$ is the magnetic field intensity as shown in Fig. 7 where T is the thickness of the material. The Hall coefficient is a material constant.

Thus, if the current is constant, the Hall output voltage depends only on the magnetic field whose intensity is a single valued function of the position in the space surrounding the magnet. If a Hall material carrying a constant current is placed in the field of a magnet, the Hall output voltage will be a function of position. Moving the Hall material along a straight line passing through the field, the output voltage will be a unique function of the distance from the magnet. If the magnet and the Hall material are placed on each one of the two parallel surfaces of a non-magnetic specimen, the output will be a function of the thickness. The Hall effect can thus be utilized to determine the thickness of non-magnetic specimens provided that the Hall coefficient is sufficiently large to yield an output which can be measured conveniently. For ordinary electrically conductive substances the Hall coefficient is negligibly small. Recently, however, semiconductors with much larger Hall coefficients have been developed and several are now commercially available.

To construct our thickness sensor, we used a Model BH-700 Hall effect device manufactured by F. W. Bell Inc. The arrangement is shown diagrammatically in Fig. 8. Here M is a small magnet, S is the specimen, H is the Hall device, S_p is a spring made from a non-magnetic metal, and C is a clamp which may be opened to install the device on one side of a stretched ring. Since the device is very light, the pressure required to keep it in contact with the specimen is negligible even with rubbers.

A Hewlett-Packard Model 6218A current supply provides the constant current. The output is preamplified through a simple home-built single-pole operational amplifier and fed to the second pen (Y_2) of the X-Y_1-Y_2 recorder which is the same as the one introduced in the previous section. Construction of the preamplifier became necessary because the one supplied by F. W. Bell proved unsatisfactory, mainly because of excessive sensitivity to changes in ambient temperature. The preamplifier and recorder have means to suppress the major portion of the Hall output so that only the change in output upon stretching a specimen is recorded.

Any pressure dependence of the Hall output voltage is negligible for our purposes. However the output is quite sensitive to temperature. A separate calibration is carried out in the pressurized tensile tester using the sliding double

wedge block gauge shown in Fig. 9. F_1 and F_2 are small frames which hold the two parts of the gauge together and also serve as convenient bench marks for calibration. The thickness of the block gauge is changed simply by sliding the accurately machined aluminum wedges past one another. To calibrate the thickness sensor, the block gauge is installed in the pressurized tensile tester, and the magnet and Hall device are clamped on. The tester is then closed, the silicone oil is pumped in, and the whole assembly is brought to constant temperature. The Hall output voltage is then measured as a function of the crosshead displacement, which had previously been related to the corresponding thickness of the block gauge by measuring the thickness as a function of bench mark separation with a cathetometer sensitive to 0.0002 cm. This relation is linear.

A typical calibration curve at 25°C is shown in Fig. 10. Although the Hall output is proportional to the intensity of the magnetic field the relation between the output and the distance from the magnet will not be linear because the intensity of the magnetic field does not change linearly with the distance from the magnet. In fact the calibration curve in Fig. 10 can be represented by the equation

$$V_H = At^2 + Bt + C \qquad (3 - 2)$$

in which t is the thickness and A, B, and C are constants depending on the temperature. The

on the temperature. The values of these constants at 25°C are shown in the figure. The dependence of the output voltage on the square of the thickness is a consequence of the geometry of the magnetic field. This is shown in Fig. 11-a where N and S are the two poles of the magnet M, and H is the Hall device. If the change of the distance between the magnet and the Hall device is quite small, the force lines passing through the small range may be considered straight lines radiating from a single point as shown in Fig. 11-b. Letting S_1 and S_2 be the arbitrary areas shown in Fig. 11-b, we can write, using a simple geometric theorem,

$$\frac{\overline{OA}}{\overline{OB}} = \frac{S_1}{S_2} \qquad (3 - 3)$$

Since the number of force lines passing through the areas S_1 and S_2 are the same, the intensity of the magnetic field B will be inversely proportional to the area, S, and hence

$$\frac{S_1}{S_2} = \frac{B_2}{B_1} \qquad (3 - 4)$$

From Eq. 3-1 the output is linearly proportional to the intensity of the magnetic field if the rest of the variables are constant,

i. e.

$$\frac{V_{H_2}}{V_{H_1}} = \frac{B_2}{B_1} \qquad (3 - 5)$$

Combining Eqs. 3-3, 3-4, and 3-5 yields

$$\frac{V_{H_2}}{V_{H_1}} = \frac{(a - t)^2}{a^2} \qquad (3 - 6)$$

where a = $\overline{OB}$ and t = $\overline{AB}$. Rearranging, Eq. 3-6 can be written as

$$V_{H_2} = V_{H_1}[1 - 2\frac{t}{a} + (\frac{t}{a})^2] \qquad (3 - 7)$$

But $V_H = V_{H_2} - V_{H_o}$, where V_{H_o} is a constant. Hence

$$V_H = (V_{H_1} - V_{H_o}) - 2\frac{V_{H_1}}{a}t + \frac{V_{H_1}}{a^2}t^2 \qquad (3 - 8)$$

which is identical with Eq. 3-2.

With our arrangement about 0. 004 inch change in thickness corresponds to 1 inch on the recorder chart. Thus in a 0. 1 inch-thick rubber specimen the thickness change resulting from a 100percent extension will register as about 7 inches

on the chart. This is quite adequate for our purpose but is not the limit of the sensitivity of the device. This could be increased by a factor of about 10 if required. The device should therfore allow determinations of Poisson's ratio in elastomers.

3.2. Material

The samples used in experiments are glass bead filled EPDM (Ethylene-propylene-terpolymer) vulcanizates. The EPDM is U. S. Rubber Co. Royalene 301T and the glass beads are 3M "Super bright" glass beads manufactured by 3M Company which have 29 micron diameters. 100 parts of rubber was milled on a 2-roll rubber mill for 10 minutes and a measured amount of glass-beads are added to be milled together for another 10 minutes. Care was taken not to overheat the mixture during the mixing. Then, 3 phr dicumyl-peroxide was added and mixed for 10 more minutes. After cooling it to the room temperature, the mixture was vulcanized by compression molding to produce sheets of 25.4x25.4x0.318 cm (10x10x1/8 in.), at 162°C for an hour. The specifications of the samples are given in TableII. The crosslinking densities shown in the last column were measured by M. Okuyama[20].

Rings of inside diameter 1.350 in. outside diameter 1.500 in. were cut out of the sheets.

3.3. Measurements and Method of Analysis

In this section the experimental procedures for measuring the stress-strain curve and the accompanying volume change of a glass-bead-filled rubber vulcanizate ring specimen will be described. The method of data analysis for obtaining volume change-stress-strain curves will follow. It will contain an estimation of end effects, the determination of the point of zero strain, and the calibration of Hall output.

3.3.1. Volume Change-Stress-Strain Curve

Preceding actual measurments, the Hall Effect thickness sensor is calibrated by the method described in Section 3.2. In calibrating the sensor, the sensitivity and range of the recorder are adjusted so that the full movement of the recorder pen across the chart approximately coincides with the change in the Hall output for the expected change in the thickness of the specimens. Stress and volume change of the samples due to deformation were measured on the pressurized tensile tester.

To begin a measurement the lower hook of the equipment is brought as close to the other hook as possible. This allows us to hang a ring specimen without deforming it over the upper hook. With the specimen on the hook, the lower hook is brought down far enough to deform the ring to an elliptical shape but

not enough to make it straightened out. At this position the specimen is still regarded as unstretched, but it does not slip around the hooks when the Hall effect thickness sensor is put on it. Care must be taken to locate the thickness sensor as close to the middle of the specimen as possible. At this stage the output from the load cell shows the sum of the forces due to the bending of the specimen and the weight of the sensor. This force is recorded. Next the cover is put over the equipment, screwed screwed in and tightened. Hydraulic liquid is introduced, and the entire system is pressurized. Temperature and pressure are carefully controlled so that the desired condition is maintained through the measurement. Before stretching the specimen, the stress output is brought back to the value indicated before the system was filled with the liquid in order to cancel the buoyancy force. The specimen is stretched at a constant speed, 3.45 cm/min., until it breaks. The stress and thickness changes are recorded on the same chart by a two-pen $X\text{-}Y_1\text{-}Y_2$ recorder. The pressures used are, 1.0, 7.9, 14.8, 27.6, 69.8, and 138.0 bar. (0, 100, 200, 400, 1,000, 2,000 psig) Each measurement is repeated three times to reduce the uncertainty of the data due to experimental error.

3.3.2. End Effect in a Ring Specimen

When a ring specimen is stretched on a pair of hooks the stretch ratio is given by

$$\lambda_a = \left[2L + \pi\left(d + \frac{w}{\sqrt{\lambda_a}}\right)\right] / \pi(D_i + w) \qquad (3 - 9)$$

where D_i is the inside diameter, d is the diameter of the hook, w is the width of the ring, L is the distance between the centers of the hooks and λ_a is the stretch ratio averaged over the cross-section. Since $D_o - D_i = 2w$, where D_o is the outer diameter of the ring, we have

$$D_a = (D_o + D_i)/2 = D_i + w \qquad (3 - 10)$$

where D_a is the average diameter. Setting $\lambda_a = 1$ in Eq. 3-9 so that L becomes L_o, the initial distance of the hooks, we may express d in terms of L_o, w, and D_i. Making the necessary substitutions, it can be shown that Eq. 3-9 is identical with the equation of Smith[21]. We prefer to use it in this form because this does not require knowledge of L_o.

Eq. 3-9 has been derived from the geometry of the ring assuming that the material is incompressible, and that there

are no end effects. In fact, however, the ring is flattened out where it is in contact with the hooks, and four "fillet sections" develop in the proximity of the hooks. For convenience in considering the end effects, a ring may be subdivided into four sections as shown in Fig. 12 in which the sections are identified by Roman numerals.

To ascertain whether the end effects could be neglected, a ring, cut from a sheet of an unfilled natural rubber vulcanizate was bench marked as shown in Fig. 12. The lengths along the inside and outside circumferences of the four sections were measured with a cathetometer to obtain the initial lengths of each section. The ring was then stretched in small increments, and the changes in the lengths of the four sections were again read with the cathetometer. The resulting stretch ratio will be denoted by λ_{meas}. Stretch ratios were then calculated using Eq. 3-9 in the form

$$\lambda_{calc} = \frac{2L}{\pi D_a} + \frac{d + w}{D_a} \qquad (3 - 11)$$

i. e. suppressing the subscript a for convenience, and neglecting the small correction for the change in the width of the ring, $1/\sqrt{\lambda_a}$. We have found that with our samples and specimen geometry this correction is indeed negligible up to stretch ratios as high as 8.

By Eq. 3-11 the stretch ratio, λ_{calc}, is a linear function of the hook distance, L. The average stretch ratio in each section was obtained by taking the mean values of the inside and outside stretches. The unfilled circles in Fig. 12 represent a plot of the average of λ_{mas} against λ_{calc}. The dotted line is the line of unit slope. The scatter of the values obtained for each section is considered to arise from slight changes in the thickness and width along the circumference of the ring.

Since the force acting on any cross section must be the same, the stress along the circumference of the ring will be inversely proportional to the cross-sectional area. Therefore, if we assume a linear relation between the stress and the stretch ratio, the latter will also be inversely proportional to the cross-sectional area along the circumference. This assumption is certanly valid for the small dimensional variations considered here. If the thickness and width of a given cross-section are denoted by t and w, and the values averaged over the circumference by t_{av} and w_{av}, respectively, we may write

$$\lambda_{corr} = \lambda_{meas} \frac{wt}{w_{av} t_{av}} \qquad (3 - 12)$$

where λ_{meas} is the cathetometrically determined stretch ratio, and λ_{corr} is the stretch ratio corrected

for changes in the cross-sectional area.

The filled circles in Fig. 12 represent the data shown by the unfilled circles corrected according to Eq. 3-12. The data fall almost exactly on the same straight line which is offset here by the arbitrary amount A for clarity. The solid line was calculated by the method of least squares from the data represented by the filled circles. This analysis shows that the scatter caused by slight changes in the thickness and width along the specimen can be corrected for in the indicated manner. It also shows that the end effects cannot be neglected in calculations demanding a high degree of accuracy. Since, however, the filled circles in Fig. 12 fall on a straight line, the true stretch ratio may be obtained from that calculated by Eq. 3-11 by the linear relation

$$\lambda_{true} = a\lambda_{corr} + b \qquad (3 - 13)$$

The constants a and b will in general, depend on the material and the ring dimensions. The constant b is small. For b = 0, $\pi D_a/a$ is an equivalent circumference analogous to the equivalent gauge length employed with dogbone shaped tensile specimens.

3.3.3. Determination of the Point of Zero Extension

When a ring is stretched in uniform extension it is first

straightened out into the "race track" shape shown in Fig. 12. Little force is required generally to affect this shape change. The load-deformation curve, therefore, shows a "toe" at small crosshead displacements where the force rises less steeply than it would if the specimen had had the race-track shape in the undeformed state. To determine the point of zero extension for the race track shape it is customary to back-extrapolate the load-deformation record using the portion of the curve just past the toe where it is generally a straight line. In the past these extrapolations were done manually. For the measurements reported here this method proved inadequate. Because of the relatively high filler content the behavior is sufficiently non-linear to prevent the determination of the point of zero extension by simple manual extrapolation with the required accuracy. We have therefore devised a method based on curve fitting which gives excellent results.

For some unfilled rubber vulcanizates the stress-strain curves in simple tension are described fairly well up to a certain strain by the equation

$$\bar{\sigma} = E \ln \lambda \qquad (3\text{-}14)$$

where $\bar{\sigma}$ is the stress, E is Young's modulus, and λ is the stretch ratio. In the case of filled elastomers, provided that the filler

is rigid and that the material is incompressible, the average deformation in the rubbery matrix, λ_R, may be approximated by

$$\lambda_R = 1 + (\lambda - 1)/(1 - \varphi) \qquad (3 - 15)$$

where λ is the overall stretch ratio and φ is the volume fraction of the filler. Substituting this expression into Eq. 3-14 we obtain

$$\overline{\sigma} = E\ln\left[1 + (\lambda - 1)/(1 - \varphi)\right] \qquad (3 - 16)$$

Although Eq. 3-15 does not describe the behavior of real filled materials, it, nevertheless, has the correct shape and may be used for the purpose of curve fitting by regarding the constants E and φ as adjustable parameters. To determine the point of zero extension by back-extrapolation using Eq. 3-16, it is necessary to add another parameter A that shifts the curve along the λ-axis without changing its shape. The result is

$$\overline{\sigma} = C\ln\left[1 + (\lambda - 1 - A)/B\right] \qquad (3 - 17)$$

where the use of the symbols A, B, and C emphasizes that no physical meaning should be attached to them, except that $C/B = E$ may be regarded as an estimate of Young's modulus at small

strains.

This procedure has been incorporated into our computer program for the reduction of the load-deformation records to the stress-strain curves. It appears to give more consistent results than back-extrapolation using a polynominal fit.

3.3.4. Calibration for the Calculation of Relative Volume Change

When a body is deformed, letting V and V_o denote the volume before and after deformation, respectively, the ratio is given by,

$$\frac{V}{V_o} = \lambda_1 \lambda_2 \lambda_3 \qquad (3 - 17)$$

where λ_1, λ_2, and λ_3 are three principal stretch ratios, respectively. If t and t_o denote the widths (thickness) of a specimen before and after deformation, respectively, the stretch ratios in the two lateral directions are

$$\lambda_2 = \lambda_3 = \frac{t}{t_o} \qquad (3 - 18)$$

As shown in section 3.4.1 the principal stretch ratio in the direction of stretching, λ_1, may be calculated by Eq. 3-12 for an unfilled elastomer. Attempts to carry out a similar

analysis on glass bead-filled EPDM rubber were unsuccessful because the specimen failed in delayed rupture when the rings were held at a constant elongation during the cathetometer reading. Therefore, an indirect method nust be used to obtain the true values of λ_1 experimentally.

If the material is incompressible we will have $\lambda_1\lambda_2^2 = 1$. Eq. 3-18 would then give

$$\lambda_1 = (\frac{t_o}{t})^2 \qquad (3-19)$$

Plotting $(t_o/t)^2$ measured by the Hall effect thickness sensor, against the separation of the hooks, L, should, by Eq. 3-19 yield a straight line if the material is incompressible. If the rubber separates from the filler particles as it is deformed, the volume does not remain constant because of the vacuole formation. As a consequence, the thickness, t, will not decrease as fast as it would if the material was incompressible. A plot of $(t_o/t)^2$ against L, therefore, would be curved downward. This is shown in Fig. 13 by the data obtained on sample A06 at atomspheric pressure (triangles), and at 138 bars pressure (squares). In both cases the curve begins as a straight line and later bends down, as expected. This shows that the composite material is incompressible until a certain stretch ratio is reached.

Although it may be possible to calculate the true values

of axial stretch ratio, λ_1, by extrapolating the straight portion of the curves in Fig. 13, it turned out that it is not accurate enough. Another method had to be developed.

The variation of the output from the Hall effect thickness sensor was shown to be a quadratic equation with respect to the thickness, both experimentally and semi-theoretically, in Section 3.2 as

$$V_H = At^2 + Bt + C \qquad (3 - 20)$$

where V_H is Hall output, t is thickness of a specimen and A, B, and C are constants. Experimentally obtained values of A, B and C will contain some amount of error and, consequently, the thickness, t, calculated from the equation will contain some error. Letting A', B', and C' represent the measured values of A, B, and C, respectively, the relation among them is given by

$$V_H = A't'^2 + B't' + C' \qquad (3 - 21)$$

where it is assumed that the Hall output, V_H can be measured accurately enough so as not to contain any error. If subscript, 'o', denotes the initial values of all the quantities under consideration, lateral stretch ratios of a specimen are defined by

$$\lambda_2 = \frac{t}{t_o} \tag{3 - 22}$$

$$\lambda_2' = \frac{t'}{t_o'} \tag{3 - 23}$$

The prime (') denotes experimental values. The volume ratio, v is given by

$$v = \frac{V}{V_o} = \lambda_1 \lambda_2^2 \tag{3 - 24}$$

$$v' = \frac{V'}{V_o'} = \lambda_1' \lambda_2'^2 \tag{3 - 25}$$

If the material is incompressible, we have $v = 1$ and λ_1 is given by

$$\lambda_1 = \frac{1}{\lambda_2^2} \tag{3 - 26}$$

The experiments described in Section 3.2 showed that the true stretch ratio, λ_1 is a linear function of crosshead displacement, and it is related to the stretch ratio calculated by Eq. 3-11, λ_1', by

$$\lambda_1 = z(\lambda_1' - 1) + 1 \tag{3 - 27}$$

This is because, according to the equation, λ_1' is also a linear

function of crosshead displacement, and z is an error factor, or more precisely, something that should be called an end effect factor.

Solving Eqs. 3-20 and 3-21 for t and substituting the solution in Eqs. 3-22 and 3-23, we can get

$$\lambda_2 = \frac{B + \sqrt{B^2 - 4A(C - V_H)}}{B + \sqrt{B^2 - 4A(C - V_{Ho})}} \qquad (3 - 28)$$

and

$$\lambda_2' = \frac{B' + \sqrt{B'^2 - 4A'(C' - V_H)}}{B' + \sqrt{B'^2 - 4A'(C' - V_{Ho})}} \qquad (3 - 29)$$

where V_{Ho} is the Hall output corresponding to the initial thickness, t_o. From Eq. 3-29 V_H is obtained as a function of λ_2 as

$$V_H = \frac{\left[\lambda_2 \{B' + \sqrt{B'^2 - 4A'(C' - V_{Ho})}\} - B\right]^2 - B'^2 + 4A'C'}{4A'} \qquad (3 - 30)$$

if the relative error in the values of the measured constants, A', B', and C' are ΔA, ΔB and ΔC, respectively, the true values are

$$A = A'(1 - \Delta A)$$

$$B = B'(1 - \Delta B) \qquad (3 - 31)$$

$$C = C'(1 - \Delta C)$$

Substituting Eqs. 3-31 in Eq. 3-28 we obtain

$$\lambda_2 = \frac{B'(1 - \Delta B) + \sqrt{B'^2(1 - \Delta B)^2 - 4A'(1 - \Delta A)[C'(1 - \Delta C) - V_H]}}{B'(1-\Delta B) + \sqrt{B'^2(1-\Delta B)^2 - 4A'(1-\Delta A)[C'(1-\Delta C) - V_{Ho}]}}$$

$$= \frac{B' \frac{1-\Delta B}{\sqrt{1-\Delta A}} + \sqrt{B'^2 \frac{(1-\Delta B)^2}{1-\Delta A} - 4A'[C'(1-\Delta C) - V_H]}}{B' \frac{1-\Delta B}{\sqrt{1-\Delta A}} + \sqrt{B'^2 \frac{(1-\Delta B)^2}{1-\Delta A} - 4A'[C'(1-\Delta C) - V_{Ho}]}} \qquad (3 - 32)$$

Replacing $(1-\Delta B)/\sqrt{1-\Delta A}$, and $(1 - \Delta C)$ by x and y, respectively, V can be written

$$\lambda_2 = \frac{B'x + \sqrt{(B'x)^2 - 4A'(C'y - V_H)}}{B'x + \sqrt{(B'x)^2 - 4A'(C'y - V_{Ho})}} \qquad (3 - 33)$$

Substitution of Eq. 3-30 into Eq. 3-33 yields

$$\lambda_2 = \frac{B'x + \sqrt{[\lambda_2'\{B' + \sqrt{B'^2 - 4A'(C' - V_{Ho})}\} - B']^2 - (B'x)^2 - B'^2 + 4A'(1-y)}}{B'x + \sqrt{(B'x)^2 - 4A'(C'y - V_{Ho})}}$$

$$(3 - 34)$$

Eq. 3-34 relates expected values of lateral stretch ratio from Eq. 3-11 to the true values. Substituting Eq. 3-27 and Eq. 3-34 into Eq. 3-24, the dilatation due to stretching can be calculated

provided that the values of x, y, and z are known.

If the material is incompressible, v will have the value of unity independent of the stretch ratio. If, however, any one or all of the parameters x, y, and z do not equal unity, v' will deviate from unity even though the material is incompressible. Calculating v' from experimental data, i. e. from the crosshead displacement and the thickness change, will lead to a curve such as that shown by the circles in Fig. 14. By contrast, the curve represented by the squares, is of the form one expects when the material is incompressible(i. e. does not dewet) until a certain value of the stretch ratio is reached. The experimental curve(circles) can be corrected to give the true curve(squares) by choosing a set of appropriate values for x, y, and z, by means of curve fitting. The result may be used to correct the data of volume change because it will be reasonably assured that the calibration constants have no relation to whether or not the volume of a specimen is increasing during the deformation. A typical example of the calibration is shown in Fig. 14. In the figure the circles show a set of experimental data of dilatational measurements. After correction the experimental values are reduced to the points represented by squares. In making this correction, measured values of A', B', and C' were used to calculate the values represented by the circles. Those values belonging to the region where the curve does not yet begin to rise sharply were compared to the expected value of 1, and the factors x, y, and z were determined by a trial-and-error method so as to give the best agreement to each other.

4. Results and Discussions

Both experimental and theoretical results will be presented and compared. First the material constants and experimental parameters of the material used are calculated. Then in the succeeding sections, the initial moduli, the stress-strain-volume change curves, and the failure properties of the samples will be presented and discussed. For the first two properties the resuts will be compared with the theoretical results.

4.1. Material Constants and Parameters

As discussed in Section 2 the strain energy function of a homogeneous and isotropic elastic material should be a function of strain invariants. Furthermore, if the material is incompressible and the time dependence is negligible, the strain energy is a function of two of the strain invariants, I_1 and I_2, and is expanded to a Taylor series of the two invariants.

$$W = \sum_{i,j=0}^{\infty} C_{ij}(I_1 - 3)^i(I_2 - 3)^j \qquad (4 - 1)$$

For the case of simple tension, I_1 and I_2 are given by

$$\begin{aligned} I_1 &= \lambda^2 + \frac{2}{\lambda} \\ I_2 &= \frac{1}{\lambda^2} + 2\lambda \end{aligned} \qquad (4 - 2)$$

The stress-strain curve is obtained by differentiating Eq. 4-1 by the stretch ratio, λ, as

$$\sigma = \frac{\partial W}{\partial \lambda} = 2(C_{10} + \frac{C_{01}}{\lambda})(\lambda - \frac{1}{\lambda^2}) + g(\lambda; C_{ij}) \quad i + j > 1 \tag{4 - 3}$$

where σ is nominal stress and $g(\lambda; C_{ij})$ is a function of λ with C_{ij} as the parameters. If $g(\lambda; C_{ij})$ is neglected Eq. 4-3 is the well known Mooney-Rivlin equation, and the constants, C_{10} and C_{01} are obtained as the intercept and the slope when $\sigma/(\lambda - \lambda^{-2})$ is plotted against $1/\lambda$. The Mooney-Rivlin equation, however, is not valid in a very wide range of stretch ratio. The Mooney stress, $\sigma/(\lambda - \lambda^{-2})$, for rubbery materials, in most cases, blows up as the stretch ratio increases indefinitely. Recently Tschoegl[25] developed a method of curve fitting to obtain the coefficients of the higher terms in Eq. 4--1. According to this method all that is needed to obtain satisfactory coincidence with the experimental data in most cases is retaining only one or two coefficients in addition to C_{10} and C_{01}. The coeffiecient for the strain energy of sample A01 (EPDM pure gum vulcanizate) was calculated according to his method. It turned out that for this material the combination of C_{10}, C_{01} and C_{22} gives the best fit to the experimental data. Mooney stresse of A01 is plotted against the inverse stretch ratio, $1/\lambda$ in Fig. 15. The solid curve was calculated from Eq. 4-3 using the following

values for the coefficients.

$C_{10} = 1.374$ bars.

$C_{01} = 3.003$ bars.

$C_{22} = 0.000783$ bars.

In the beginning of Section 2 the model for the composite system with the representative dimensions, a, b, and c was introduced. The relation between these parameters, however, was left undetermined. Obviously the relation must depend on the volume fraction of filler in some way. By definition, the volume fraction, φ, is related to a, b, and c by

$$\varphi = \frac{\frac{4}{3}\pi a^3}{2\pi bc^2} = \frac{2a^3}{3bc^2} \qquad (4 - 4)$$

While ψ is defined by $\psi = a/b$, if we let b = c, then φ and ψ are related by

$$\varphi = \frac{2}{3}\psi^3 \qquad \text{or} \qquad \psi = \sqrt[3]{\frac{3}{2}\varphi} \qquad (4 - 5)$$

If this relation holds over the whole range of possible filler loading ratios, ψ increases as φ increases and reaches 1 at $\varphi = \frac{2}{3}$ or 66.7 %. Since it is obvious that ψ can not exceed 1, as long as this condition holds, 66.7 % is the upper limit

of the possible loading fraction of filler. On the other hand, experiments show that the limit of loading ratio ranges from 60 to 63 %[26] and that this range is fairly close to the maximum loading ratio of our choice. It may be reasonable to assume that at maximum loading all the filler particles are effectively in contact with each other so that the whole composite system behaves as a rigid body. If this is true we may modify Eq. 4-5 by replacing 2/3 by φ_m,

$$\psi = \sqrt[3]{\frac{\varphi}{\varphi_m}} \qquad (4 - 6)$$

where φ_m is the maximum loading ratio of filler particles.

The adequacy of the choice will be tested in the following section.

4.2. Initial Modulus of a Filled Elastomer

As mentioned in Section 1 there are a number of theories for predicting the effects of filler particles on the Young's modulus of filled elastomers. Although calculating the modulus is not the main purpose of this work, it will serve to check the feasibility of the theory.

With the strain energy of a filled elastomer known as a function of stretch ratio and volume change, the Young's modulus E, of the system is given by

$$E = \left.\frac{\partial^2 W}{\partial \lambda^2}\right|_{\lambda=1} \qquad (4-7)$$

where λ is the stretch ratio of a simple tension deformation. As will be shown in the next section, the volume change due to the dewetting under deformation does not begin until a certain stretch ratio is reached unless the hydrostatic pressure is zero. We, therefore, can use the strain energy function for the case of no vacuole formation obtained in Section 2 to compute the Young's modulus. Values of second derivative of the strain energy function were computed numerically to obtain the Young's modulus, using the constants and the parameter, ψ, obtained in the previous section.

The experimental values of Young's moduli of glass bead filled EPDM rubber were calculated as the slopes of the tangents of stress-strain curves at $\lambda = 1$. The results are shown in the second columns of Tables III to IX, where $\overline{G}$ is obtained by dividing E by 3. Contrary to the prediction, the experimental values of the moduli show a slight dependence on the pressure at high loading ratios at low pressures. This, however, can reasonably be attributed to the fact that in a highly loaded system, the dewetting begins at such a low stretch ratio that it becomes difficult to measure the initial slope of a stress-strain curve precisely before the effect of volume change initiates.

The crosslink densities[20] of the rubber matrices in the

samples are shown in Tables III to IX. The crosslink density of the pure gum vulcanizate A01 is 2.72×10^{-4} mol/cc. Molecular kinetic theory shows that the modulus of crosslinked polymers is proportional to the crosslink density. These data allow us to correct the experimental values of the moduli in order to appropriatedly compare them with the theoretical results. If we assume that the material constants obtained in the previous section vary in the same proportion as the crosslink density, the resulting values of the moduli vary at the same rate. That is, if the crosslink density of a rubber matrix increases by a factor of 2, the modulus of the composite doubles its value. Omitting the data in the second columns of the tables that are obviously affected by the decrease of the apparent modulus due to dewetting, the moduli were averaged over the pressures for each sample, and the results were multiplied by the ratio of the crosslink density of rubber matrix to that of A01. That is,

$$\bar{G}_{corr} = \bar{G}_{av}\left(\frac{\nu_e}{\nu_{eo}}\right) \qquad (4 - 8)$$

where $\bar{G}_{av}$ is the average of the moduli over the pressures, $\bar{G}_{corr}$ is the corrected value, and ν_e and ν_{eo} are the crosslink densities of the sample and of A01, respectively. $\bar{G}_{corr}$ normalized by the value of the unfilled binder, $\bar{G}_o$, are plotted as $\bar{G}/\bar{G}_o$ in Fig. 16. The solid curve was calculated from Eq. 4 - 7 using the material constants and the parameter, ψ,

obtained in the previous section. The coincidence is fairly good in spite of the scatter among the experimental data.

4.3. Volume Change-Stress-Strain Curves.

4.3.1. General Observations

A few typical examples of volume change-stress-strain curves of glass bead-filled EPDM vulcanizates are shown in Fig. 19. These are the results of the measurements on sample A08 at 5 different pressures.

The figure exhibits most of the characteristic features of the pressure dependence of stress response and dilatational behavior of non-reinforcing filler-filled rubber vulcanizates.

Dilatation of a filled system does not begin until a certain stretch ratio is reached. After passing through a transitional region, where the rate of dilatational change gradually increases from zero to a certain positive value, the volume of the system increases linearly with stretch ratio.

In order to obtain a general idea concerning the dependence of dilatational behavior on pressure and filler fraction, it is convenient to characterize the volume change-strain curve by as few characteristic parameters as possible. Considering the typical nature of a curve described above, two parameters are necessary and also sufficient for the purpose, namely a stretch ratio, λ_d, at which volume change begins and the final

rate of volume increase, m. For the sake of convenience we define λ_d as the stretch ratio where back extrapolation of the linear part of a volume change-strain curve intersects with the λ-axis. Although this is obviously not the real point of volume change initiation, it will serve the purpose.

These characteristic values for each experiment are shown in Tables III to IX. Despite the fact that fairly large scatter in the data makes it difficult to obtain precise information one can observe that λ_d depends strongly on pressure but that it depends little on volume fraction of filler, if it does at all.

λ_d is plotted against pressure in the lower half of Fig. 17. The circles represent the averages over several different filler fractions ranging from 0.089 to 0.485. A range of experimental scatter is shown by a solid vertical line segment and a pair of short horizontal bars at both ends. According to the results, λ_d increases with pressure. In other words the volume change in the system is delayed by superposed hydrostatic pressure. The change in λ_d from 1 bar to 10 bars is about 0.15 and the corresponding value is about 0.30 in the interval from 10 to 100bars. This implies that much more change happens in the low pressure region than does in the higher pressure region.

Tables III to IX show that m decreases with pressure, suggesting a lower rate of volume increase at higher pressure. The decisiveness of these observations, however, is obscured

by the amount of experimental scatter, and if the observations are true the pressure dependence of m is less conspicuous than the dependence on the change in filler fraction. Values of m are plotted against filler fraction, φ, in Fig. 18 in a manner similar to Fig. 17, i.e. a circle represents an average value of m over several different pressures ranging from 1 to 140 bars and the range of experimental scatter is shown by a vertical line segment and a pair of short horizontal bars at both ends. As expected the slope of volume change increases with volume fraction of filler, the more so, the higher the filler fraction.

In order to show the change in stress-strain relations due to increase in filler content, Fig. 20 shows the experimental results from the samples with several different filler fractions at 14.8 bars. As clearly seen, the more highly loaded with filler a specimen is, the stronger the force necessary to stretch it in the early stage of deformation. This relation is reversed as the stretch ratio increases, i.e. at a highly stretched state, the least loaded system shows the highest stress and the most highly loaded one has the lowest stress. This implies that all the stress-strain curves cross each other at certain stretch ratios. Although experiments show that the points of intersection fall in a fairly narrow range of stretch ratios-- sometimes it looks almost like one point -- this is probably purely coincidental.

The stresses corresponding to λ_d, denoted by $\bar{\sigma}_d$, are shown in the upper half of Fig. 17. $\bar{\sigma}_d$ is a monotonically increasing function of pressure and the rate of increase is higher for a more highly filled system. $\bar{\sigma}_d$ also increases with the fraction of filler except at the lowest pressure.

4.3.2. Comparison with Theory

Consider a system of elastic material in simple tension which is in equilibrium at hydrostatic pressure, P, nominal stress, σ (stress based on the original cross section of the system), stretch ratio, λ, and the ratio of the deformed volume to the original volume, v. If the stored energy in this system is $W(\lambda, v)$ the change in strain energy caused by small changes in the variables is obtained from the following energy balance relation.

$$dW = \sigma d\lambda - P dv$$

or

$$\frac{\partial W}{\partial \lambda} d\lambda + \frac{\partial W}{\partial v} dv + P dv - \sigma d\lambda = 0 \qquad (4 - 9)$$

If λ is constant we get

$$\frac{\partial W}{\partial v} dv + P dv = 0$$

or

$$P = -\frac{\partial W}{\partial v} \qquad (4 - 10)$$

If v is constant we obtain

$$\frac{\partial W}{\partial \lambda} d\lambda - \sigma d\lambda = 0$$

or

$$\sigma = \frac{\partial W}{\partial \lambda} \qquad (4 - 11)$$

In Section 2.5.2 we assumed that the strain energy of a composite system was given by Eq. 2-54. As an example of the function, $f(\lambda, v/v_o(\lambda))$ we can select the following expression.

$$f(\lambda, v/v_o(\lambda)) = (1 - v/v_o(\lambda))^{h(\lambda)} \qquad v \leq v_o(\lambda) \qquad (4 - 12)$$

If $h(\lambda)$ is always larger than 1, this expression for $f(\lambda, v/v_o(\lambda))$ satisfies the conditions mentioned in Section 2. That is, $f = 1$ at $v = 0$, and the function has a minimum, 0 at $v = v_o(\lambda)$. Furthermore, this form is simple enough to allow us to treat it mathematically.

Substituting Eq. 2-54 into Eq. 4-10 we can obtain

$$P = -[W_o(\lambda) - W_{min}(\lambda)]\frac{\partial f}{\partial \lambda} \qquad (4 - 13)$$

Substituting Eq. 4-12 into Eq. 4-13, P is obtained as

$$P = [W_o(\lambda) - W_{min}(\lambda)]h(\lambda)(1 - \frac{v}{v_o(\lambda)})^{h(\lambda)-1}\frac{1}{v_o(\lambda)} \qquad (4 - 14)$$

Similar calculations using Eqs. 2-54 and 4-11 give

$$\sigma = \frac{\partial W_{min}}{\partial \lambda} + (1 - \frac{v}{v_o(\lambda)})^{h(\lambda)}\frac{\partial}{\partial \lambda}[W_o(\lambda) - W_{min}(\lambda)]$$

$$+ [W_o(\lambda) - W_{min}(\lambda)]h(\lambda)(1 - \frac{v}{v_o(\lambda)})^{h(\lambda)-1}\frac{1}{v_o(\lambda)} \qquad (4 - 15)$$

From Eq. 4-14 the volume ratio v is obtained as a function of P as

$$\frac{v}{v_o(\lambda)} = 1 - \left[\frac{Pv_o(\lambda)}{h(\lambda)\{W_o(\lambda) - W_{min}(\lambda)\}}\right]^{\frac{1}{h(\lambda)-1}} \qquad (4 - 16)$$

Substitution of Eq. 4-16 into Eq. 4-15 gives the nominal stress, σ, as a function of stretch ratio, λ, and hydrostatic pressure, P.

Functions $h(\lambda)$ and $v_o(\lambda)$ were chosen so that they give reasonable agreement with the experimental data on sample A11 with filler fraction, 0.398 (cf. Fig. 24),

$$h(\lambda) = 6\lambda^3 \qquad (4 - 17)$$

$$v_o(\lambda) = \varphi(\lambda - 1)^{1.3} \qquad (4 - 18)$$

Stress-strain curves and volume changes for glass-bead-filled EPDM samples were calculated numerically using the material constants and parameters obtained in Section 4.1.

Fig. 21 through 24 show the results for samples A02, A04, A08 and A11, respectively. The volumetric loading fraction of filler increases from 0.089 to 0.398 in this order. In plotting the data the values were corrected by the same method used for determining the Young's moduli in Section 4.2.

In each figure experimental values of stress-strain and volume change-strain are shown by solid lines for pressures, 1.0, 14.8 and 138.0 bars. The theoretical results are indicated by broken lines for 1.0 and 138.0 bars. As expected the agreement between the experimental and theoretical data becomes poorer as the volume fraction of filler increases; however, the agreement is fairly good considering the arbitrariness in choosing the functional form of the strain energy $W(\lambda, v)$. Although it may be possible to choose a more complicated form for $f(\lambda, v/v_o(\lambda))$ to improve the agreement of the results, we may not be able to obtain a closed form for the stress, σ because it may be impossible to rewrite Eq. 4-13 to a form equivalent to Eq. 4-16 in such a case.

Unlike the agreement in the stress-strain curves, the

volume changes predicted by the theory
than those of the experimental data. This is rather strange considering the fact that the theoretically obtained strain energy function describes the stress-strain behavior fairly well not just for one, but for three variables, namely volume fraction of filler, stretch ratio and hydrostatic pressure. For examle, in Fig. 23 the theory predicts not only the approximate heights of stress-strain curves but also the characteristic shapes of the curves, which are not monotonous functions. This deviation from the experimental data of the volume changes predicted by the theory may be because of the special choice of the functions, $h(\lambda)$, and $v_o(\lambda)$ we made.

From the observation discussed above we may conclude that, if we choose the functions, $h(\lambda)$ and $v_o(\lambda)$, so that the results of the theoretical calculations show reasonable agreement with the experimental data at a volume fraction of 0.398, then the theory satisfactorily predicts the stress-strain behavior as a function of stretch ratio, volumetric loading of filler, and pressure for volume fractions below 0.398, and pressures up to about 140 bar.

At higher volume fractions the specimens broke before dewetting fully developed. The stress-strain curves up to the relatively short stretch ratio, λ_b, at which the specimens failed were practically straight lines, the slope of which are given

by the initial moduli tabulated on Tables Ⅲ to Ⅸ.

The effect of filler-elastomer adhesion on the reinforcement of mechanicala behavior of filled elastomer is quite obvious in Figs. 21 to 24.

Superposed hydrostatic pressure prevents filler-elastomer separation to some extent as shown by the volume change-strain curves in the lower parts of the figures. As soon as the elastomer begins to separate from the filler particles, the rate of stress increase sharply drops. The higher the loading fraction of filler is, the more remarkable the phenomenon appears. In the case of no vacuole formation, the theory predicts a nominal stress of 860 bars at $\lambda = 2.5$, $\varphi = 0.4$; experiments give only 11.4 bars for the same material even at the highest pressure, 138 bars, which was actually used. Of course this does not mean that this composite will really show a stress of 860 bars if dewetting is completely prevented. There will be many factors that prevent the achievement of this extreme strength. For example, the maximum internal stretch ratio of a composite system with filler fraction of 0.4 at $\lambda = 2.5$ reaches as high as $\lambda = 10.6$ according to Eq. 2-42. Considering that the stretch ratio at break of unfilled EPDM sample A01 has a value of about 3.5, it is highly improbable that the stretch ratio exceeds the value of 10 even locally. However, the theoretical speculation gives an idea about the importance of filler-elastomer adhesion on reinforcing effect of filler.

4.4. Failure

4.4.1. General Observations

In systems heavily loaded with glass beads, a stress-strain curve often has a maxima. Sometimes this phenomenon may be genuinely the reflection of a sudden decrease in strain energy due to vacuole formation in the composite material, but at other times it is caused by local growth of flaws. If the latter is the case, caution is needed in determining the true mechanical properties at break.

Fig. 25 shows the results of measurements on two different specimens of A13(φ = 0.459) at 13.8 bars(gauge). In spite of the excellent reproducibility of the data, both in stress-strain curves and in volume change-strain curves at stretch ratios lower than 1.1, they deviate from each other at higher deformation. Moreover, the shape of the curves becomes quite irregular as soon as the volume change-strain curve begins to deviate from 1. Not to mention the fact that $\Delta V/V_o$ could not be negative, it is obvious that the deformation in this region is not uniform any longer. Visual observations of the specimens under deformation revealed that a large flaw sometimes develops locally in the specimen at it is stretched. To be accurate, the stress and the corresponding stretch ratio at which a stress-strain curve begins to show an irregularity in shape are taken

as the properties at break. The failure data are shown in the last three columns of Tables III to IX.

The data for a few of the samples are shown in Fig. 26 and Fig. 27. In Fig. 26 stretch ratios at break for samples A02, A08 and A14 are plotted against hydrostatic pressure, and the corresponding stresses are shown in Fig. 27.

Of the three cases sample A14, which is the most highly loaded system in the series, is of most interest. In A02 and A08 the stretch ratios at break more or less smoothly increase with hydrostatic pressure. On the other hand the behavior of A14 is quite unique; that is, λ_b exhibits a dramatical drop at a pressure of about 10 bars. It becomes clear that this is not simply experimental error when one looks into the other properties. In spite of the unusual behavior of λ_b in A14, the dependence of the stress at break, $\bar{\sigma}_b$, is hardly distinguishable from the other two samples as shown in Fig. 27. Inspection of the dilatational behavior of these specimens shows that the volume of specimens under stretching at 1 and 7.9 bars increases quite rapidly, as expected from the high loading ratio of filler. In the other four cases, measured at higher pressures, the specimens break before they show any indication of dilatation. This observation suggests that at lower pressures the release of large internal deformation due to vacuole formation which causes a large stress concentration is strongly responsible

for keeping the specimens from breaking. It further suggests that the properties at break of the rubber matrix itself are not at all or only slightly affected by hydrostatic pressure.

4.4.2. Failure Surfaces

If an elastic material is subjected to a deformation, the stress tensor as the response can be characterized by three principal values, σ_1, σ_2 and σ_3. When the values at rupture are plotted in three-dimensional stress space with σ_1, σ_2 and σ_3 as the base axes, they will fall on a characteristic surface, which is called the failure surface. Since in an isotropic material interchanging σ_1, σ_2 and σ_3 does not alter the mode of deformation, a failure surface must have the space diagonal as an axis of six-fold rotational symmetry as the most general case. A space diagonal is defined as a straight line consisting of all the equidistant points from the three stress axes in the first and eighth octants, where σ_1, σ_2 and σ_3 all have the same sign.

Lim and Tschoegl[16], assuming that a failure surface is a surface of revolution whose axis is the space diagonal, attempted to express it by two variables. Those are

$$\sigma_{on} = \frac{1}{3}(\sigma_1 + \sigma_2 + \sigma_3)$$
$$\sigma_{os} = \frac{1}{3}[(\sigma_1 - \sigma_2)^2 + (\sigma_2 - \sigma_3)^2 + (\sigma_3 - \sigma_1)^2]^{\frac{1}{2}} \qquad (4 - 14)$$

Both σ_{on} and σ_{os} are symmetric with respect to σ_1, σ_2 and σ_3, and consequently any equation containing σ_{os} and σ_{on} as the variables defines such a surface of revolution that was described above. Geometrically, $\sqrt{3}\,\sigma_{on}$ is the length of the projection of a position vector in stress space on the space diagonal, and $\sqrt{3}\,\sigma_{os}$ is the distance of the point from the space diagonal.

Lim and Tschoegl obtained values of σ_{on} and σ_{os} at break, which are denoted by $\sigma_{on,b}$ and $\sigma_{os,b}$, from their simple tension measurments under hydrostatic pressure on glass bead-filled EPDM vulcanizates. In simple tension the principal stresses at break $\sigma_{1,b}$, $\sigma_{2,b}$, and $\sigma_{3,b}$ are related to the stress at break by

$$\begin{aligned} \sigma_{1,b} &= \bar{\sigma}_b - P \\ \sigma_{2,b} &= -P \\ \sigma_{3,b} &= -P \end{aligned} \qquad (4-15)$$

where P is the superposed hydrostatic pressure and $\bar{\sigma}_b$ is the true stress at break. Substituting Eqs. 4-15 into Eq. 4-14 we obtain $\sigma_{on,b}$ and $\sigma_{os,b}$ as

$$\begin{aligned} \sigma_{on,b} &= \frac{\bar{\sigma}_b}{3} - P \\ \sigma_{os,b} &= \frac{2}{3}\bar{\sigma}_b \end{aligned} \qquad (4-16)$$

Plotting $(\sqrt{3}\sigma_{os,b})^2$ against $\sqrt{3}\sigma_{on,b}$, they found that the failure surfaces consisted of a paraboloidal and a cylindrical section corresponding to the higher and lower pressure regions, respectively. They refered to the critical pressure at which the transition from a cylinder to a paraboloid takes place as $\sigma_{on,b}(trans)$ and speculated that vacuole formation is completely prevented atpressures higher than $\sigma_{on,b}(trans)$.

Unfortunately at the time they did not have a practical method for measuring the volume change in a stretched specimen.

In order to obtain principal stresses one must know the true stress of deformation and consequently one must know the dilatational properties as well as the force-displacement relation for a specimen. Naturally their data could not avoid the error caused by the lack of knowledge of the dilatation.

In this section the volume change-strain curves for the samples which were used in their measurements were calculated by interpolating the data from the curves obtained for the samples we measured and correcting the stress-strain curves to obtain the true stresses at break. The results show considerable differences from the conclusions they reached.

$\sqrt{3}\sigma_{os,b}$ is plotted against $\sqrt{3}\sigma_{on,b}$ in Fig. 28, and 29, for all the samples measured. Attempts to fit these data by a continuous and smooth power function were not successful. As clearly shown in the figures each curve consists of two

straight line segments. As for the shape of a failure surface, this implies that it consists of two cones with different opening angles, provided that it is a surface of revolution. This assumption may be reasonable for an isotropic system, including a system such as filled polymers that is homogeneous only from a macroscopic point of view. However , one could not expect a dewetted glassbead-filled polymer to be isotropic; i. e. the shape of vacuoles formed around particles will depend on the mode of deformation, and consequently the mechanical properites will also depend on the mode of deformation. In order to discuss the characteristic of failure surfaces appropriately, it will be essential to measure the properties at break by not only simple tension deformation but also at least one other type of deformation such as, simple shear, pure shear, biaxial, etc. In the following discussion, however, we assume that the failure surfaces are surfaces of revolution, simply for convenience.

The curves shown in Fig. 28 and 29 are the intersections of failure surfaces with a plane that contains the σ_1 axis and the space diagonal. All the curves in Fig. 28. and 29 are replotted on Fig. 30 for comparison. Each curve can be expressed by the following two equations.

$$\sigma_{os,b} = -C_1\sigma_{on,b} + C_2 \qquad \sigma_{on,b} \leqq \sigma_{on,b}(\text{trans})$$

$$\sigma_{os,b} = -C_3\sigma_{on,b} + C_4 \qquad \sigma_{on,b} \geqq \sigma_{on,b}(\text{trans}) \qquad (4\text{-}17)$$

In the equations, $\sigma_{on,b}(trans)$ is the value of $\sigma_{on,b}$ at which the two straight lines intersect, and C_1, C_2, C_3 and C_4 are constants. We will call the portion of a curve belonging to the region, $\sigma_{on,b} \leq \sigma_{on,b}(trans)$ the first cone and the other the second cone. At first glance all the curves look parallel, and for the second cones this is true because there is no significant dependence of the slope on the volume fraction of filler. A closer inspection of the first cones, however, reveals that the slope increases with the filler concentration from A02 ($\varphi = 0.089$) to A07 ($\varphi = 0.258$). (with the exception of A05 ($\varphi = 0.200$)), and decreases again as the filler concentration further increases. This may be too consistent to be neglected as experimental error.

C_1 and C_3 are plotted in Fig. 31 as a function of filler concentration. C_1 has a sharp maximum at about $\varphi = 0.22$ while C_3 remains constant regardless of the value of filler concentration.

C_2 and C_4 are shown in Fig. 32 also as a function of the volume fraction of filler. Both decrease linearly with the filler concentration in the range of experiments. Since the value (24.4 bars) of C_2 at $\varphi = 0.0$ is much higher than the value expected from linear behavior, it may be more reasonable to assume that the C_2- and C_4-curves are concave upward. Experiments show that the failure properties of unfilled EPDM do not depend on pressure; i.e. the value of C_1 and C_3 of A01

is 0. Although the values of C_3 in Fig. 31 show a slight indication of a drop at φ =0. 089 and 0. 132, a sharp drop must take place in the narrow range between φ = 0. 1 and 0. 0.

The values of $\sigma_{on,b}$(trans) range from -5. 77 to -24. 2bars, and they do not show any consistent dependence on filler concentration. This range is quite narrow compared to the range of hydrostatic pressure where the experiments were performed so that one can safely say $\sigma_{on,b}$(trans) is a critical value independent of pressure. The behavior of $\sigma_{os,b}$(trans) is almost identical to that of C_2 and C_4.

The significance of $\sigma_{on,b}$(trans) as a critical value is not clear. This could not correspond to the initiation of vacuole formation because, according to the experiments described in the previous section, only A12 and A14 among the samples break under deformation before vacuoles are formed. Even for these highly filled samples it happens only at high pressures. $\sigma_{on,b}$(trans) may be related to the release of stress concentration due to vacuole formation.

In conclusion the failure surfaces consist of two cones, provided that they are surfaces of revolution, and the pair of cones intersect at a constant value of $\sigma_{on,b}$ regardless of the filler concentration.

5. Conclusions

Mechanical behavior described in preceeding sections may be summarized as;

1. A glass bead filled - EPDM vulcanizate behaves as a typical non-reinforcing filler-filled elastomer at atmospheric pressure.
2. Typically, the volume of a glass bead-filled EPDM vulcanizate begins to increase as the stretch ratio reaches a certain value. After a transitional region the volume increases linearly with the stretch ratio. The initiation of volume change is delayed by hydrostatic pressure, but it does not depend on volume fraction of filler. The steady rate of volume increase is an increasing function of volume fraction of filler. This also seems to be a decreasing function of pressure, although it is not conclusive because of experimental scatter.
3. The theory for the strain energy of composite systems derived in Section 2 had good agreement with the experimental data in the Young's moduli and stress-strain curves of glass bead-filled EPDM vulcanizates as functions of appropriate variables; i. e. volume fraction of filler in the Young's moduli and volume fraction of filler, stretch ratio, and hydrostatic pressure in stress-strain

behavior.

4. The failure surface of a glass bead-filled EPDM vulcanizate consists of a pair of cones. The value of $\sigma_{on,b}$ at which a transition from one cone to the other occurs does not depend on volume fraction of filler.

Appendix 1. Deformation Tensor in a Cylindrical Coordinate System

If a pair of closely located points are given the coordinates (r, θ, z) and $(r+dr, \theta+d\theta, z+dz)$ in a cylindrical coordinate system and the corresponding cartesian coordinates are (x, y, z) and $(x+dx, y+dy, z+dz)$, respectively, there exist the following relations between them

$$\begin{aligned} x &= r\cos\theta \\ y &= r\sin\theta \\ z &= z \end{aligned} \qquad \text{(A - 1)}$$

and

$$\begin{aligned} dx &= \cos\theta\, dr - r\sin\theta\, d\theta \\ dy &= \sin\theta\, dr + r\cos\theta\, d\theta \\ dz &= dz \end{aligned} \qquad \text{(A - 2)}$$

Since the distance between a pair of positions is given as the square root of the sum of the squares of differences of each coordinate in a cartesian coordinate, the distance ds_o is given by

$$(ds_o)^2 = dx^2 + dy^2 + dz^2 \qquad \text{(A - 3)}$$

Substituting Eq. A-2 in Eq. A-3 yields

$$(ds_o) = dr^2 + r^2 d\theta^2 + dz^2 \qquad (A - 4)$$

If the two points move to $(r + u, \theta + \frac{v}{r}, z + w)$ and $(r + dr + u', \theta + d\theta + \frac{v'}{r + dr}, z + dz + w')$, respectively, after a certain amount of deformation of the system, u', v', and w' can be related to u, v, and w by simple relations, where u, v, and w are radial, tangential and axial displacement. Because dr, $d\theta$ and dz are small quantities, we can write

$$u' = u + du = u + \frac{\partial u}{\partial r} dr + \frac{\partial u}{\partial \theta} d\theta + \frac{\partial u}{\partial z} dz$$

$$v' = v + dv = v + \frac{\partial v}{\partial r} dr + \frac{\partial v}{\partial \theta} d\theta + \frac{\partial v}{\partial z} dz \qquad (A - 5)$$

$$w' = w + dw = w + \frac{\partial w}{\partial r} dr + \frac{\partial w}{\partial \theta} d\theta + \frac{\partial w}{\partial z} dz$$

and

$$\frac{v'}{r + dr} = \frac{v + dv}{r + dr} = \frac{v}{r} + \frac{dv}{r} - \frac{v dr}{r^2} \qquad (A - 6)$$

neglecting the higher terms of differentials.

Similar to Eq. A-4, the distance between the two points after the deformation, ds, can be written

$$(ds)^2 = (dr+du)^2 + (r+u)^2\left(d\theta + \frac{dv}{r} - \frac{v\,dr}{r^2}\right)^2 + (dz+dw)^2 \qquad (A-7)$$

Using Eqs.A-5 into Eq. A-7, one can rewrite it, using matrices as,

$$(ds)^2 = (dr,\ r\,d\theta,\ dz)\begin{bmatrix} 1+\frac{\partial u}{\partial r} & (1+\frac{u}{r})(\frac{\partial v}{\partial r} - \frac{v}{r}) & \frac{\partial w}{\partial r} \\ \frac{1}{r}\frac{\partial u}{\partial \theta} & (1+\frac{u}{r})(1+\frac{1}{r}\frac{\partial v}{\partial \theta}) & \frac{1}{r}\frac{\partial w}{\partial \theta} \\ \frac{\partial u}{\partial z} & (1+\frac{u}{r})\frac{\partial v}{\partial z} & 1+\frac{\partial w}{\partial z} \end{bmatrix}$$

$$\times \begin{bmatrix} 1+\frac{\partial u}{\partial r} & \frac{1}{r}\frac{\partial u}{\partial \theta} & \frac{\partial u}{\partial z} \\ (1+\frac{u}{r})(\frac{\partial v}{\partial r} - \frac{v}{r}) & (1+\frac{u}{r})(1+\frac{1}{r}\frac{\partial v}{\partial \theta}) & (1+\frac{u}{r})\frac{\partial v}{\partial z} \\ \frac{\partial w}{\partial r} & \frac{1}{r}\frac{\partial w}{\partial \theta} & 1+\frac{\partial w}{\partial z} \end{bmatrix}\begin{bmatrix} dr \\ r\,d\theta \\ dz \end{bmatrix}$$

$$(A-8)$$

Comparing Eq. A-8 with Eq .A-6 the deformation tensor α_{ij} is

$$\alpha_{ij} = \begin{bmatrix} 1+\frac{\partial u}{\partial r} & \frac{1}{r}\frac{\partial u}{\partial \theta} & \frac{\partial u}{\partial z} \\ (1+\frac{u}{r})(\frac{\partial v}{\partial r} - \frac{v}{r}) & (1+\frac{u}{r})(1+\frac{1}{r}\frac{\partial v}{\partial \theta}) & (1+\frac{u}{r})\frac{\partial v}{\partial z} \\ \frac{\partial w}{\partial r} & \frac{1}{r}\frac{\partial w}{\partial \theta} & 1+\frac{\partial w}{\partial z} \end{bmatrix}$$

(A - 9)

If a system is axially symmetric the tangential displacement is always zero, and in addition all derivatives with respect to θ vanish. The deformation tensor then becomes

$$\alpha_{ij} = \begin{bmatrix} 1+\frac{\partial u}{\partial r} & 0 & \frac{\partial u}{\partial z} \\ 0 & 1+\frac{u}{r} & 0 \\ \frac{\partial w}{\partial r} & 0 & 1+\frac{\partial w}{\partial z} \end{bmatrix} \qquad (A - 10)$$

The Cauchy-Green tensor, γ_{ij}, is given by

$$\gamma_{ij} = \alpha_{ki}\alpha_{kj}$$

$$= \begin{bmatrix} (1+\frac{\partial u}{\partial r})^2 + (\frac{\partial w}{\partial r})^2 & 0 & (1+\frac{\partial u}{\partial r})\frac{\partial w}{\partial r} + \frac{\partial u}{\partial z}(1+\frac{\partial w}{\partial z}) \\ 0 & (1+\frac{u}{r})^2 & 0 \\ (1+\frac{\partial u}{\partial r})(\frac{\partial w}{\partial r}) + (\frac{\partial u}{\partial z})(1+\frac{\partial w}{\partial z}) & 0 & (1+\frac{\partial w}{\partial z})^2 + (\frac{\partial u}{\partial z})^2 \end{bmatrix}$$

(A - 11)

This is the necessary relation.

Appendix 2. Strain Energy Function of Dewetting Composite System

Rigorously, vacuoles will be allowed to take only one shape, which gives the minimum total strain energy at the same volume. One must choose a certain function to define the shape of the vacuoles, however, because it is quite unlikely for one to be able to obtain the precise mathematical expression for the shape of the vacuoles. In making an appropriate choice we must keep in mind that the approximation should satisfy as many experimentally observed conditions as possible while it should be simple enough not to hamper the mathematical treatment. After having tried several possibilities we came to the conclusion that the following function may best serve the purpose. The necessary notations are schematically shown in Fig. 3 with the general idea of the derivation. Since the system is axially symmetric, the shape of a vacuole must be a surface of revolution. We use a two dimensional rectangular coordinate system, (X, Y) in the discussion for convenience. The correspondence between the new coordinate system and the (R, θ, ℓ') system used before should be obvious from Fig. 3. The origin of the rectangular coordinate system coincides with the center of the circle at the bottom. If the distance of a point on the circle from the X-axis is given by bx, at $X = R$, x is given by

$$x = \psi \cos\theta \qquad (A - 12)$$

where $\psi = a/b$, a is the radius of the circle and b is the half distance between the centers of two circles. If a point represented by x moves by the distance from the X-axis, by, after vacuole formation, the internal stretch ratio, λ', which has the same physical significance as in the Section 2.5.1, is given by,

$$\lambda' = \frac{\lambda - y}{1 - x} \qquad (A - 13)$$

Determining the functional form of y is equivalent to deciding the profile of the vacuole as a function of x, or R. y should have a maximum at $x = \psi$ or $R = 0$, and the value of the maximum increases as the volume of the vacuole increases. However, the value can not increase indefinitely because the space between the surfaces of the spheres facing each other is limited. Consequently, it is reasonable to set a limit on the value of y at $x = \psi$, the corresponding internal stretch ratio is given by Eq. A-13,

$$\frac{\lambda - \eta\psi}{1 - \psi}$$

and by the physical restriction this value must be positive. That is,

$$\frac{\lambda - \eta\psi}{1 - \psi} > 0 \qquad \text{or} \qquad \eta < \frac{\lambda}{\psi} = \eta_o \tag{A - 14}$$

where η_o is the physically possible upper limit of η. Consider an ellipse described by

$$\frac{X^2}{A^2} + \frac{Y^2}{\eta^2} = a^2 \tag{A - 15}$$

which passes a point $(0, \eta a)$. If we assume that (X_d, Y_d) are the coordinates of the intersection of the ellipse with the circle representing a filler particle and that Y_d decreases linearly from a to 0 as η increases from 1 to η_0, we can obtain the following relation which gives the necessary information about internal stretch ratio and volume change for calculating the strain energy. The details of the derivation are given in Appendix 3.

From the definition of x, y, X and Y, the following relations between them exist.

$$\begin{aligned} Y &= by \\ X &= b(\psi^2 - x^2)^{\frac{1}{2}} \end{aligned} \tag{A - 16}$$

Denoting the value of x corresponding to (X_d, Y_d) by x_d, from the assumption concerning Y_d mentioned above, x_d is given by

$$x_d = \frac{\eta_o - \eta}{\eta_o - 1}\psi \tag{A - 17}$$

From the condition that the ellipse given by Eq. A-15 intersects with the circle at $x = x_d$, A^2 is obtained as

$$A^2 = \frac{\psi^2 - x_d^2}{\psi^2 - x_d^2/\eta^2} \qquad (A - 18)$$

Consequently y is given by

$$y = \eta \sqrt{\psi^2 - \frac{\psi^2 - x_d^2/\eta^2}{\psi^2 - x_d^2}(\psi^2 - x^2)} \qquad (A - 19)$$

In case of vacuole formation the volume of the region enclosed by the broken lines and the two horizontal lines passing through the upper and lower ends in Fig. 3 is not the same as that of the original cylinder. The increase in the enclosed volume is the difference between the volume of the shaded regions of the vacuoles and the corresponding volume of the sphere. The ratio of enclosed volume, μ, after the necessary calculations is given by

$$\mu = 1 + \frac{\eta}{3}\left[\frac{2\psi^2}{\psi + \sqrt{\psi^2 - (\psi^2 - \frac{x_d^2}{\eta^2})\frac{\psi^2 - x^2}{\psi^2 - x_d^2}}} - \sqrt{\psi^2 - (\psi^2 - \frac{x_d^2}{\eta^2})\frac{\psi^2 - x^2}{\psi^2 - x_d^2}} \right] / (1 - x)$$

$$- \frac{1}{3} \frac{(\psi-x)(2\psi+x)}{(1-x)(\psi+x)} \qquad \text{(A - 20)}$$

in the range $x_d < x < \psi$. At $x=x_d$, the value of μ, denoted by μ_d, becomes

$$\mu_d = 1 + \frac{1}{3}\left[\frac{(2\eta\psi+x_d)(\eta\psi-x_d)}{(\eta\psi+x_d)(1-x_d)} - \frac{(2\psi+x_d)(\psi-x_d)}{(\psi+x_d)(1-x_d)} \right] \qquad \text{(A - 21)}$$

In the range, $0 \leqq x \leqq x_d$ ($R_d \leqq R \leqq a$), the absolute value of the increase of enclosed volume is constant and is given by

$$2\pi b^3 (1 - x_d)(\psi^2 - x_d^2)\mu_d$$

Since the original value of the enclosed volume at a certain x is

$$2\pi b^3 (1 - x)(\psi^2 - x^2)$$

the ratio of enclosed volume, μ, is given, in the range, $0 \leqq x \leqq x_d$ by

$$\mu = 1 + (\mu_d - 1) \frac{(1-x_d)(\psi^2-x_d^2)}{(1-x)(\psi^2-x^2)} \qquad 0 \leqq x \leqq x_d \qquad \text{(A - 22)}$$

Similarly, in the range, $a < R < c$, μ is given by

$$\mu = 1 + (\mu_d - 1)\frac{(1-x_d)(\psi^2 - x_d^2)}{\psi^2}\frac{a^2}{R^2} \qquad a < R < c \qquad (A-23)$$

Eqs. A-20, A-22 and A-23 give all the information needed for the value of μ. Corresponding to Eqs. A-20, A-22, and A-23 the internal stretch ratios in these three regions are given by

$$\begin{aligned} \lambda' &= \frac{\lambda - y}{1 - x} && x_d < x \leqq \psi \quad (0 \leqq R < R_d) \\ \lambda' &= \frac{\lambda - x}{1 - x} && 0 \leqq x \leqq x_d \quad (R_d \leqq R \leqq a) \\ \lambda' &= \lambda && a \leqq R \leqq c \end{aligned} \qquad (A-24)$$

The total strain energy is obtained by carrying out the integration in Eq. 2-32. However, in this case, the interval of integration must be divided into three ranges,

$$W = 2\pi\int_0^{R_d} W_{IN,d} R\ell_o \, dR + 2\pi\int_{R_d}^{a} W_{IN,nd} R\ell_o \, dR + 2\pi b\int_a^c W_{OUT} R \, dR \qquad (A-25)$$

where $W_{IN,d}$, $W_{IN,nd}$, and W_{OUT} are the strain energy in dewetted, non-dewetted, and outer shell regions, respectively. These are given by the same form as Eq. 2-37,

$$W_N = \sum_{i,j=0}^{\infty} C_{ij} W_{1,N}^{\,i} W_{2,N}^{\,j} \qquad (A-26)$$

where the subscript N is a dummy to be replaced by, IN, d, IN, nd, and OUT, respectively, corresponding to each case. Constants and functions needed in the calculations are summarised in Table I.

The integrations can be carried out numerically.

Appendex 3. Ratio of Enclosed volume

Consider an ellipse described in a rectangular coordinate system, (X, Y), by

$$\frac{X^2}{A^2} + \frac{Y^2}{\eta^2} = a^2 \qquad \text{(A - 27)}$$

If the ellipse intersects a circle of radius, a, with the center on the origin at a point (X_d, Y_d), X_d and Y_d will satisfy the following simultaneous equations,

$$\frac{X_d^2}{A^2} + \frac{Y_d^2}{\eta^2} = a^2$$

$$X_d^2 + Y_d^2 = a^2 \qquad \text{(A - 28)}$$

We introduce a new coordinate system (x, y) which is related to (X, Y) by

$$Y = by$$

$$X = b(\psi^2 - x^2) \qquad \text{(A - 29)}$$

Geometrically, x is the normalized distance of a point on the circle from the X-axis given by $\psi \cos\theta$ and y is defined as the

ratio between the distance of a pair of points on the ellipse and the circle with the same X-coordinate and $\psi = a/b$. Substituting Eq. A - 29 into Eq. A - 27, we obtain

$$\frac{\psi^2 - x^2}{A^2} + \frac{y^2}{\eta^2} = \psi^2 \qquad \text{(A - 30)}$$

The circle is given by

$$y = x \qquad \text{(A - 31)}$$

The simultaneous equations A-28 are converted to

$$\frac{\psi^2 - x_d^2}{A^2} + \frac{y_d^2}{\eta^2} = \psi^2$$

$$y_d = x_d \qquad \text{(A - 32)}$$

The internal stretch ratio, λ', is given by

$$\lambda' = \frac{\lambda - y}{1 - x} \qquad \text{(A - 33)}$$

from the definitions of x and y, because the original distance between the facing circles at a certain value of x is

$$2(b - bx)$$

and the length after deformation is

$$2(\lambda b - by)$$

From Eq. A-29, y is $\eta\psi$ at $x = \psi$ $(X = 0)$. While the internal stretch ratio, λ', is given by $(\lambda - \eta\psi)/(1 - \psi)$ at $x = \psi$, and the value decreases as η increases, λ' must be positive for obvious reasons. When $\lambda' = 0$, $\eta\psi = \lambda$ or $\eta = \lambda/\psi$. Since the minimum value of η is obviously 1, η could vary at most from 1 to λ/ψ. If we assume that the profile of a vacuole is expressed by the ellipse of Eq. A-27 and that the value of x at the point of contact with the surface of the sphere, x_d, linearly decreases from ψ to 0 as η increases from 1 to η_o $(=\lambda/\psi)$. x_d is given by

$$x_d = \frac{\eta_o - \eta}{\eta_o - 1}\psi \qquad (A - 34)$$

Eliminating y_d from Eqs. A-33 and solving it for A^2. we obtain

$$A^2 = \frac{\psi^2 - x_d^2}{\psi^2 - x_d^2/\eta^2} \qquad (A - 35)$$

Substituting Eq. A-35 into Eq. A-30, y is obtained, after re-arrangement, as

$$y = \eta \sqrt{\psi^2 - \frac{\psi^2 - \frac{x_d^2}{\eta^2}}{\psi^2 - x_d^2}(\psi^2 - x^2)} \qquad (A - 36)$$

While the nature of a vacuole is described by Eqs. A-35 and A-33. the volume of the region enclosed by the surface, the profile of which is shown by the broken lines in Fig. 3 and the two horizontal planes on both ends, increases as the system is stretched and/or the size of the vacuole increase. The region was originally a circ ular cylinder of radius, R, and length, $2\ell_o$. The amount of increase of the volume is the same as the difference between the part of the vacuoles represented by the shaded area and the corresponding portion of the spheres in Fig. 3. The original volume of the cylinder, V_o, is obtained from geometrical relations.

$$V_o = 2\pi R^2 \ell_o = 2\pi b^3 (\psi^2 - x^2)(1 - x) \qquad (A - 37)$$

The volume of the shaded region of the vacuoles, V_a is computed by carrying out the integration $\int_Y^{\eta a} X^2 dY$. The result of the computation is

$$V_a = 2\pi b^3 \frac{\psi^2 - x^2}{3} \eta \left[\frac{2\psi^2}{\psi + \sqrt{\psi^2 - (\psi^2 - \frac{x_d^2}{\eta^2}) \frac{\psi^2 - x^2}{\psi^2 - x_d^2}}} - \sqrt{\psi^2 - (\psi^2 - \frac{x_d^2}{\eta^2}) \frac{\psi^2 - x^2}{\psi^2 - x_d^2}} \right] \qquad (A - 38)$$

The corresponding part of the spheres, V_{ao}, is calculated similarly to give

$$V_{ao} = \frac{2\pi b^3}{3} (\psi - x)^2 (2\psi + x)$$

The ratio of enclosed volume, μ, is obtained from the definition,

$$\mu = 1 + \frac{V_a - V_{ao}}{V_o}$$

$$= 1 + \frac{\eta}{3}\left[\frac{2\psi^2}{\psi + \sqrt{\psi^2 - (\psi^2 - \frac{x_d^2}{\eta^2})\frac{\psi^2 - x^2}{\psi^2 - x_d^2}}} - \sqrt{\psi^2 - (\psi^2 - \frac{x_d^2}{\eta^2})\frac{\psi^2 - x^2}{\psi^2 - x_d^2}}\right]$$

$$/(1 - x) - \frac{1}{3}\frac{(\psi^2 - x)(2\psi + x)}{(1 - x)(\psi + x)} \qquad \text{(A - 39)}$$

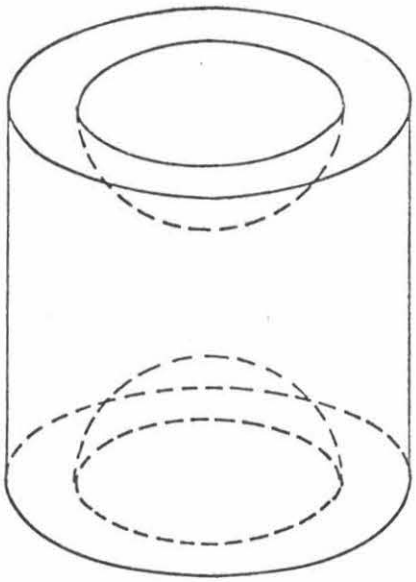

(a)

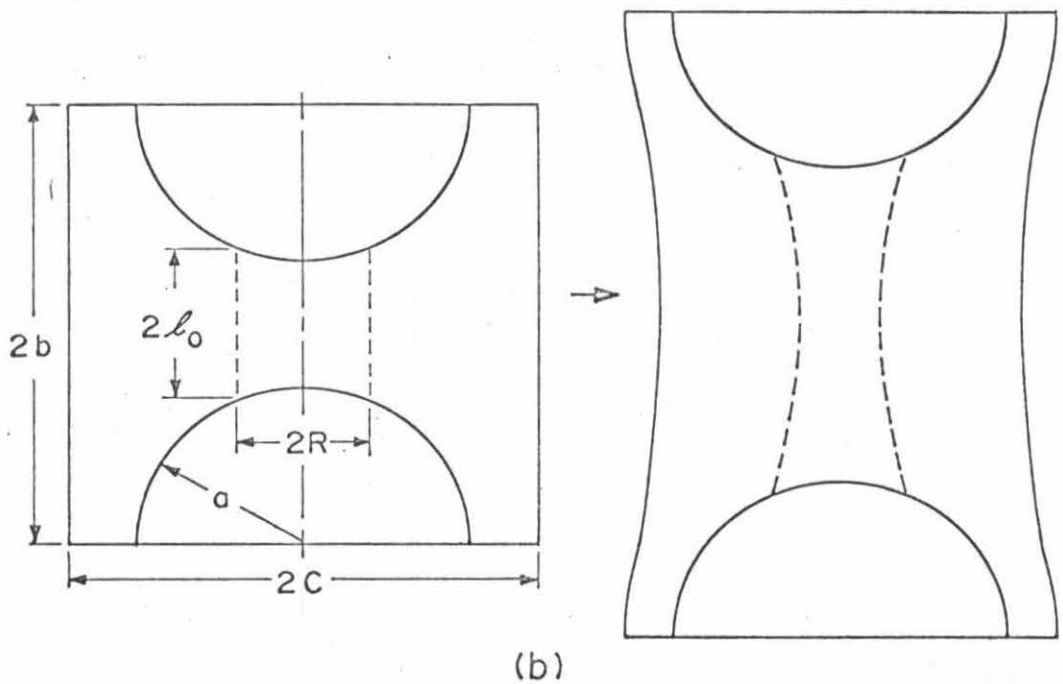

(b)

Fig. 1 Illustration of a Model of Composite Systems

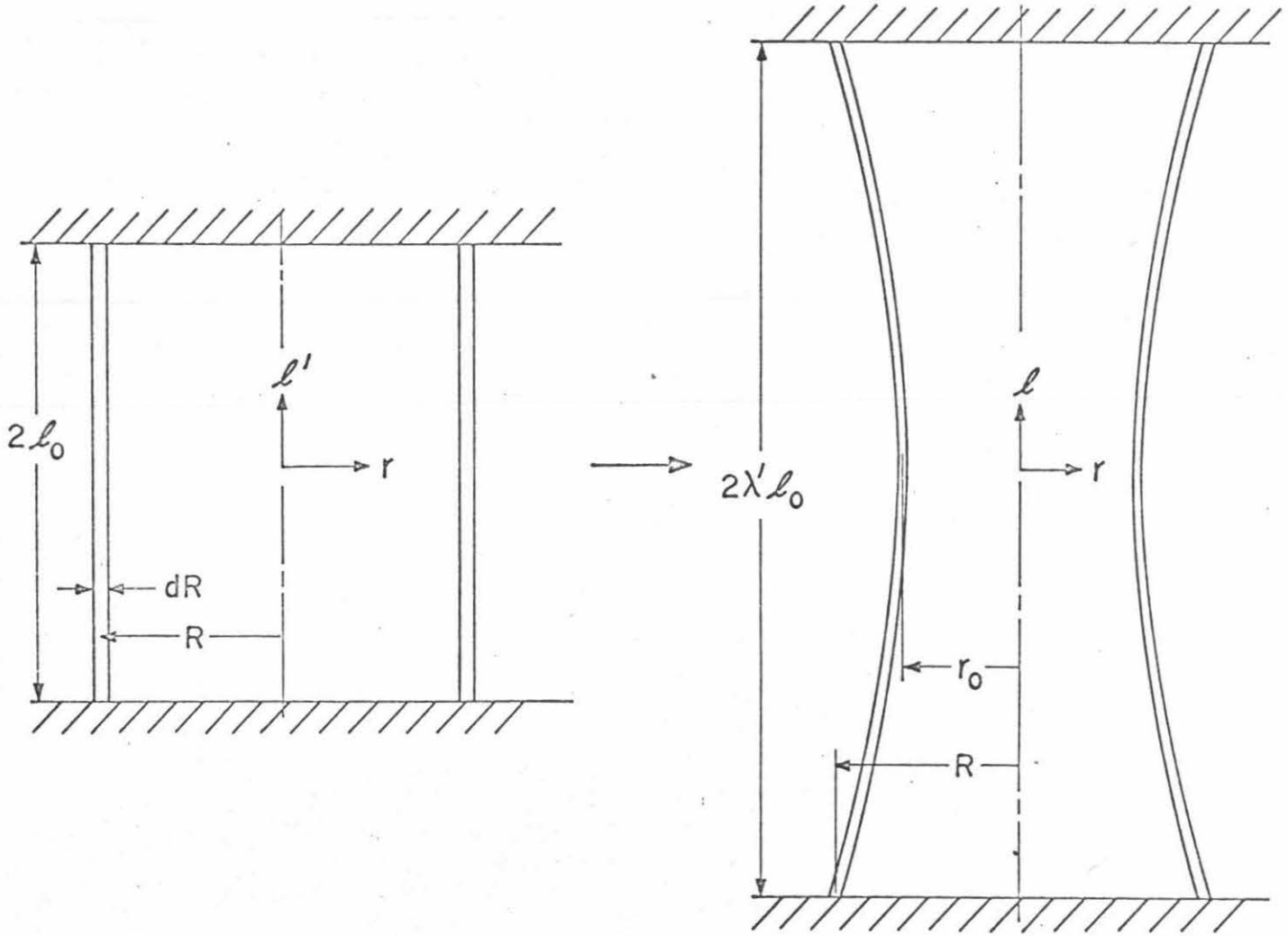

Fig. 2 Schematic Explanation of the Deformation of a Thin-shelled Cylinder

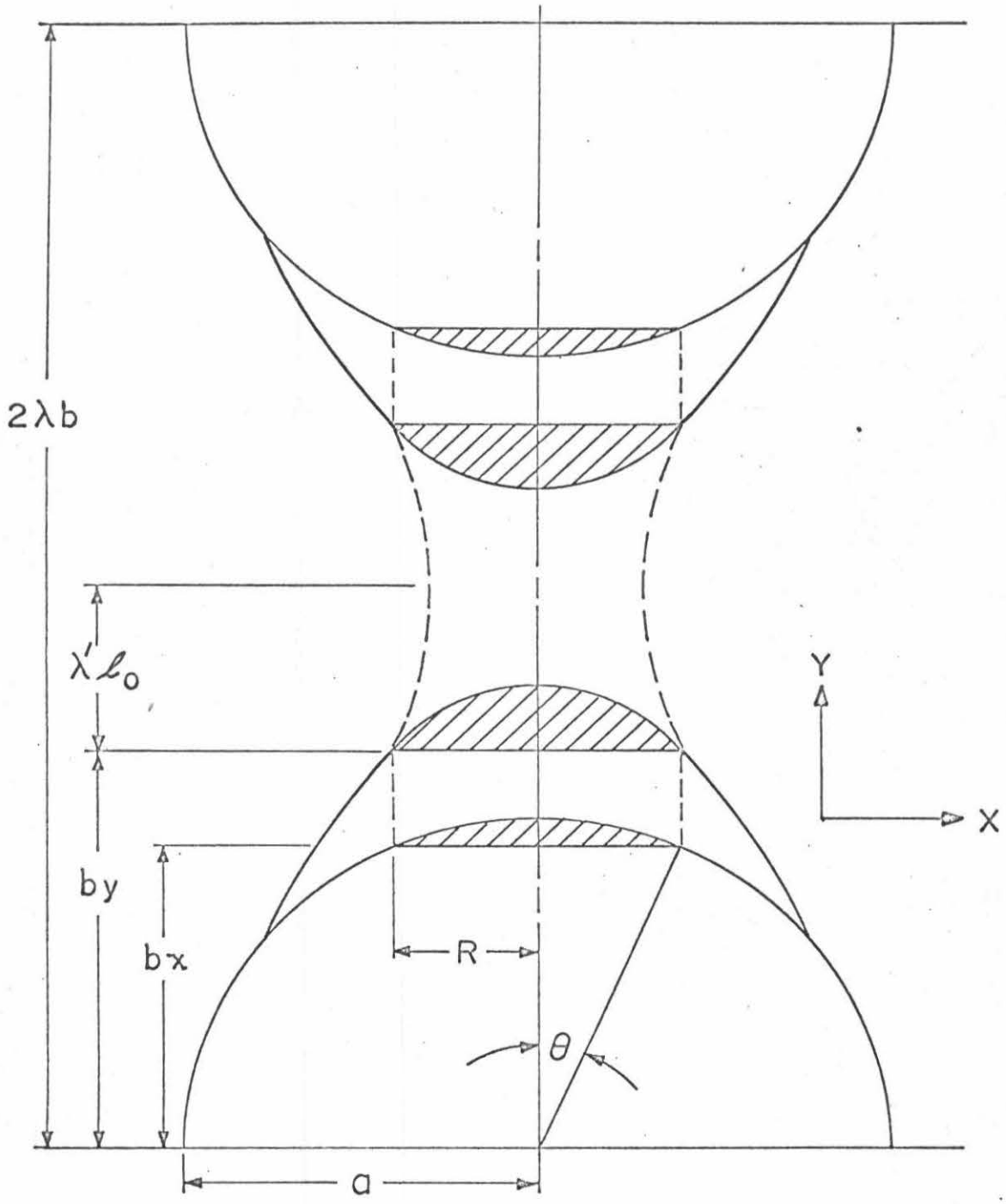

Fig. 3 Schematic Explanation of the Internal Deformation for the Case of Vacuole Formation

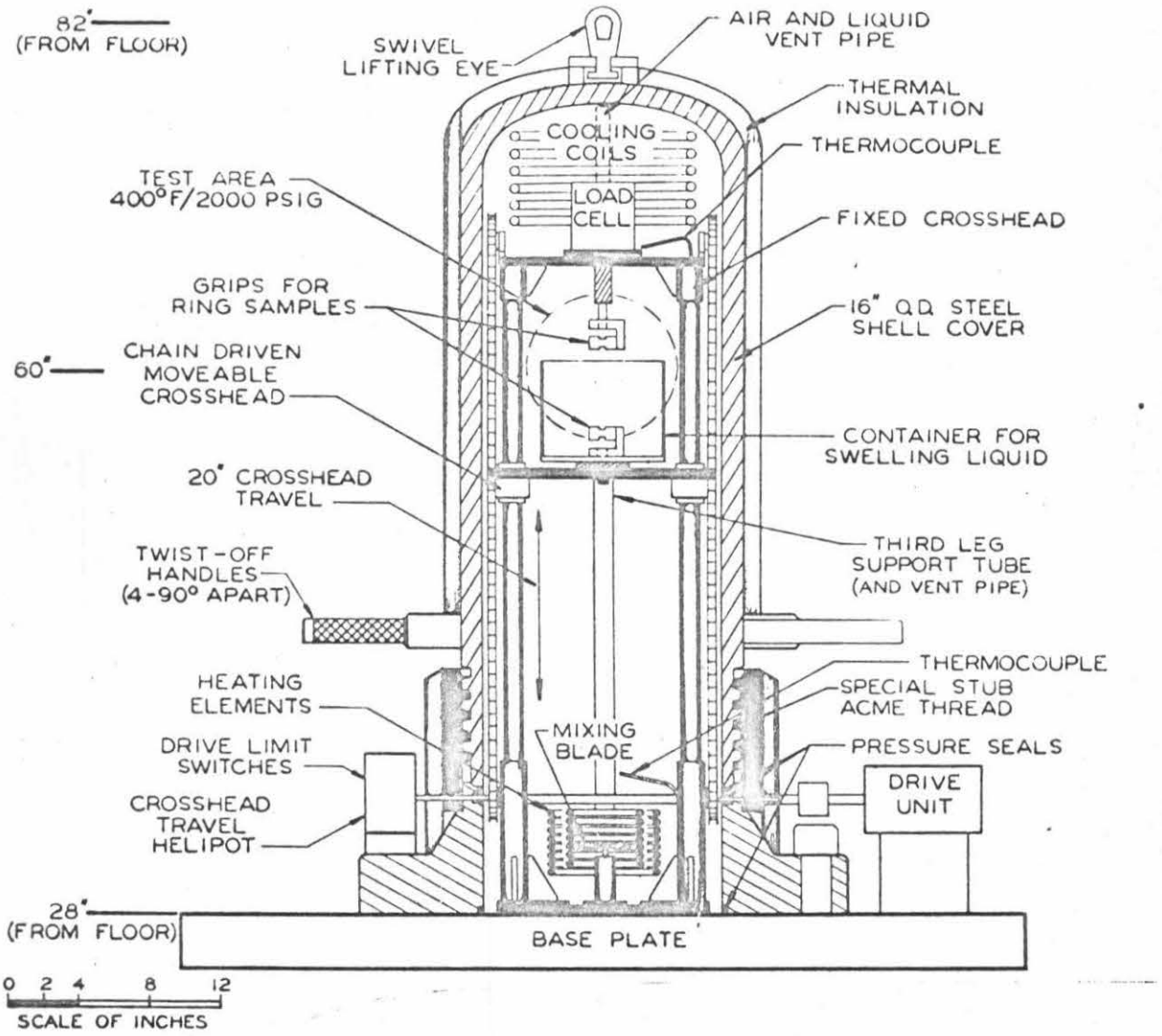

Fig. 4 Schematic of the Pressurized Tensile Tester.

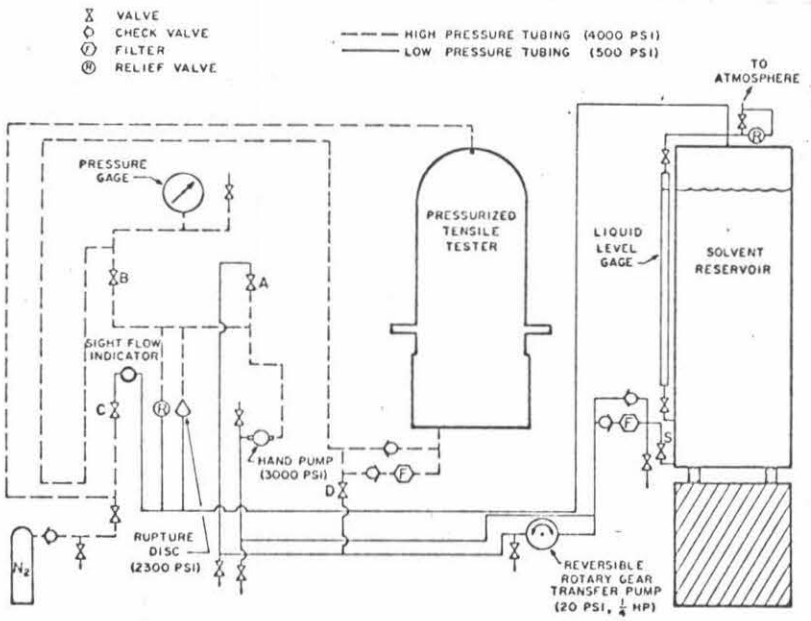

Fig. 5 Piping Schematic for the Pressurized Tensile Tester.

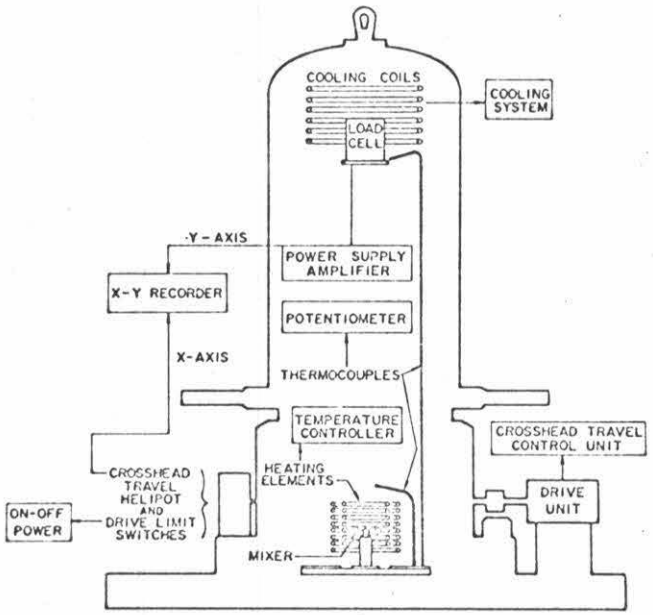

Fig. 6 Electric Schematic for the Pressurized Tensile Tester.

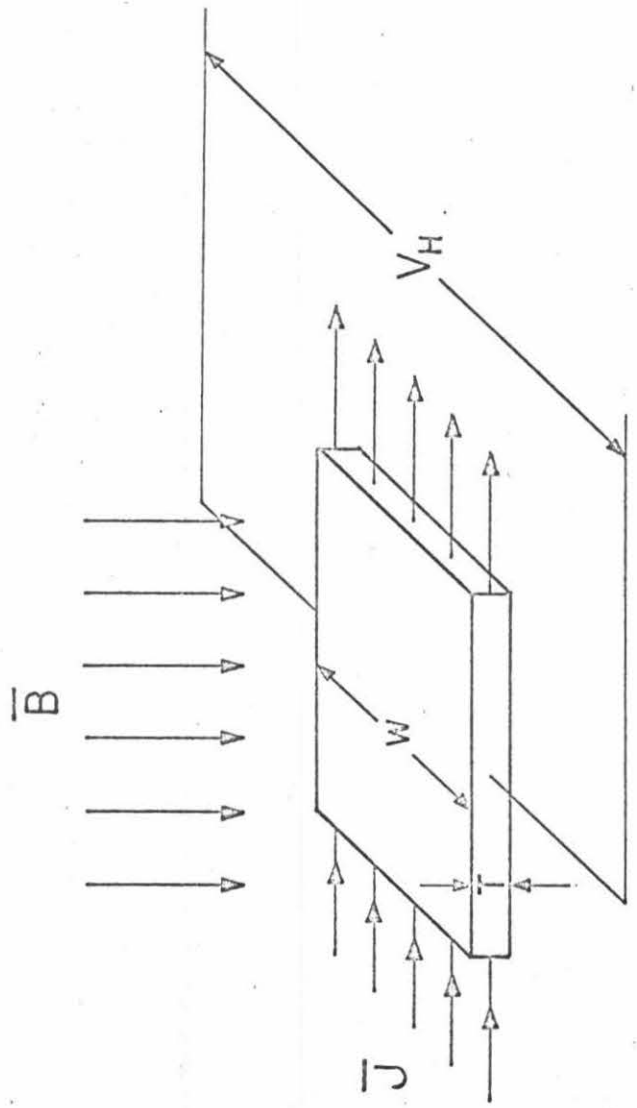

Fig. 7 Schematic Illustraion of Hall Effect

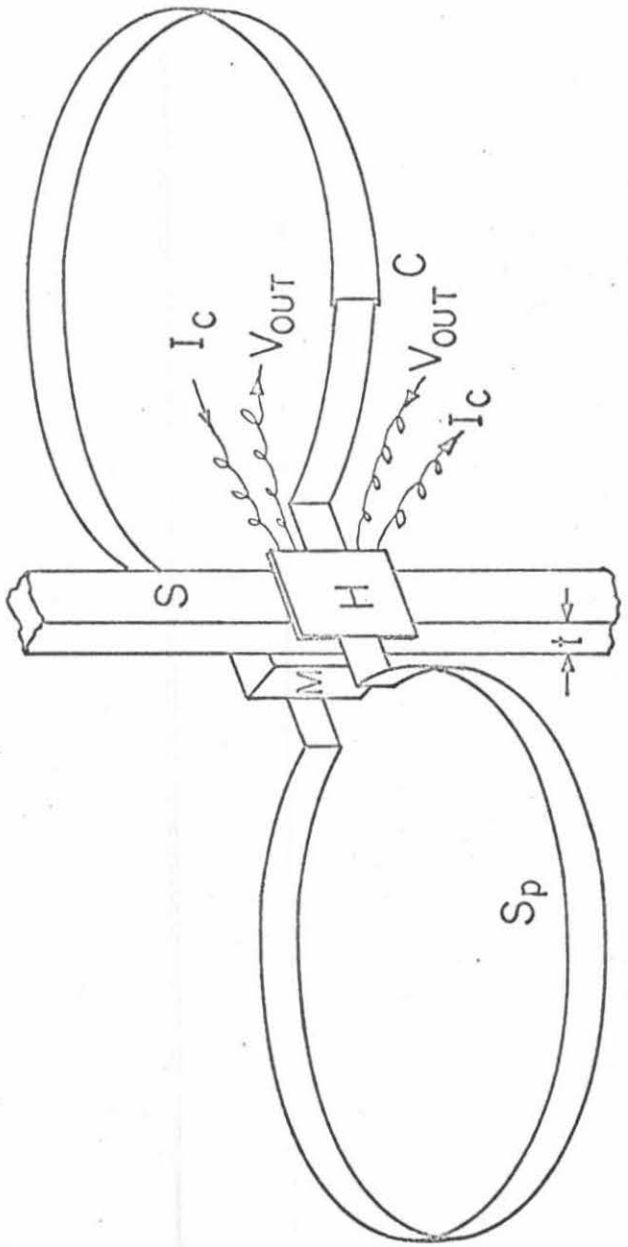

Fig. 8 Schematic of Hall Effect Thcikness Sensor

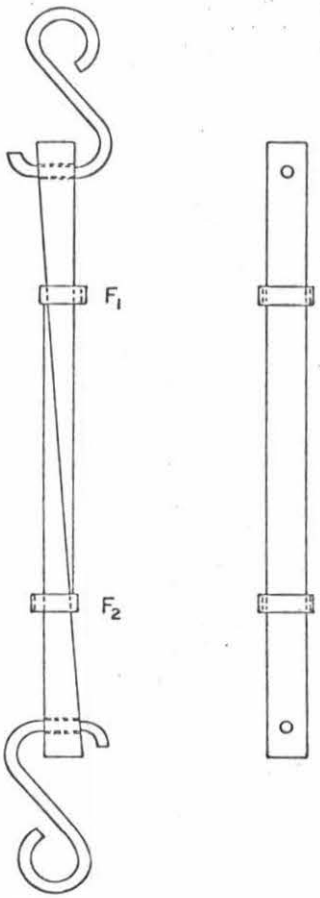

Fig. 9 Sliding Wedge Block Gauge for Calibration of Hall Effect Thickness Sensor.

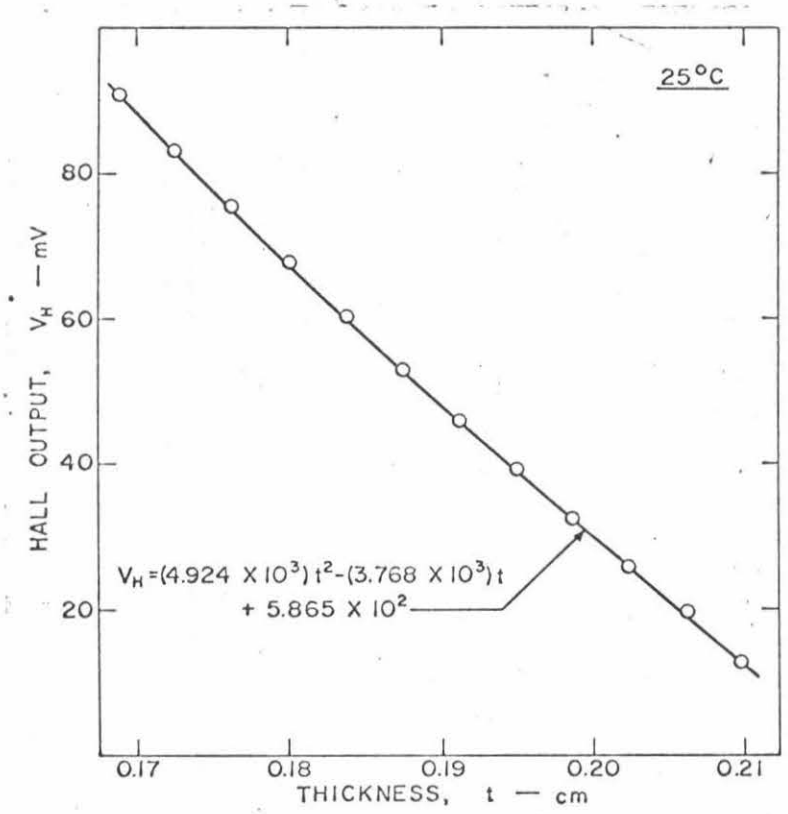

Fig. 10 Typical Calibration Curve for Hall Effcet Thickness Sensor

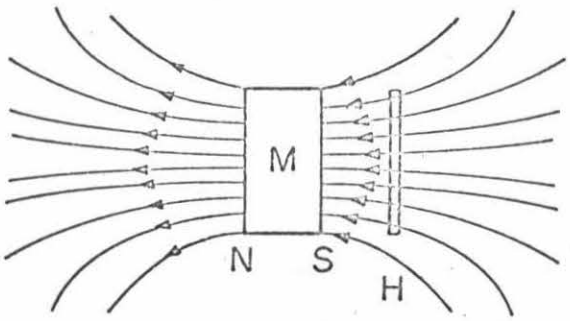

(a)

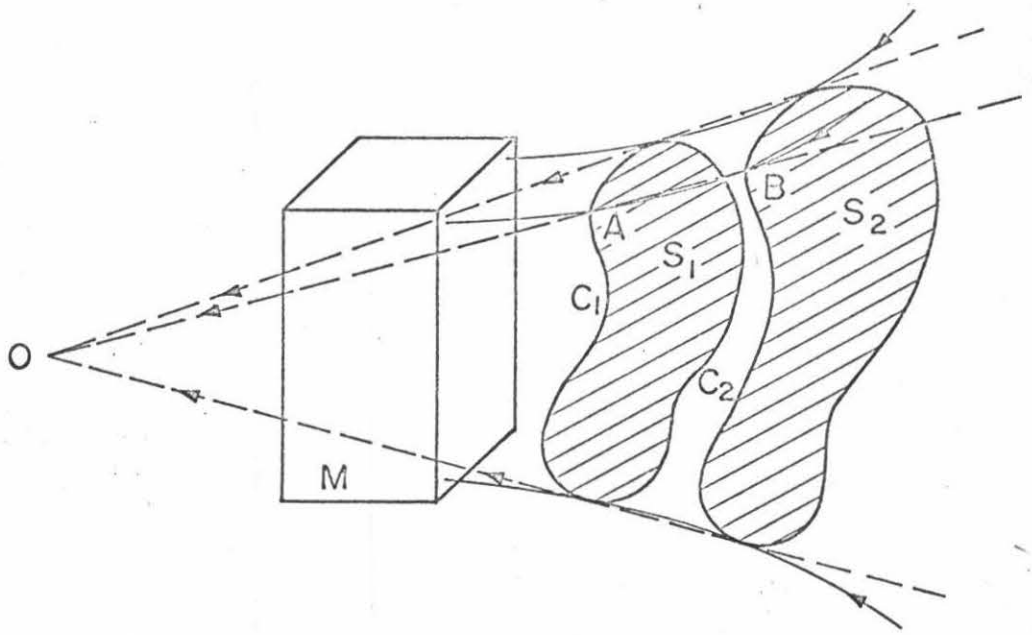

(b)

Fig. 11 Schematic Explanation of Quadratic Dependence of the Hall Output on the Thickness

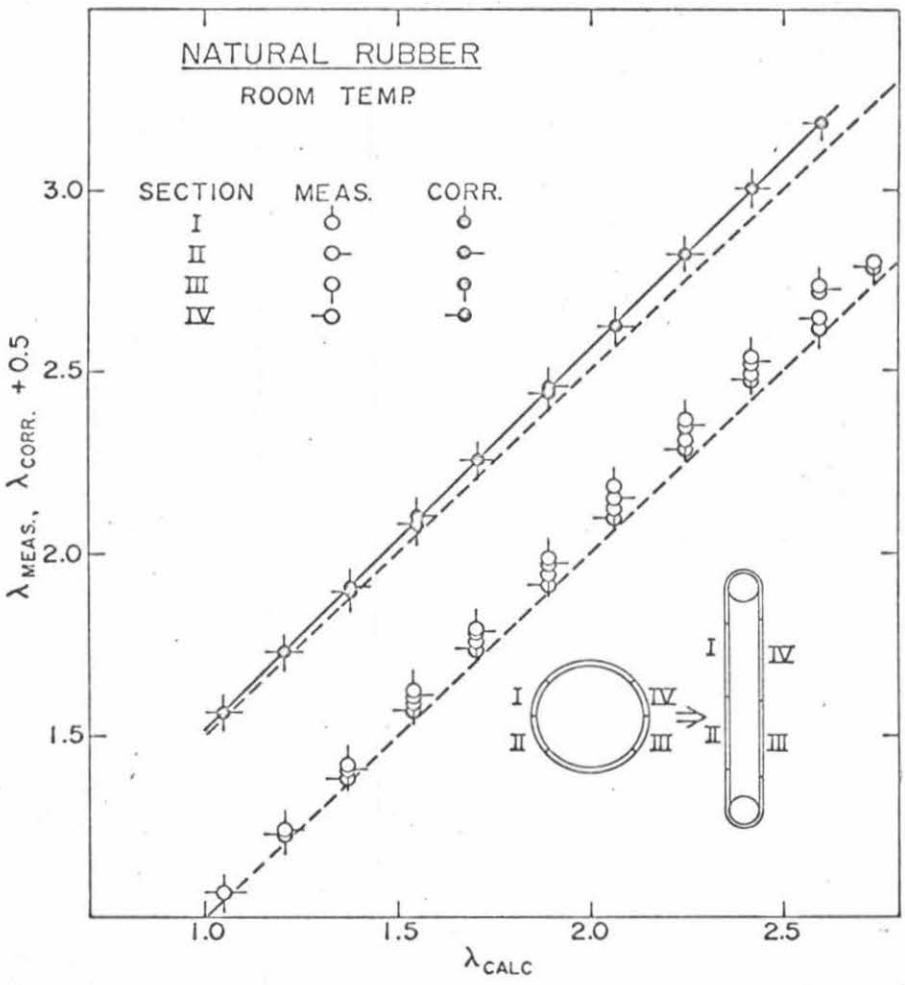

Fig. 12 Measured, and Corrected, Stretch Ratio as Function of Calculated Value.

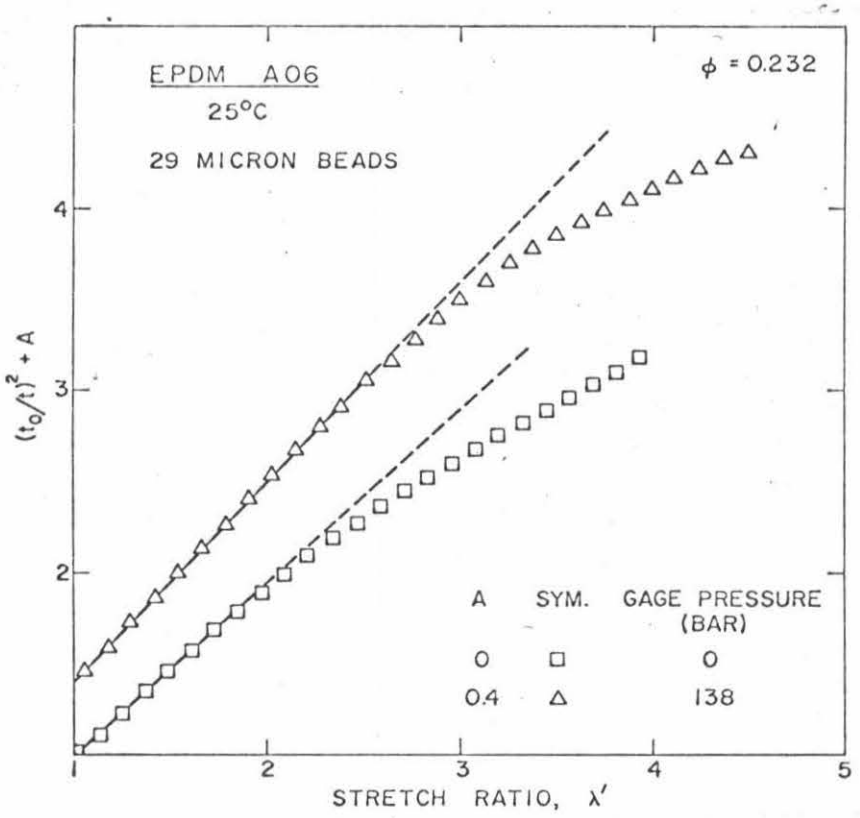

Fig. 13 Reciprocal of the Square of the Lateral Contraction, Measured with the Hall Effect Thickness Sensor as Function of the Stretch Ratio, λ'.

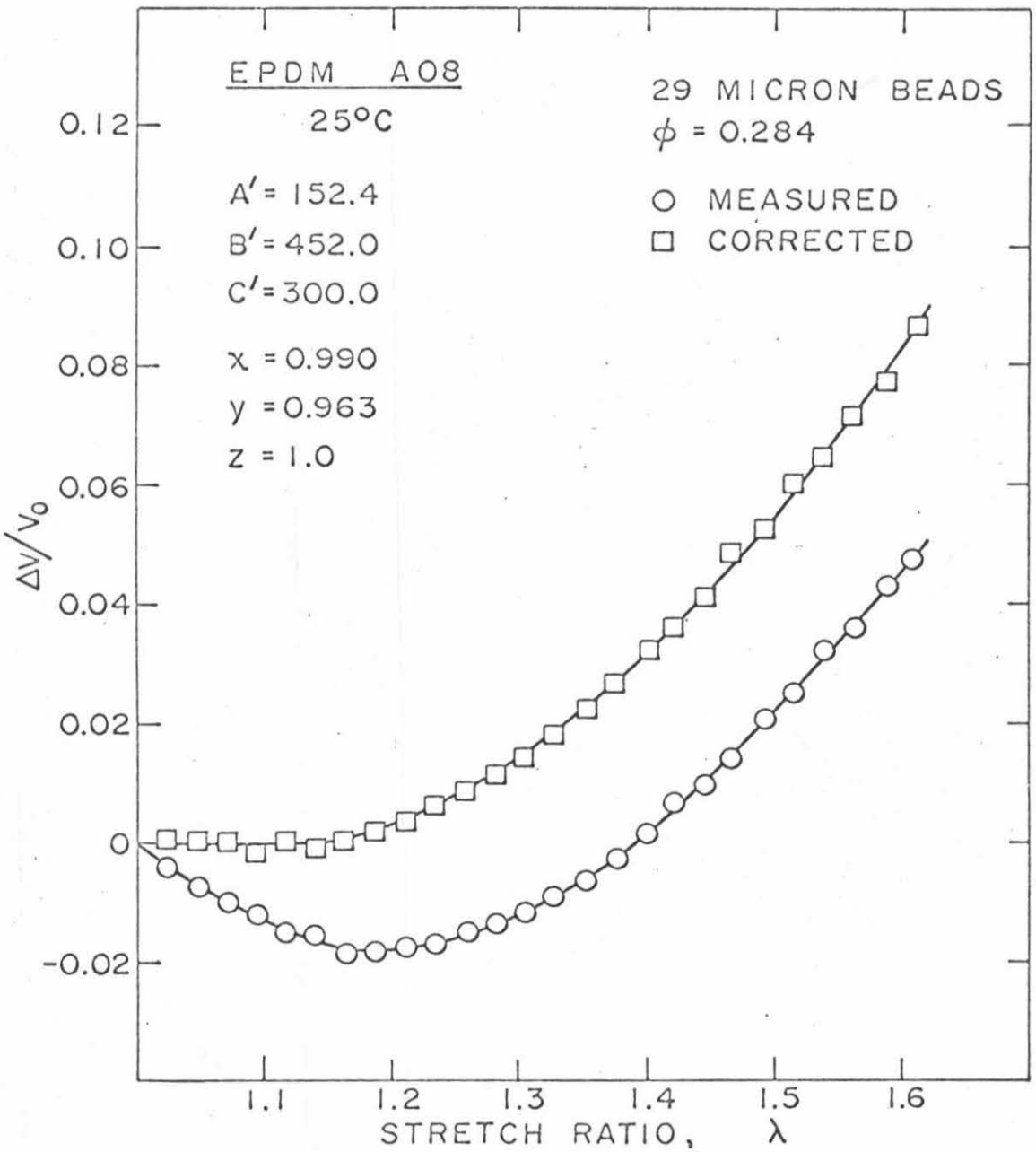

Fig. 14 Volume Change-Stress-Strain Curve. Comparison between the Measured and Corrected Values

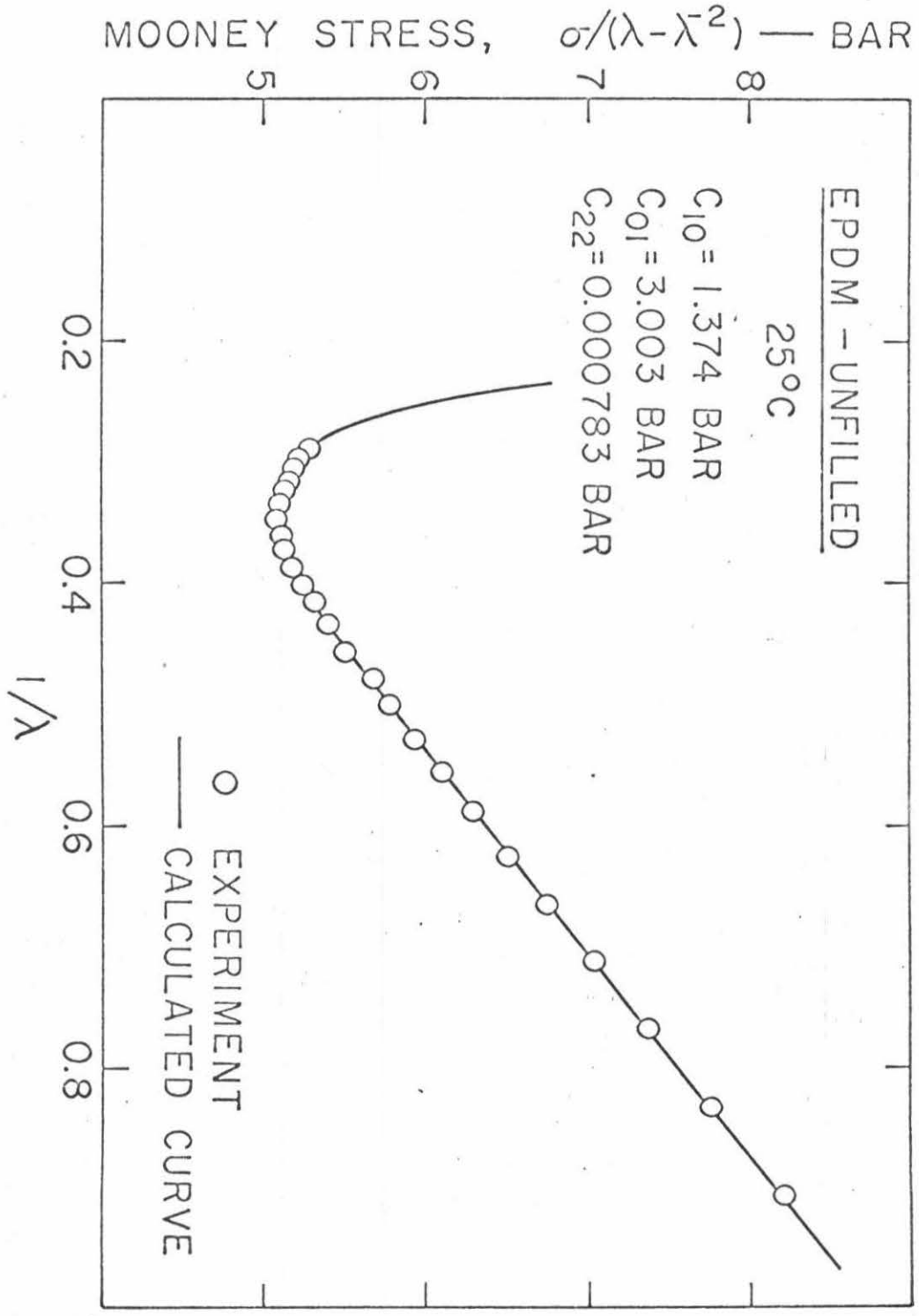

Fig. 15 Mooney-Rivlin Plot of Unfilled EPDM Vulcanizates

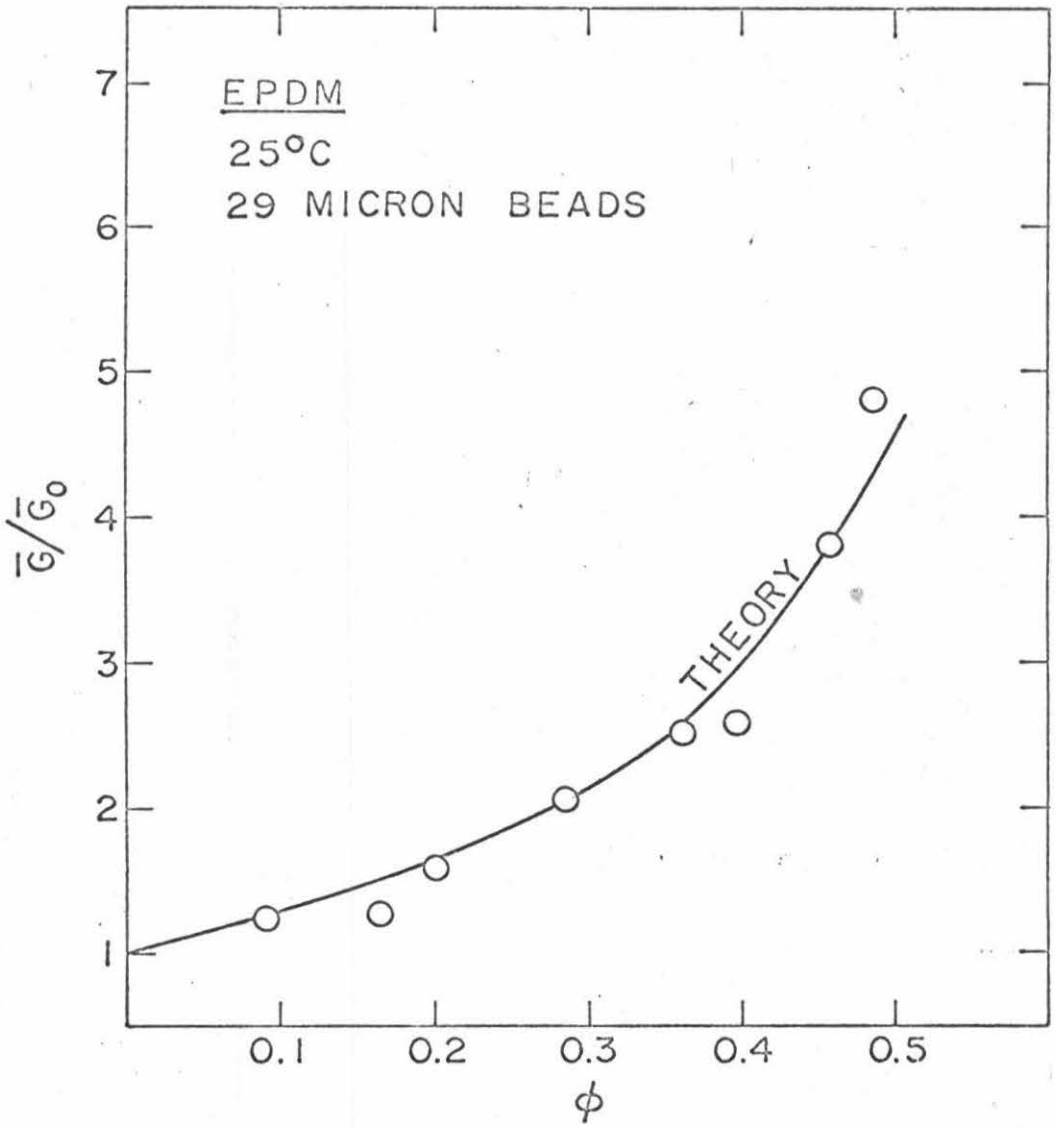

Fig. 16 Initial Moduli of Glass Bead-Filled EPDM Vulcanizates

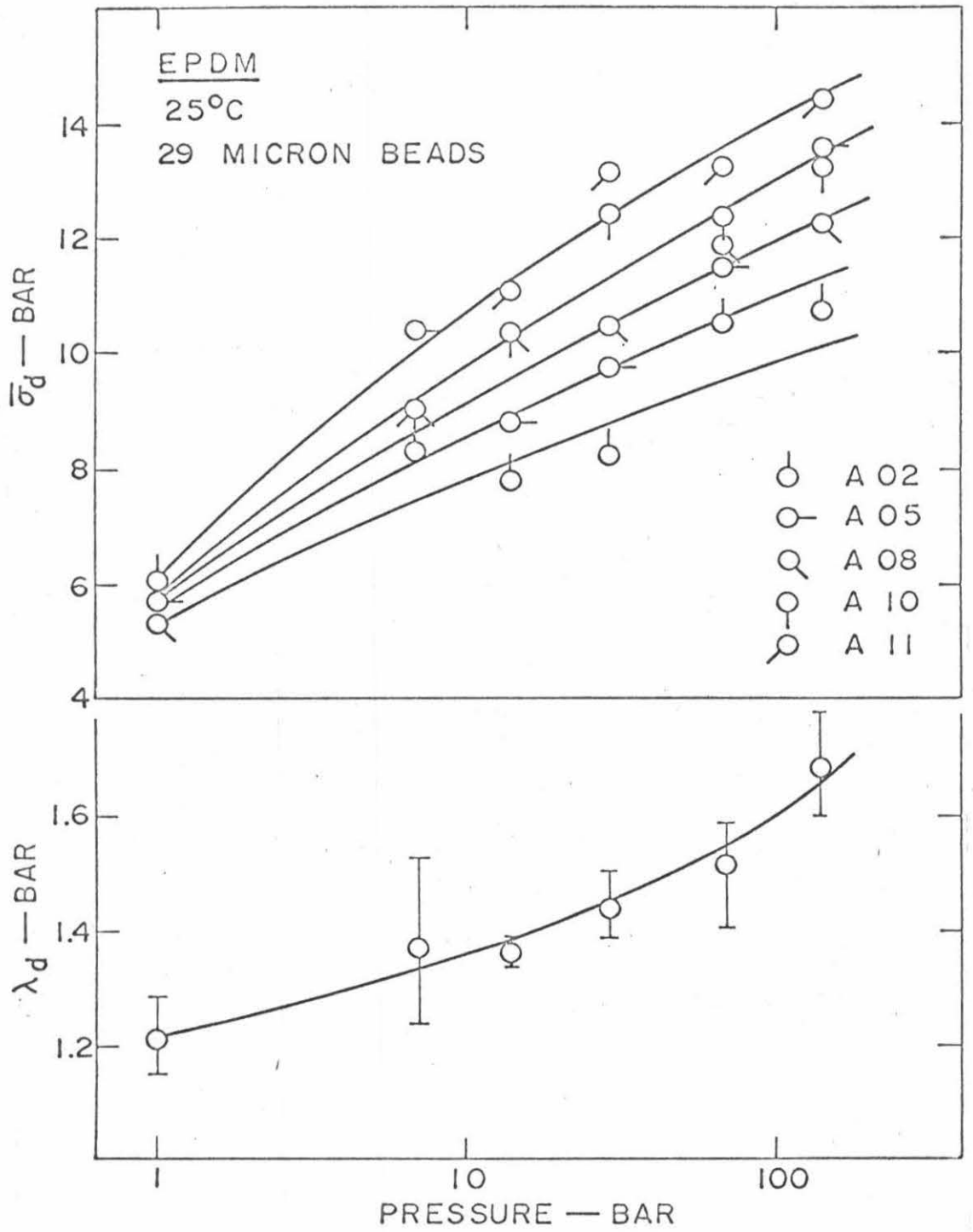

Fig. 17 Dependence of Stretch Ratio and Stress at Dewetting Initiation on Hydrostatic Pressure

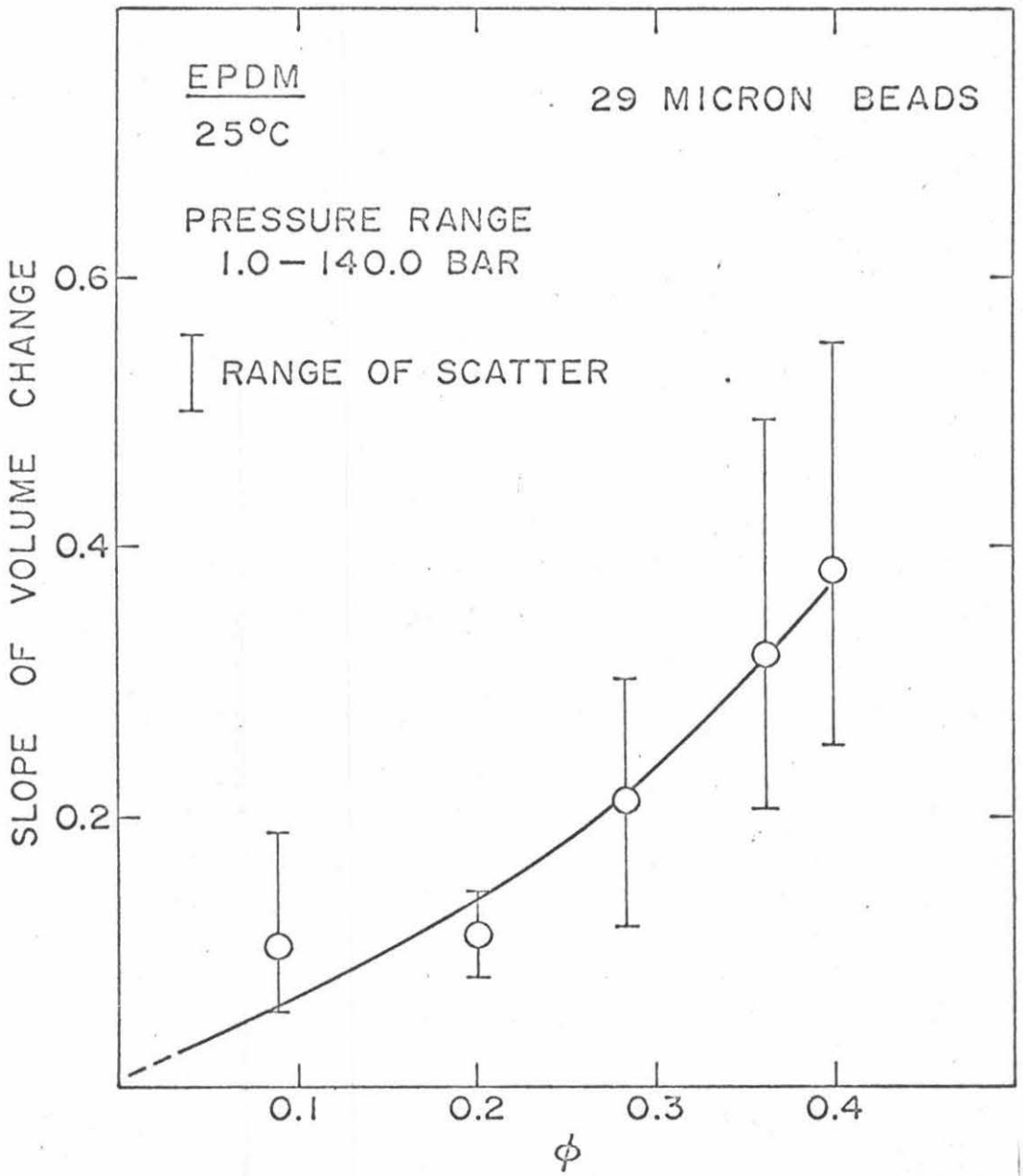

Fig. 18 Dependence of Final Slope of Volume Change-Strain Curve on Volumetric Filler Fraction

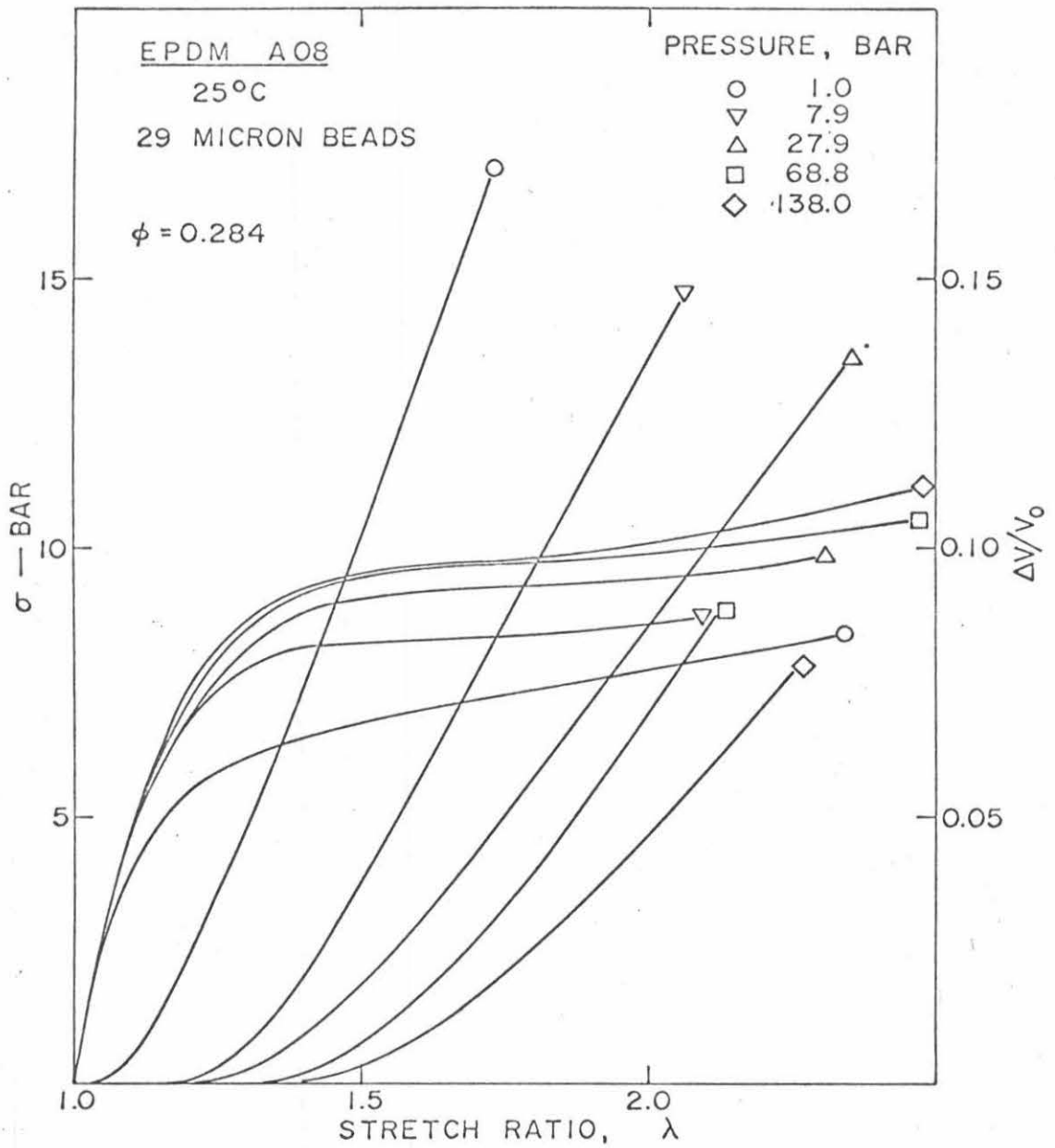

Fig. 19 A Few of Typical Examples of Volume Change-Stress-Strain Curves of Glass Bead-Filled EPDM Vulcanizates

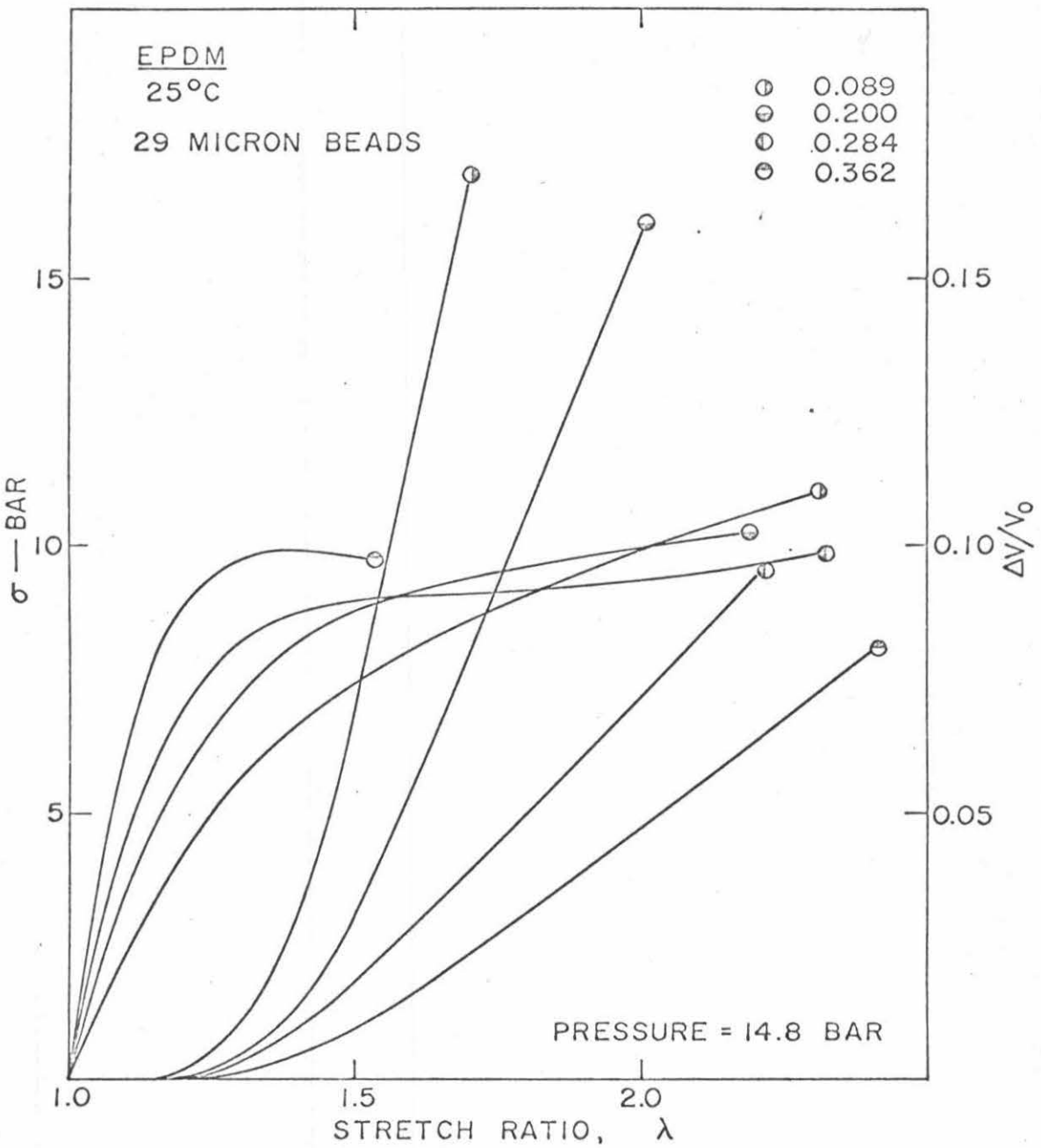

Fig. 20 A Few of Typical Examples of Volume Change-Stress-Strain Curves of Glass Bead-Filled EPDM Vulcanizates

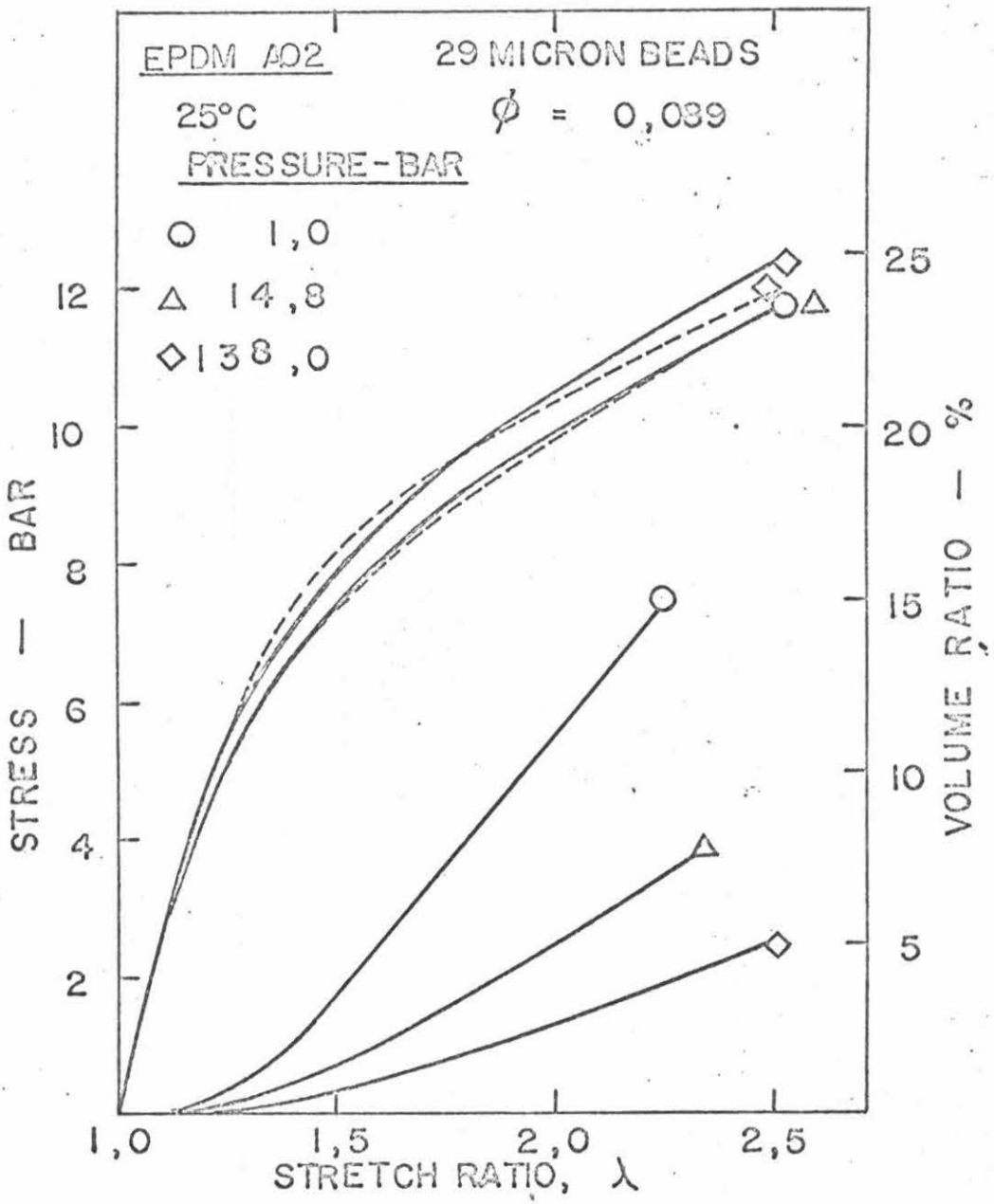

Fig. 21 Volume Change-Stress-Strain Curves of Sample A02. Comparison with Theory

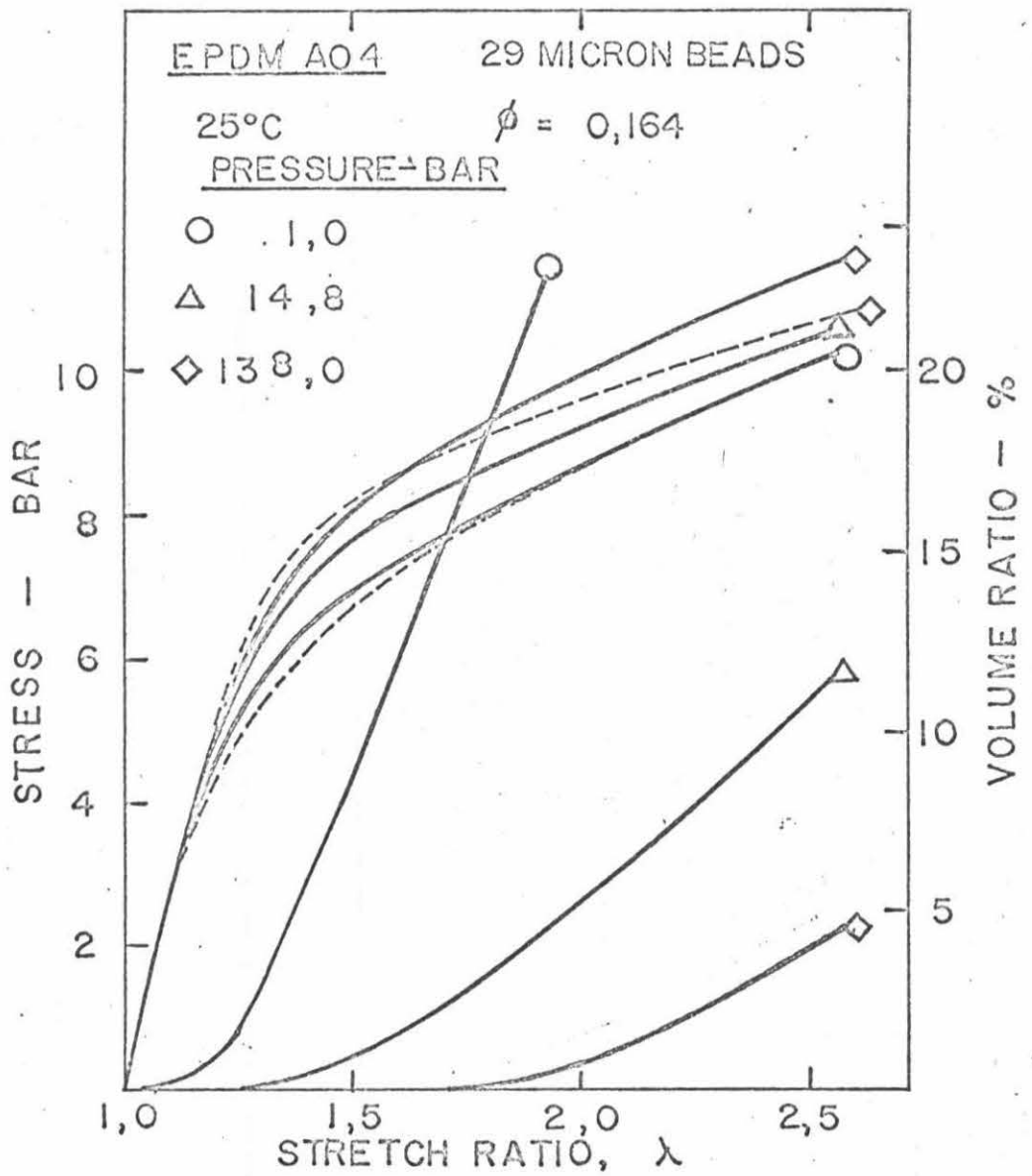

Fig. 22 Volume Change -Stress-Strain Curves of Sample A04. Comparison with Theory

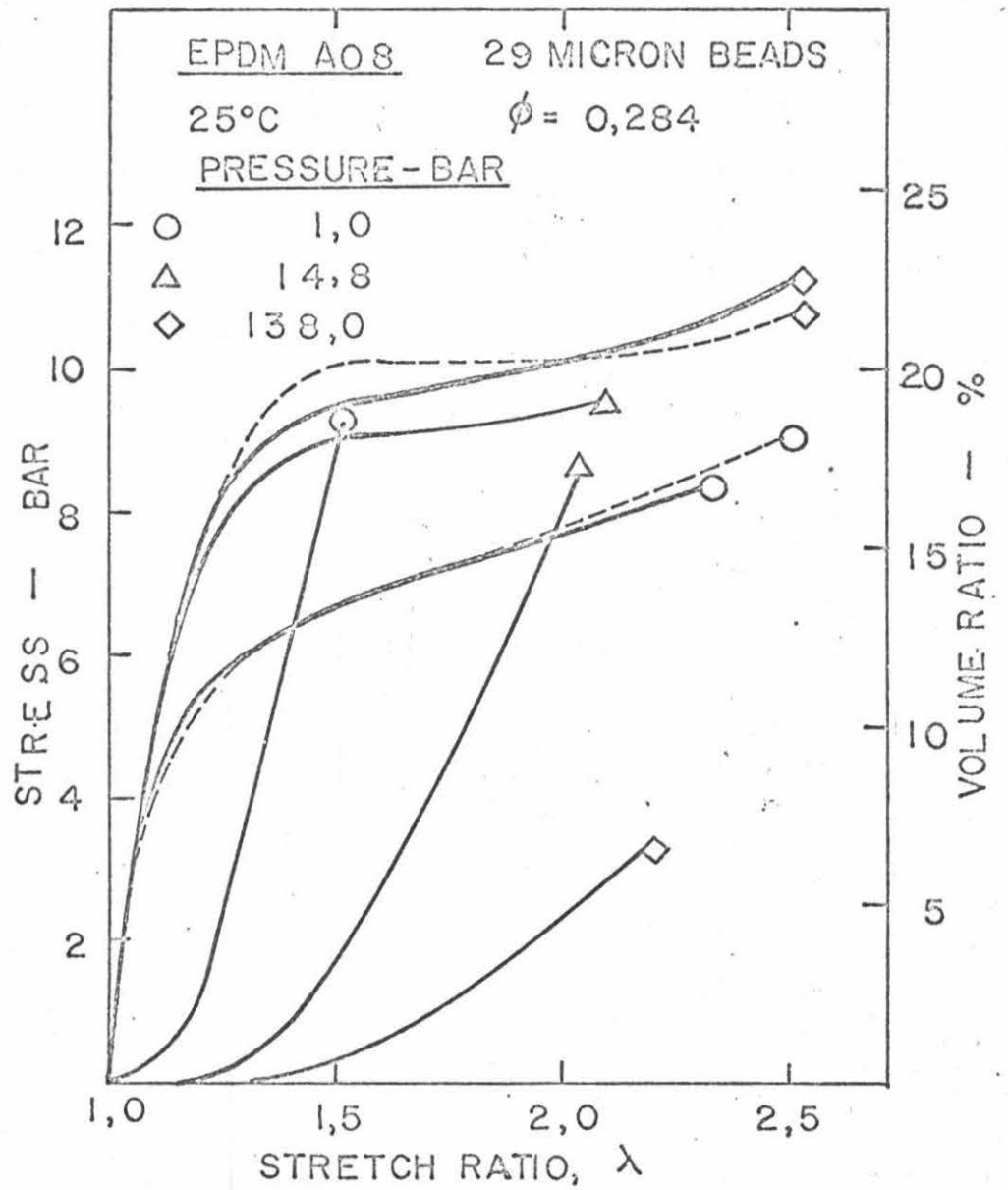

Fig. 23 Volume Change-Stress-Strain Curves of Sample A08 Comparison with Theory

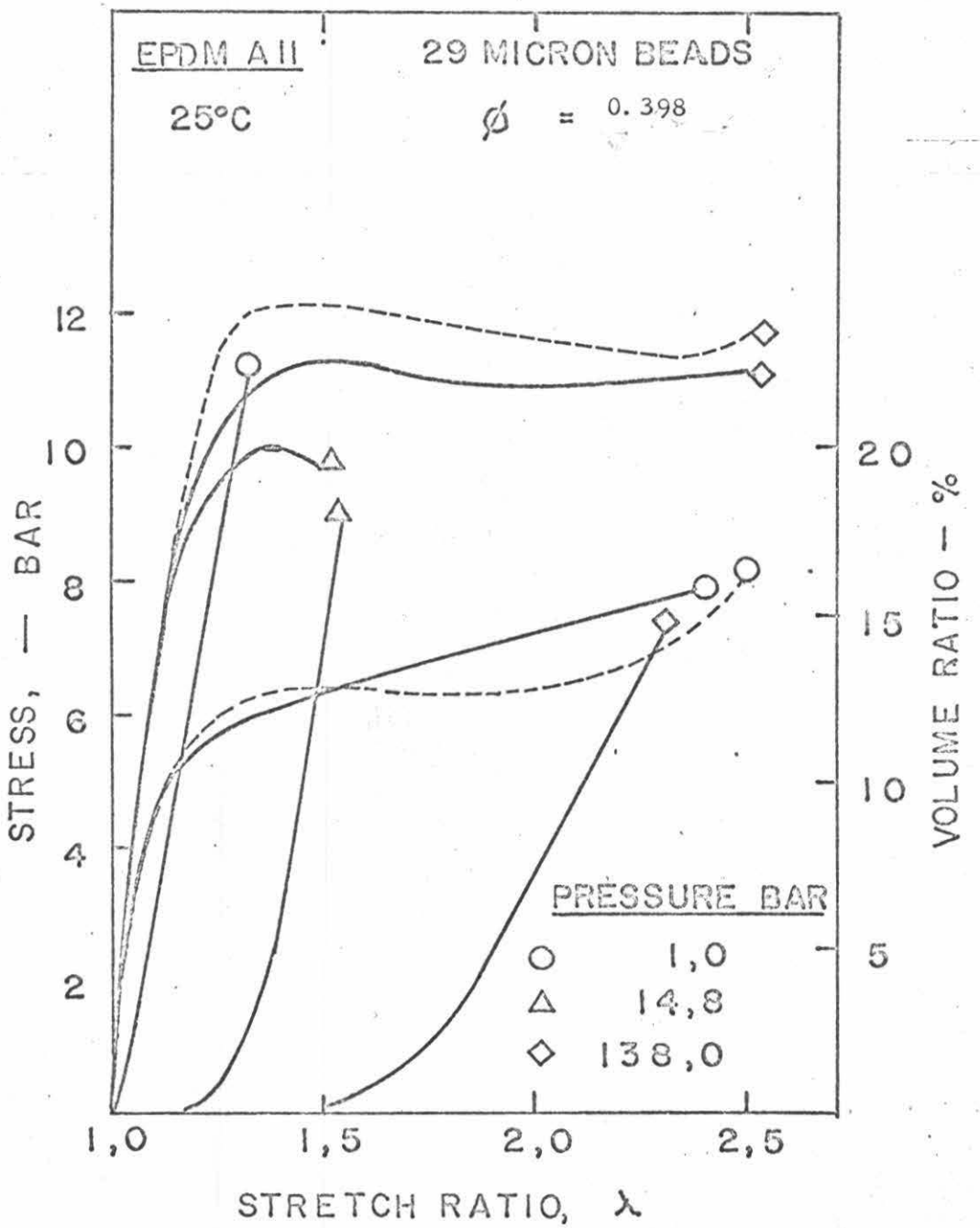

Fig. 24 Volume Change-Stress-Strain Curves of Sample A11. Comparison with Theory

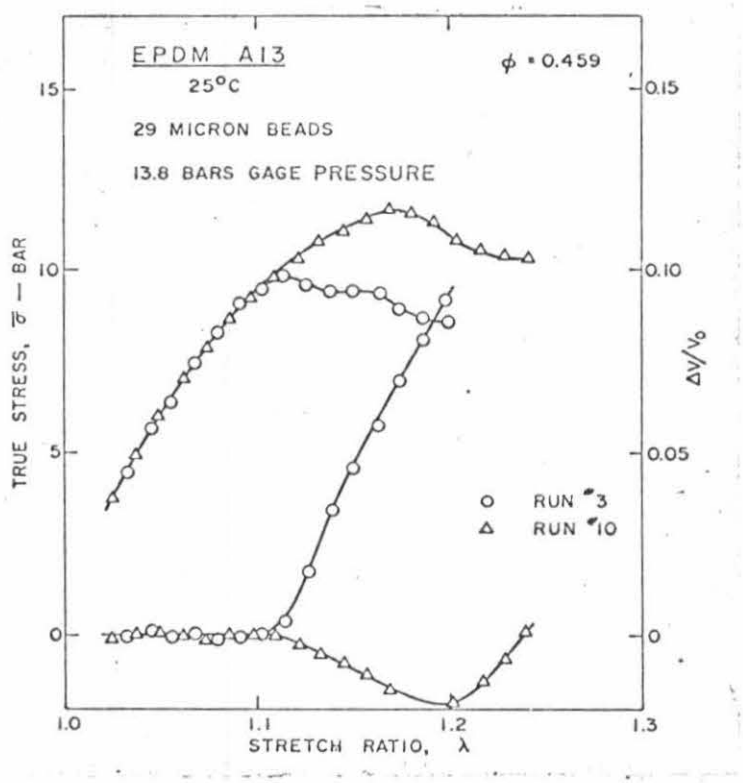

Fig. 25 Example of Abnormal Behavior in Highly Filled Elastomer

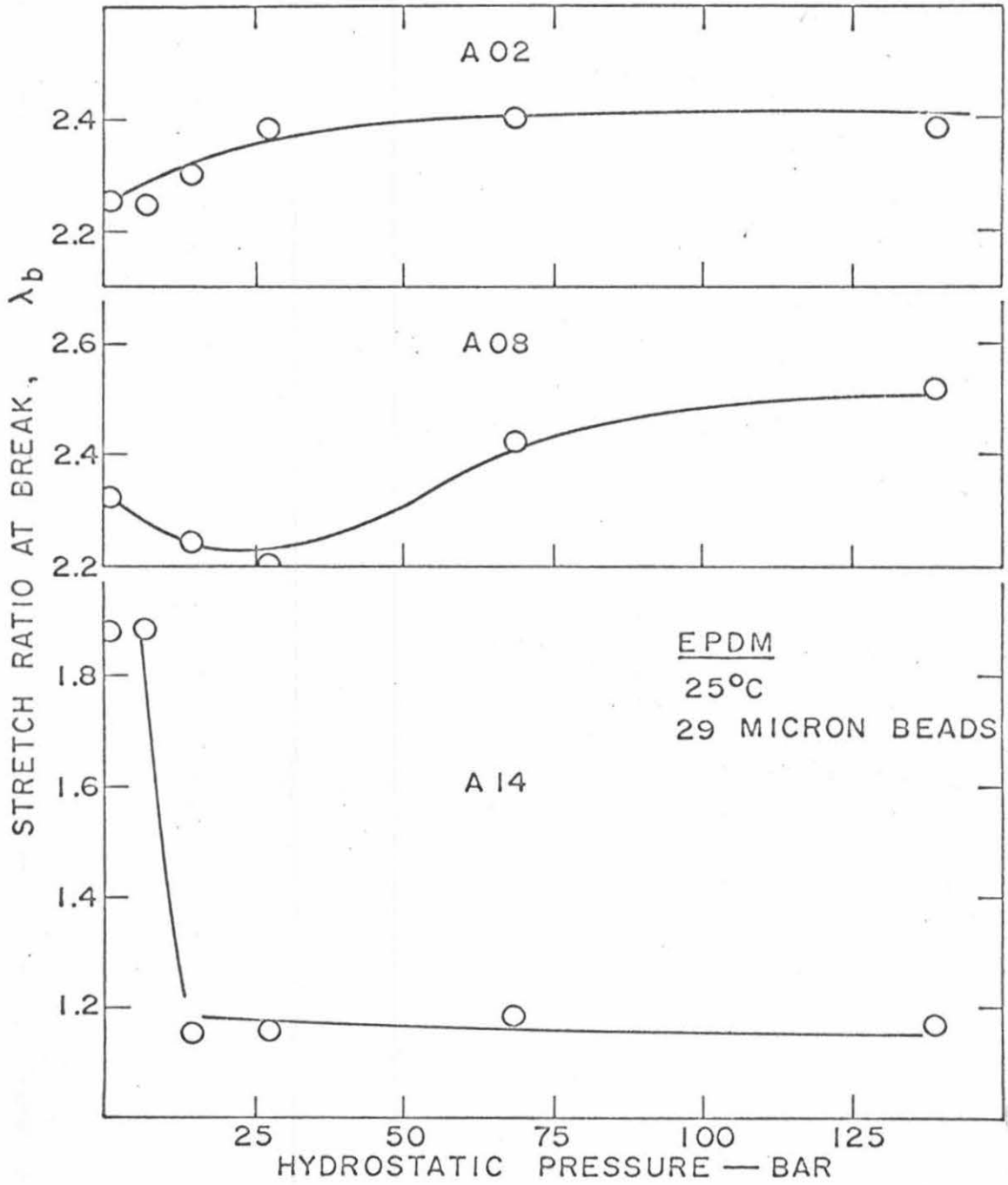

Fig. 26 Stretch Ratio at Break as Function of Hydrostatic Pressure

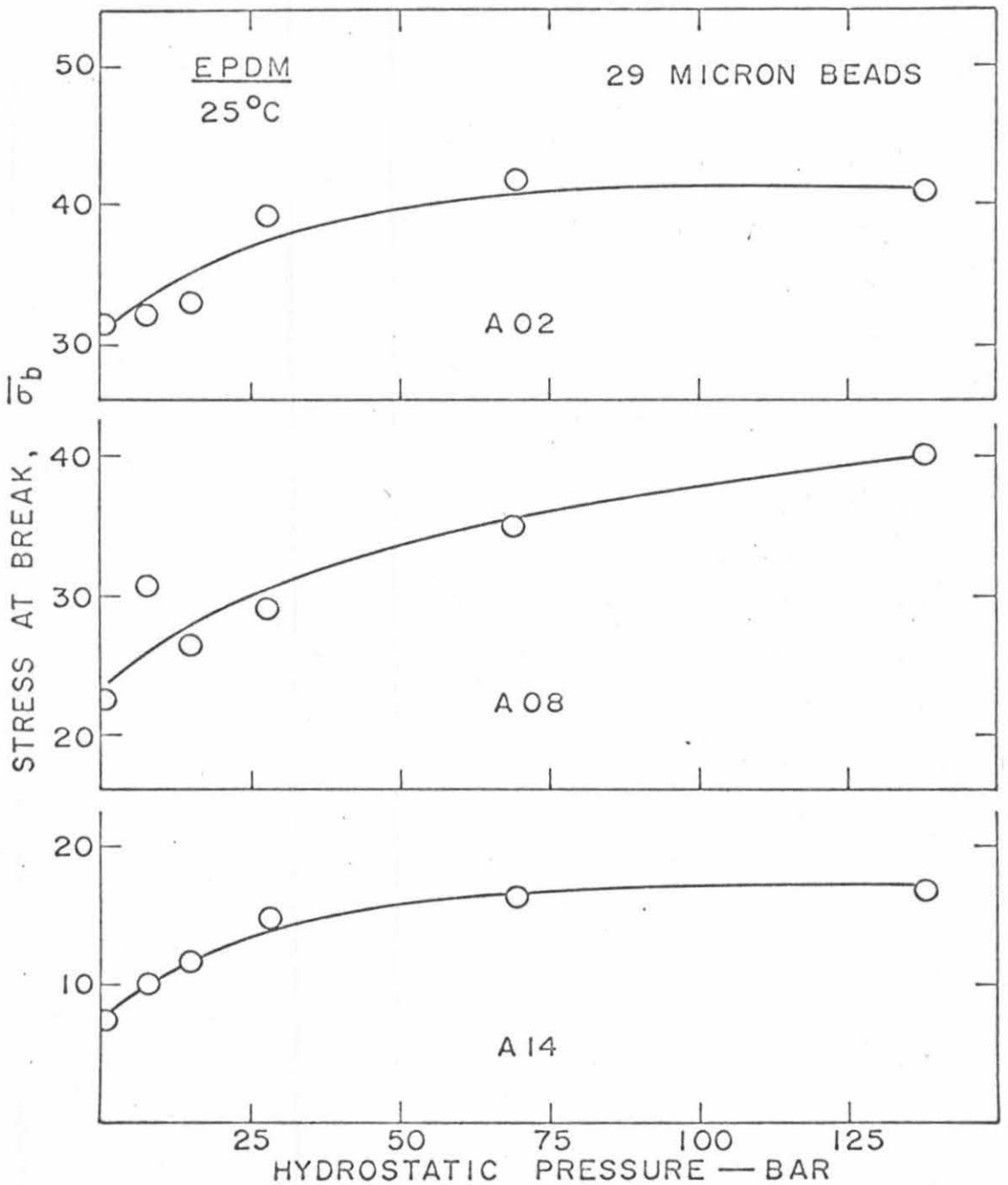

Fig. 27 Stress at Break as Function of Hydrostatic Pressure

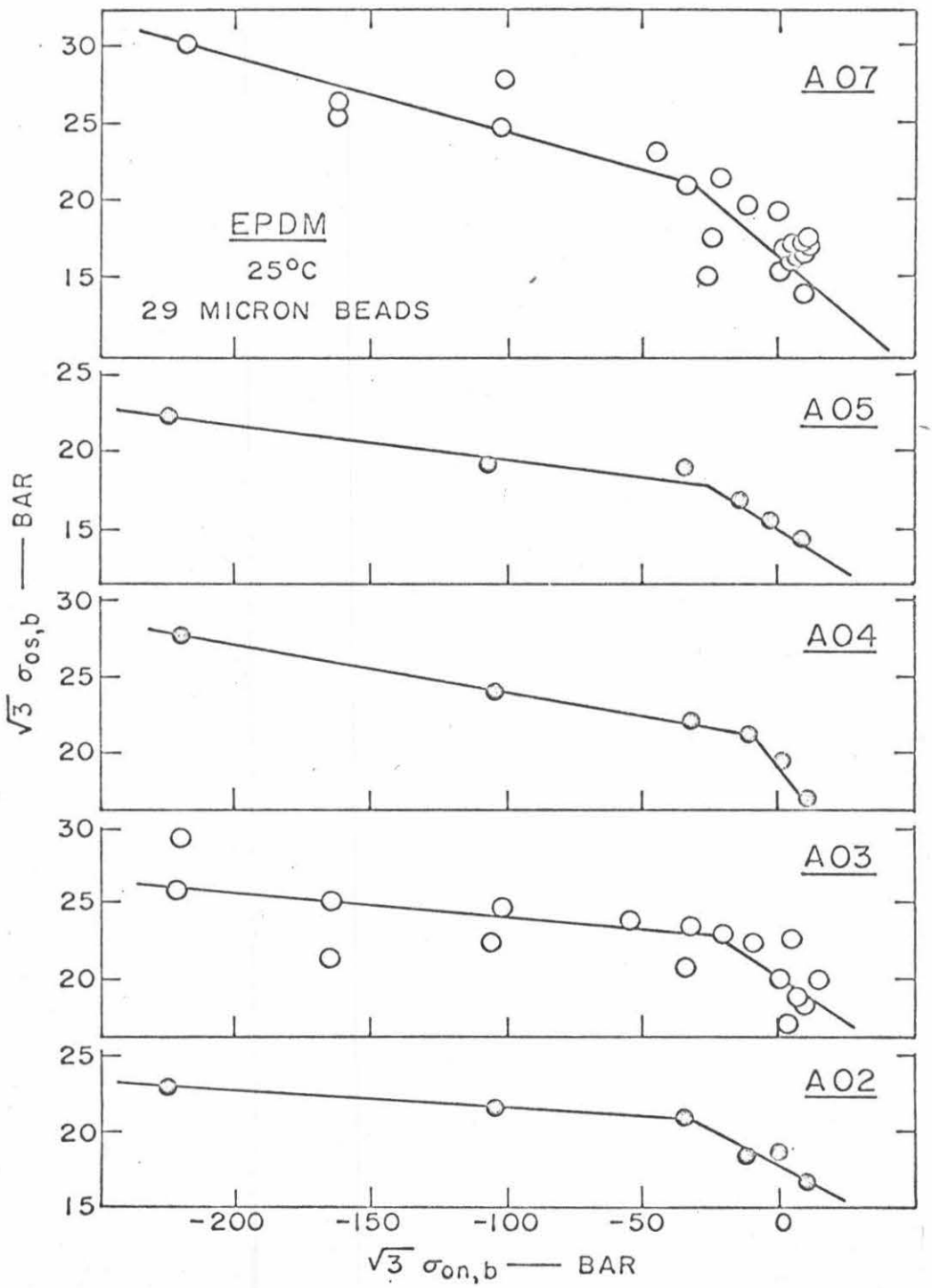

Fig. 28 Profile of Failure Surface

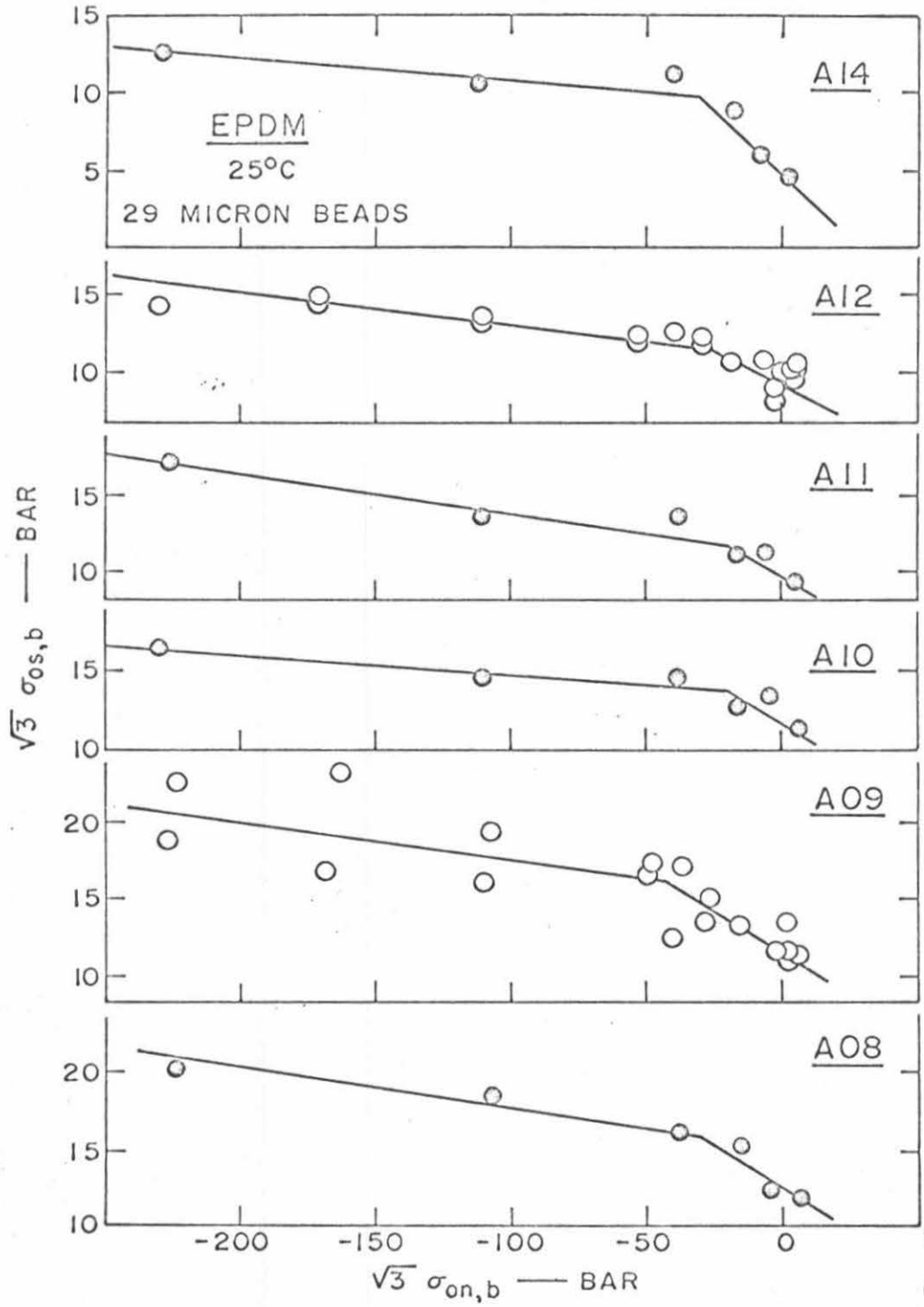

Fig. 29 Profile of Failure Surface

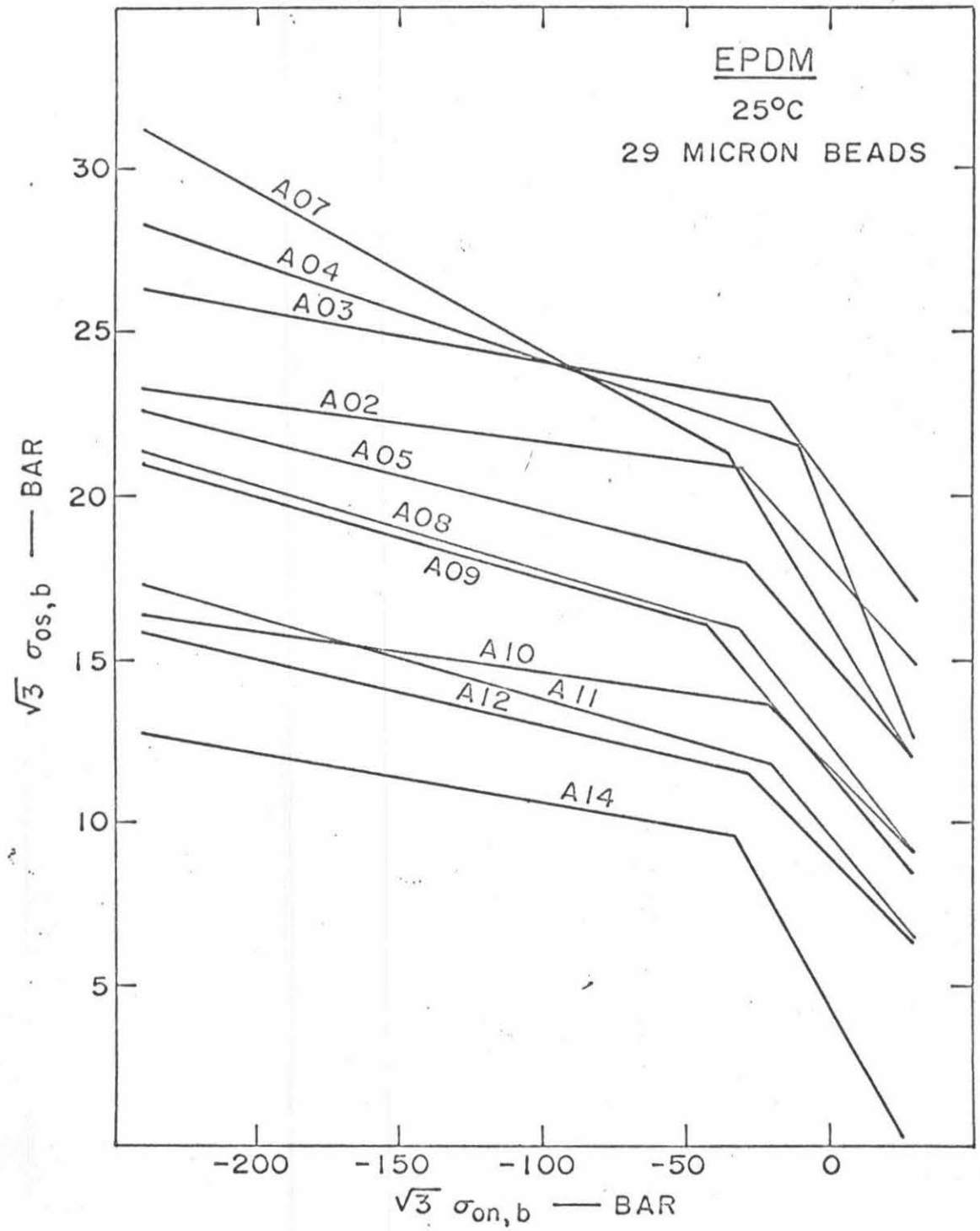

Fig. 30 Profile of Failure Surface. Effect of Volumetric Loading

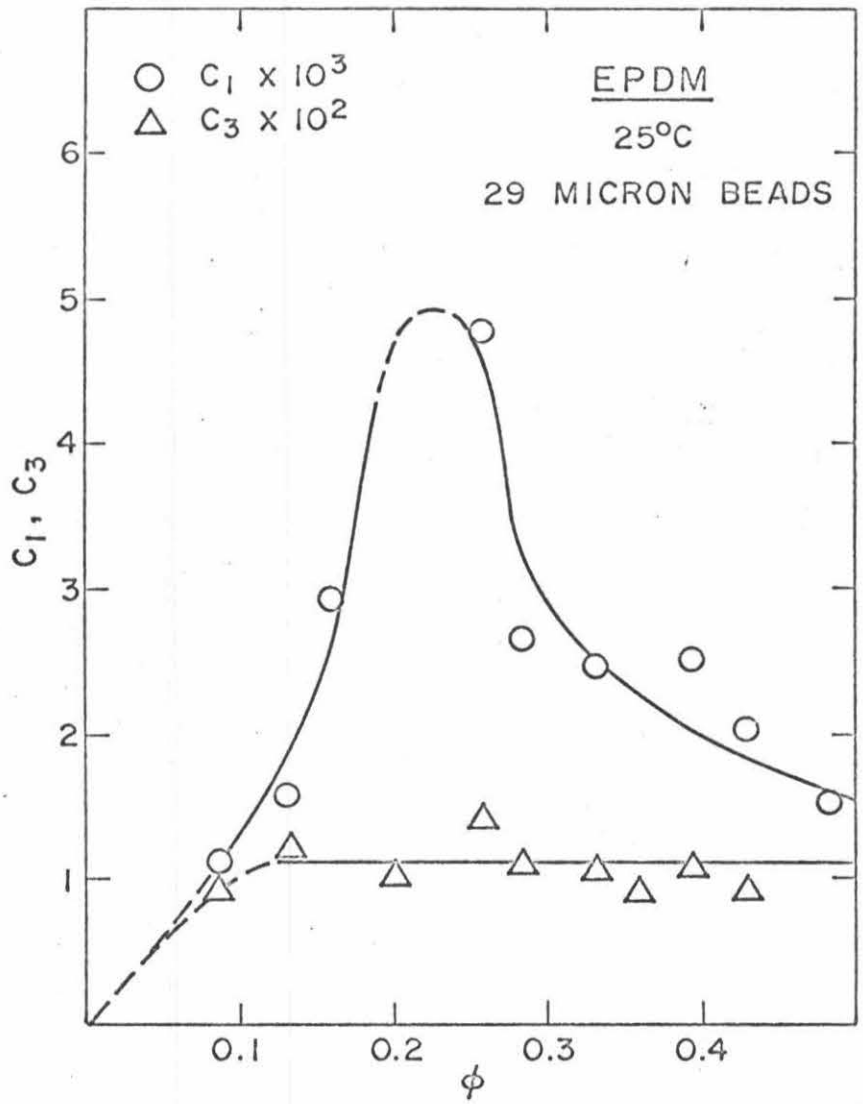

Fig. 31 Characteristic Constants, C_1 and C_3 of Failure Surface as Function of Isotropic Component of Stress at Break

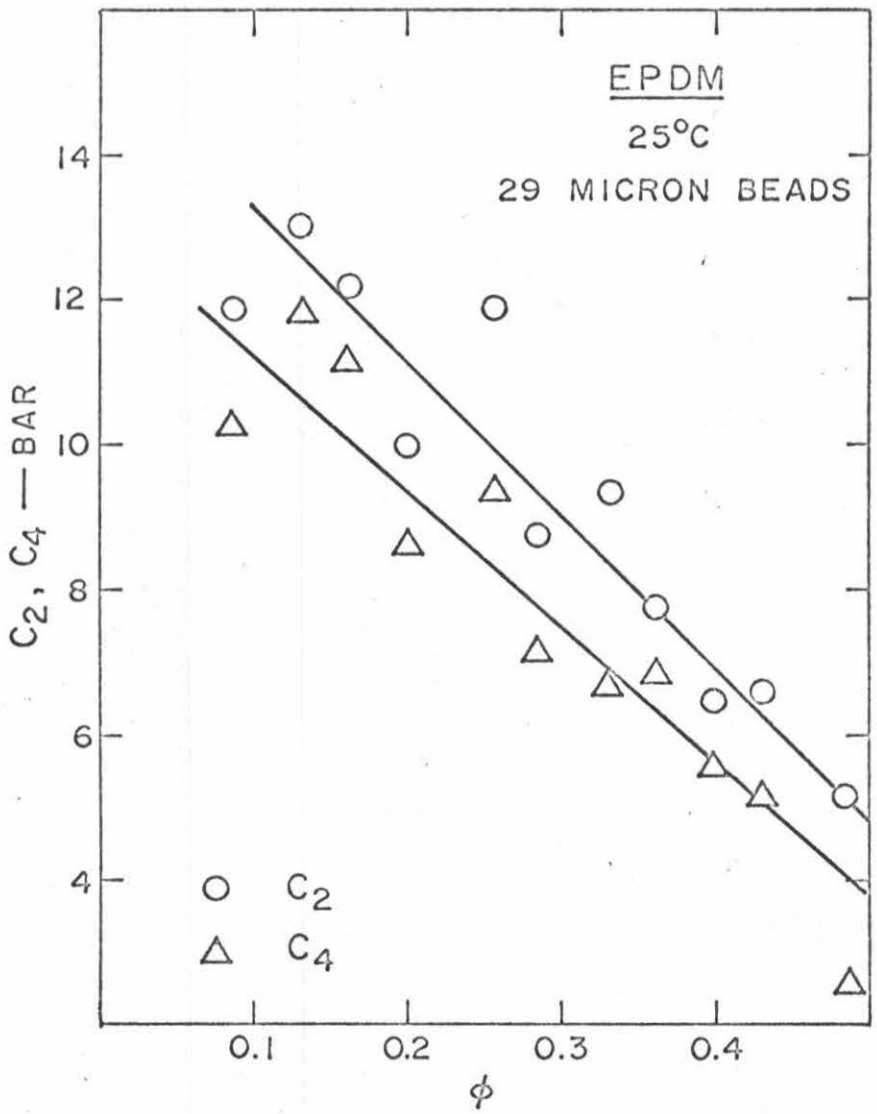

Fig. 32 Characteristic Constants, C_2, and C_4 of Failure Surface as Function of Isotropic Component of Stress at Break

Table I

Summary of the Theoretical Results

No Vacuole Formation

$$W = 2\pi\int_0^a W_{IN} R\ell_o \, dR + 2\pi b\int_a^c W_{OUT} R \, dR$$

(1) (2)

Vacuole Formation

$$W = 2\pi\int_0^{R_d} W_{IN,d} R\ell_o \, dR + 2\pi\int_{R_d}^a W_{IN,nd} R\ell_o \, dR$$

(3) (4)

$$+ 2\pi b\int_a^c W_{OUT} R dR$$

(5)

$$W_N = 2 \sum_{i,j=0}^{\infty} C_{ij} W_{1,N}^{\,i} W_{2,N}^{\,j} \qquad N = IN,\ OUT,\ IN,d,\ IN,nd,\ OUT$$

$$W_{1,N} = \frac{1}{\beta^2\lambda'^2} F + \frac{[\nu \beta R(1-\alpha)]^2}{\ell_o^2} \frac{1}{2\nu - 1}$$

$$+ \beta^2[\alpha^2 + 2\alpha \frac{(1-\alpha)}{\nu+1} + \frac{(1-\alpha)^2}{2\nu+1}] + \lambda'^2 - 3$$

Table I (Cont'd)

$$W_{2,N} = \frac{1}{\lambda'^2} + \frac{[\nu\beta R(1-\alpha)]^2}{\ell_o^2}\left[\frac{\alpha^2}{2\nu-1} + \frac{2\alpha(1-\alpha)}{3\nu-1} + \frac{(1-\alpha)^2}{4\nu-1}\right]$$

$$+ \beta^2\lambda'^2\left[\alpha^2 + \frac{2\alpha(1-\alpha)}{\nu+1} + \frac{(1-\alpha)^2}{2\nu+1}\right] + \frac{1}{\beta^2}F - 3$$

$$F = \frac{1}{\ell_o}\int_0^{\ell_o} \frac{d\ell'}{\left[\alpha + (1-\alpha)\left(\frac{\ell'}{\ell_o}\right)^\nu\right]^2}$$

$$\alpha = \left(\frac{\mu}{\beta^2\lambda'}\right)\frac{\beta^2\lambda'/\mu - 1 + R/\ell_o}{2(\beta^2\lambda'/\mu - 1) + R/\ell_o}$$

$$\nu = \frac{-(3\alpha_o - 2\alpha - 1) + \sqrt{(3\alpha_o - 2\alpha - 1)^2 - 8(\alpha_o - \alpha^2)(\alpha_o - 1)}}{4(\alpha_o - \alpha^2)}$$

$$\left.\begin{aligned} \beta &= 1 && \text{for (1), (3) and (4)} \\ \beta &= \sqrt{\frac{1}{\lambda} + \left(1 - \frac{1}{\lambda}\right)\frac{a^2}{R^2}} && \text{for (2) and (5)} \end{aligned}\right]$$

$$\lambda' = \frac{\lambda - y}{1 - x} \qquad \text{for (1), (3), and (4)}$$

$$\left[\begin{aligned} y &= x && \text{for (1) and (4)} \\ y &= \eta\sqrt{\psi^2 - \left(\psi^2 - \frac{x_d^2}{\eta^2}\right)\frac{\psi^2 - x^2}{\psi^2 - x_d^2}} && \text{for (3)} \end{aligned}\right.$$

$$x_d = \frac{\eta_o - \eta}{\eta_o - 1}\,\psi$$

Table I (Cont'd)

$$\lambda' = \lambda \qquad \text{for (2) and (5)}$$

$$\left.\begin{aligned} \ell_o &= b(1 - x) \\ R &= b(\psi^2 - x^2)^{\frac{1}{2}} \end{aligned}\right\} \qquad \text{for (1), (3) and (4)}$$

$$\left.\begin{aligned} \ell_o &= b \\ R &= R \end{aligned}\right\} \qquad \text{for (2) and (5)}$$

$$\mu = 1 + \frac{\eta}{3}\left[\frac{2\psi^2}{\psi + \sqrt{\psi^2 - (\psi^2 - \frac{x_d^2}{\eta^2})\frac{\psi^2 - x^2}{\psi^2 - x_d^2}}} - \sqrt{\psi^2 - (\psi^2 - \frac{x_d^2}{\eta^2})\frac{\psi^2 - x^2}{\psi^2 - x_d^2}} \right] / (1-x) - \frac{1}{3}\frac{(\psi - x)(2\psi + x)}{(1-x)(\psi + x)} \qquad \text{for (3)}$$

$$\mu = 1 + (\mu_d - 1)\frac{(1-x_d)(\psi^2 - x_d^2)}{(1-x)(\psi^2 - x^2)} \qquad \text{for (4)}$$

$$\mu = 1 + (\mu_d - 1)\frac{(1-x_d)(\psi^2 - x_d^2)}{\psi^2}\frac{a^2}{R^2} \qquad \text{for (5)}$$

$$\mu_d = 1 + \frac{1}{3}\left[\frac{(2\eta\psi + x_d)(\eta\psi - x_d)}{(\eta\psi + x_d)(1 - x_d)} - \frac{(2\psi + x_d)(\psi - x_d)}{(\psi + x_d)(1 - x_d)} \right]$$

$$\mu = 1 \qquad \text{for (1) and (2)}$$

Table II

Composition and Properties

of

Glass Bead-Filled EPDM Vulcanizates

29 μ glass beads diameter

Identification	Parts by Weight	Volume Fraction	Density (g/cc)	Crosslink Density ($\times 10^4$ mol/cc)
A01	0.0	0.0	0.875	2.72
A02	26.0	0.089	0.986	1.32
A03	40.0	0.131	1.048	3.11
A04	52.0	0.164	1.076	2.80
A05	66.0	0.200	1.141	3.14
A06	80.0	0.232	1.204	3.32
A07	92.0	0.258	1.237	3.50
A08	105.0	0.285	1.266	3.53
A09	132.0	0.333	1.330	4.18
A10	150.0	0.362	1.348	3.93
A11	175.0	0.398	1.369	3.95
A12	200.0	0.430	1.472	4.75
A13	225.0	0.459	1.491	3.91
A14	250.0	0.485	———	———

Table III

Sample A02 $\varphi = 0.089$ $\nu_e = 1.32 \times 10^{-4}$ mol cc

Pressure (Bar)	$\bar{G}$ (Bar)	Dewetting λ_d	Dewetting $\bar{\sigma}_d$ (Bar)	Slope	Failure λ_b	Failure σ_b (Bar)	Failure $\bar{\sigma}_b$ (Bar)	ΔV_b
1.0	9.23	1.288	6.10	0.1525	2.254	16.06	31.56	0.147
7.90	10.43	1.418	8.35	0.1862	2.242	16.52	32.12	0.153
14.80	9.57	1.385	7.80	0.0788	2.303	15.94	32.99	0.0645
27.90	9.53	1.414	8.25	0.0843	2.389	17.76	39.20	0.0822
68.80	10.03	1.588	10.07	0.0545	2.403	18.15	41.75	0.0444
138.90	10.63	1.605	10.75	0.0648	2.376	18.06	40.86	0.0500

Table IV

Sample A04 $\varphi = 0.164$ $\nu_e = 2.80 \times 10^{-4}$ mol cc

Pressure (Bar)	$\bar{G}$ (Bar)	Dewetting λ_d	Dewetting σ_d (Bar)	Slope	Failure λ_b	Failure σ_b (Bar)	Failure $\bar{\sigma}_b$ (Bar)	ΔV_o
1.0	12.07	1.220	5.40	0.314	2.594	16.83	30.51	0.431
7.90	12.20	1.423	8.60	0.154	2.584	17.20	37.70	0.1786
14.80	12.37	1.524	10.03	0.113	2.635	18.28	42.78	0.1259
27.90	12.60	1.662	11.46	0.0977	2.630	18.64	44.78	0.0946
68.80	11.37	1.860	13.03	0.0607	2.640	19.39	48.87	0.0473
138.90	12.37	1.967	13.92	0.0701	2.908	21.80	59.46	0.0660

Table V

Sample A05 $\varphi = 0.200$ $\nu_e = 3.14 \times 10^{-4}$ mol cc

Pressure (Bar)	$\bar{G}$ (Bar)	Dewetting λ_d	Dewetting σ_d (Bar)	Slope	Failure λ_b	Failure σ_b (Bar)	Failure $\bar{\sigma}_b$ (Bar)	ΔV_b
1.0	14.33	1.203	5.78	0.1231	2.263	14.45	28.92	0.1305
7.90	17.30	1.530	10.37	0.1367	2.197	14.57	29.33	0.0912
14.80	14.13	1.337	8.80	0.1097	2.150	15.30	30.20	0.0892
27.90	15.47	1.398	9.72	0.1419	2.293	16.79	34.16	0.1270
68.80	15.80	1.533	11.44	0.0810	2.252	16.60	35.22	0.0852
138.00	16.13	1.779	13.58	0.0927	2.511	18.72	44.02	0.0679

Table VI

Sample A08 $\varphi = 0.284$ $\nu_e = 3.53 \times 10^{-4}$ mol/cc

Pressure (Bar)	$\bar{G}$ (Bar)	Dewetting λ_d	Dewetting σ_d (Bar)	Slope	Failure λ_b	Failure σ_b (Bar)	Failure $\bar{\sigma}_b$ (Bar)	ΔV_b
1.0	26.3	1.150	5.30	0.298	2.319	12.82	22.05	0.348
7.90	25.2	1.306	8.96	0.1970	1.949	11.99	30.73	0.137
14.80	21.5	1.383	10.26	0.257	2.246	14.33	26.34	0.222
27.90	22.4	1.393	10.49	0.1423	2.198	14.65	28.90	0.144
68.80	22.6	1.549	11.95	0.1568	2.422	16.50	35.14	0.137
138.00	25.5	1.593	12.27	0.1161	2.519	17.54	39.87	0.108

Table VII

Sample A10 $\varphi = 0.362$ $\nu_e = 3.93 \times 10^{-4}$ mol/cc

Pressure (Bar)	$\bar{G}$ (Bar)	Dewtting λ_d	Dewtting σ_d (Bar)	Slope	λ_b	Failure σ_b (Bar)	Failure $\bar{\sigma}_b$ (Bar)	ΔV_b
1.0	65.7	-----	-----	0.336	2.499	12.78	17.35	0.840
7.90	43.8	1.250	9.08	0.298	2.076	12.40	20.85	0.234
14.90	36.5	1.353	10.32	0.495	2.009	12.97	19.66	0.325
27.90	38.9	1.502	12.42	0.252	2.161	14.28	26.46	0.166
68.80	36.9	1.407	12.30	0.333	1.590	12.77	19.13	0.0609
138.00	48.0	1.654	13.20	0.204	2.281	15.27	30.87	0.128

Table VIII

Sample A11 $\varphi = 0.398$ $\nu_e = 3.95 \times 10^{-4}$ mol/cc

Pressure (Bar)	$\bar{G}$ (Bar)	Dewetting λ_d	Dewetting σ_d (Bar)	Slope	Failure λ_b	Failure σ_b (Bar)	Failure $\bar{\sigma}_b$ (Bar)	ΔV_b
1.0	36.2	-----	-----	0.337	2.105	10.83	13.34	0.709
7.90	40.0	1.242	8.97	0.268	1.883	11.58	18.60	0.172
14.80	37.4	1.352	11.00	0.476	1.427	11.25	15.49	0.0357
27.90	36.4	1.463	13.12	0.550	1.767	13.65	20.66	0.1672
68.80	36.5	1.488	13.18	0.410	1.567	13.34	20.24	0.0324
138.0	37.1	1.712	14.37	0.254	2.144	15.86	30.63	0.1097

Table IX

Sample A14 φ = 0.485

Pressure (Bar)	$\bar{G}$ (Bar)	Dewetting λ_d	Dewetting σ_d (Bar)	Slope	Failure λ_b	Failure σ_b (Bar)	Failure $\bar{\sigma}_b$ (Bar)	ΔV_b
1.0	56.9	-----	-----	-----	1.878	7.48	(7.48)	-----
7.90	128.7	-----	-----	-----	1.883	10.01	(10.01)	-----
14.80	90.5	-----	-----	-----	1.150	10.04	11.55	-----
27.90	117.8	-----	-----	-----	1.160	12.64	14.66	-----
68.80	82.8	-----	-----	-----	1.186	13.66	16.20	-----
138.00	137.7	-----	-----	-----	1.170	14.12	16.52	-----

Table X

Failure Surface Parameters of Glass Bead-Filled EPDM Vulcanizates

Sample		First Cone		Second Cone		Transition	
		$C_1 \times 10^3$	C_2 (Bar)	$C_3 \times 10^3$	C_4 (Bar)	$\sigma_{on,b}$(trans) (Bar)	$\sigma_{os,b}$(trans) (Bar)
A01	0.0						
A02	0.089	1.136	11.83	9.64	10.28	-18.0	12.06
A03	0.131	1.565	13.00	12.13	11.82	-11.55	13.39
A04	0.164	2.93	12.25	22.1	11.13	- 5.77	12.47
A05	0.200	2.93	12.25	22.1	11.13	-16.17	10.38
A07	0.258	4.78	11.89	14.4	9.37	-20.5	12.3
A08	0.284	2.63	8.73	11.1	7.20	-18.13	9.21
A09	0.333	2.48	8.66	10.6	6.69	-24.2	9.26
A10	0.362	1.273	7.70	9.19	6.82	-11.55	7.85
A11	0.398	2.52	6.50	10.8	5.57	-11.55	6.81
A12	0.430	2.05	6.30	8.98	5.19	-16.28	6.64
A14	0.485	1.512	5.20	15.9	2.52	-18.60	5.51

REFERENCES

1 A. Einstein: Ann. Physik 19, 289 (1906); 34, 591 (1911)

2 H. von Eilers: "Die Viscosität von Emulsionen Hochviskoser Stoffe als Funktion der Konzentration", Koll.-Z., 97, 313 (1941)

3 E. Guth, "Theory of Filler Reinforcement", J. Appl. Phys., 16, 20 (1945)

4 H. M. Smallwood: "Limiting Law of Reinforcement of Rubber", J. Appl. Phys., 15, 798 (1954)

5 C. van der Poel: "On the Rheology of Concentrated Dispersions", Rheologica Acta, 1, No. 2 - 3, 198 (1958)

6 N. A. Frankel, and A. Acrivos: "On the Viscosity of a Concentrated Suspension of Solid Spheres", Chem. Eng. Sci., 22, 847 (1967)

7 Y. Sato and J. Furukawa: "A Molecular Theory of Filler Reinforcement Based upon the Conception of Internal Deformation (A Rough Approximation of the Internal Deformation)", Rubber Chem. Tech., 36, 1081 (1963)

8 R. F. Fedors and R. F. Landel: JPL Space Program Summary, 37-41, 4, No. 10, 97

9 N. Fishman, and J. A. Rinde, "Solid Propellant Mechanical Properties Investigations", SRI Project PRU-4673 (1964)

10 R. J. Farris, "The Influence of Vacuole Formation on the Response and Failure of Filled Elastomers", Trans. Soc.

Rheology, 12, 315 (1968)

11 A. C. Eringen: "Nonlinear Theory of Continuous Media", McGraw-Hill (1962)

12 M. Yamamoto: "Rheology", Maki-Shoten (1964)

13 F. R. Eirich: "Rheology", Chapter 10, Academic Press (1956)

14 I. S. Gradshteyn and I. M. Ryzik: "Table of Integrals and Products", p. 284, Academic Press (1965)

15 R. F. Landel and N. W. Tschoegl: "A Research Program on Solid Propellant Physical Behavior", MATSCIT PS 67-1, California Institute of Technology, Pasadena, 1967, AFRPL-TR-67-193, Volume 1, June 1967, pp. II-1 to II-49

16 C. K. Lim and N. W. Tschoegl, W. G. Knauss, R. F. Landel, et al.: "A Research Program on Solid Propellant Physical Behavior", CHECIT PL-69-1, California Institute of Technology, AFRPL-TR-69-180, Edward AFB, California, August 1969

17 E. H. Hall, Am. J. Mathematics, 2, 287 (1879)

18 M. Epstein, et al.: Proc. of National Electronics Conference, 15, 241 (1959)

19 "The Hall Effect and Its Applications", pamphlet by F. W. Bell Inc.

20 M. Okuyama, Personal communication

21 T. L. Smith, Technical Documentary Report No. ASD-TDR-62-572, Air Force Systems Command, June 1962

22 R. C. Sampson: "Observation of Damage in Rigid-Particle Filled Elastomer Models", CPTA Publication No. 177 1968, p. 221

23 E. H. Kerner: "The Electrical Conductivity of Composite Media", Proc. Phys. Soc., B, 69, 802 (1956)

24 E. H. Kerner: "The Elastic and Thermo-elastic Properties of Composite Media", Proc. Phys. Soc. B, 69, 808 (1956)

25. N. W. Tschoegl: "Constitutive Equations for Elastomers", to be published

26. H. Kausch and N. W. Tschoegl, N. W. Tschoegl, R. F. Landel, et al.:" A Research Program on Solid Propellant Physical Behavior", CHECIT PL 68-1, California Institute of Technology, AFRPL-68-106, June 1968, pp. II-1 to II-29